Article

Novel Multi-Target Directed Triazinoindole Derivatives as Anti-Alzheimer Agents

Dushyant V Patel, Nirav R Patel, Ashish M Kanhed, Sagar P Patel, Anshuman Sinha, Deep
D Kansara, Annie R Mecwan, Sarvangee B Patel, Pragnesh N Upadhyay, Kishan B Patel,
Dharti B Shah, Navnit K Prajapati, Prashant R. Murumkar, Kirti V Patel, and Mange Ram Yadav

Just Accepted

Novel Multi-Target Directed Triazinoindole Derivatives as Anti-Alzheimer Agents

Dushyant V. Patel, Nirav R. Patel, Ashish M. Kanhed, Sagar P. Patel, Anshuman Sinha, Deep D. Kansara, Annie R. Mecwan, Sarvangee B. Patel, Pragnesh N. Upadhyay, Kishan B. Patel, Dharti B. Shah, Navnit K. Prajapati, Prashant R. Murumkar, Kirti V. Patel, Mange Ram Yadav[a*]

Faculty of Pharmacy, Kalabhavan Campus,
The Maharaja Sayajirao University of Baroda, Vadodara- 390001
Gujarat, India

Abstract: The multifaceted nature of Alzheimer's disease (AD) demands treatment with multitarget-directed ligands to confront the key pathological aberrations. A novel series of triazinoindole derivatives were designed and synthesized. In vitro studies revealed that all the compounds showed moderate to good anti-cholinesterase activity; the most active compound **23e** showing IC_{50} value of 0.56 ± 0.02 μM for AChE and IC_{50} value of 1.17 ± 0.09 μM for BuChE. These derivatives are also endowed with potent anti-oxidant activity. To understand the plausible binding mode of the compound **23e**, molecular docking studies and molecular dynamics simulation studies were performed and the results indicated significant interactions of **23e** within the active sites of AChE as well as BuChE. Compound **23e** successfully diminished H_2O_2-induced oxidative stress in SH-SY5Y cells and displayed excellent neuroprotective activity against H_2O_2 as well as Aβ-induced toxicity in SH-SY5Y cells in a concentration dependent manner. Furthermore, it did not show any significant toxicity in neuronal SH-SY5Y cells in the cytotoxicity assay. Compound **23e** did not show any acute toxicity in mice at doses up to 2000 mg/kg, and significantly reversed scopolamine-induced memory deficit in mice model. Additionally, compound **23e** showed notable in silico ADMET properties. Taken collectively, these findings project compound **23e** as a potential balanced MTDL in the evolution process of novel anti-AD drugs.

Keywords: Alzheimer's disease, MTDL, anticholinesterase, antioxidant, neuroprotection, triazinoindole

1

Introduction

Alzheimer's disease (AD) is an irrevocable age-related neurodegenerative disorder clinically identified by progressive deterioration in memory, cognitive deficit, abnormal behavior and incoherent language.[1] It is the most prominent form of dementia. More than 50 million people are suffering from it worldwide, and the number will significantly rise up to 152 million by 2050 if no cure or preventive measures are found.[2] This burgeoning number of people suffering from AD, in both developed and developing countries, has drawn the attention of medicinal chemists to accelerate research on drug discovery in this area.

The etiology of AD is still enigmatic. Different factors, like low levels of neurotransmitter acetylcholine (ACh),[3] aggregation of the β-amyloid peptide,[4,5] accumulation of hyperphosphorylated tau protein,[6,7] dyshomeostasis of biometals,[8] oxidative stress,[9] mitochondrial dysfunction[10] and neuroinflammation[11-13] are proposed to play pivotal roles in the pathogenesis of AD. To combat AD like diseases having a complex etiology, development of multitarget-directed ligands (MTDLs) is recognized as one of the most assuring drug discovery approaches.[14-17] Drugs acting on a single target even though having high affinity and selectivity for their targets might not influence the mysterious etiology of the disease satisfactorily. An MTDL having moderate, but balanced affinities for the targets can still exert more beneficial effects compared to a single-targeted molecule. Concurrent effects on several therapeutic targets make MTDLs superior in altering the complex equilibrium of the cellular network.[18,19] A mild and balanced activity on multiple therapeutic targets might secure higher safety, and reduce the risk of therapeutic resistance.[20]

After perusal of current research in this field, we focused our attentions on inhibition of cholinesterase and anti-oxidant potential of new chemical entities (NCEs) as the core objectives

of anti-AD drug design. Two types of cholinesterase enzymes (ChEs) namely acetylcholinesterase (AChE) (EC 3.1.1.7) and butyrylcholinesterase (BuChE) (EC 3.1.1.8), are found in the central nervous system. Both these enzymes belong to the carboxylesterase family of enzymes and play an important role in cholinergic transmission through hydrolysis of the neurotransmitter ACh. Although AChE and BuChE are produced by different genes they are highly homologous with more than 65 % similarity in their active sites.[21,22] AChE has two major binding sub-sites, a peripheral anionic site (PAS) and the other a catalytic active site (CAS).[23] The CAS of the enzyme is actively involved in the maintenance of cholinergic neurotransmission. PAS is involved in the formation of β-amyloid fibrils that are associated with plaque deposition.[24,25] AChE inhibitors blocking both CAS and PAS simultaneously could alleviate the cognitive defect in AD patients by elevating ACh levels and have also been endowed with disease modifying ability by inhibiting the amyloid plaque formation.[26] In healthy brains, AChE is more active than BuChE and can hydrolyze about 80 % of ACh. Current studies have demonstrated that as the disease progresses, the ability of BuChE increases by 40-90 %, and that of AChE declines in the hippocampus and temporal cortex areas of the brain.[27-29] BuChE plays several roles both in neural and non-neural functioning. Clinical data suggested that the high cortical levels of BuChE were associated with some important AD hallmarks, such as extracellular deposition of the Aβ and aggregation of hyper-phosphorylated tau protein.[21,30,31] This reflects the important role played by both the cholinesterases and the necessity to develop MTDLs which could act on both these ChEs.[32]

Recent research has emphasized the significance of oxidative stress in the fundamental molecular mechanism of AD.[8,9] Oxidative stress occurs when there is an inequity between the formation and quenching of free radicals formed from oxygen species. These reactive oxygen species (ROS) are regarded as the other major etiological factor of AD, since the role of the ROS

in the formation of both amyloid plaques and neurofibrillary tangles is confirmed.[33] Through pathological oxidation-reduction steps, ROS can denature biomolecules like proteins, lipids and nucleic acids. This can cause tissue damage through necrosis and apoptosis.[34] Thus, oxidative stress plays a central role in the pathogenesis of AD leading to neuronal dysfunction and cell death.[35]

Considering the facts that inhibition of AChE provides a symptomatic treatment to AD, increase in levels of BuChE are observed in the brains of AD patients, and the ROS system plays a vital role in neurodegeneration, a series of triazinoindole derivatives were designed, synthesized and evaluated in the current report for their multifactorial anti-AD activities, including cholinesterase inhibitory activity, antioxidant activity, cytoprotective effect against H_2O_2/Aβ-induced cell injury and acute toxicity in animal models. The in silico ADMET properties of the synthesized derivatives were predicted and the structure-activity relationship of these novel derivatives has been discussed. Molecular modeling studies were performed to offer an insight into the binding mode of the derivatives with the target proteins, and these findings were supported by the time dependent stability analysis of the ligand-receptor complex of the most active ligand and the receptor under study, by means of molecular dynamics simulations.

Designing aspects

To combat a disease like AD having complex etiology, development of MTDLs has been recognized as one of the most assuring drug discovery approaches. In spite of considerable research on new targets available for AD treatment, the cholinesterase inhibitors still remain the drugs of choice, although they provide symptomatic and transient benefits to the patients. Oxidative stress plays an important role in pathogenesis of AD. However antioxidant molecules all alone might not be enough to treat such highly complex pathological disease

4

like AD.[36] So dual cholinesterase inhibitors endowed with additional anti-oxidant and neuroprotective properties could increase the chances of combating AD successfully.

Indole ring is prodigiously present in many natural compounds possessing invaluable medicinal and biological properties.[37,38] Melatonin is an indole ring containing pineal neurohormone whose levels decrease during aging, especially in AD patients.[39-41] It is endowed with strong free radical scavenging properties.[42] The high reactivity of melatonin with ROS is apparently due to its electron-rich indole ring, acting as an electron donor. Recent studies have also shown that melatonin offers protective effects against Aβ-induced apoptosis,[43] glutamate-induced excitotoxicity,[44] nitric oxide toxicity,[45] decreases neurofilament hyperphosphorylation and augments learning and memory in rats. In recent years, many indole based hybrids e.g. tacrine-melatonin hybrids,[46] donepezil-chromone-melatonin hybrids,[47] melatonin-*N,N*-dibenzyl(*N*-methyl)amine hybrids,[48] and carbamate derivatives of indolines,[49] have been designed to act as multifunctional agents for the treatment of AD. Furthermore, the indole moiety is present in several CNS-active drugs like rizatriptan and oxypertine. Thus indole ring offers a privileged scaffold for CNS-active drugs which could augment the search for new therapeutics for AD. 1,2,4-Triazine nucleus is another important structural system present in several biologically active compounds.[50] The significance of triazines in neuropharmacology is explored progressively for their potential anti-AD,[51-54] antianxiety,[55] antiepileptic[56] and anti-depressant[57] activities. Some triazine derivatives have been reported to be potent neuroprotective agents against H_2O_2-induced cell death in PC12 cell line.[58] In recent past our research group had reported substituted diaryltriazines as potential anti-AD entities.[59] Reports of remarkable biological activities associated with the indole ring and the 1,2,4-triazine nucleus prompted us to fuse these two

privileged scaffolds into a single moiety which could potentially offer multiple favorable activities

for the treatment of AD.
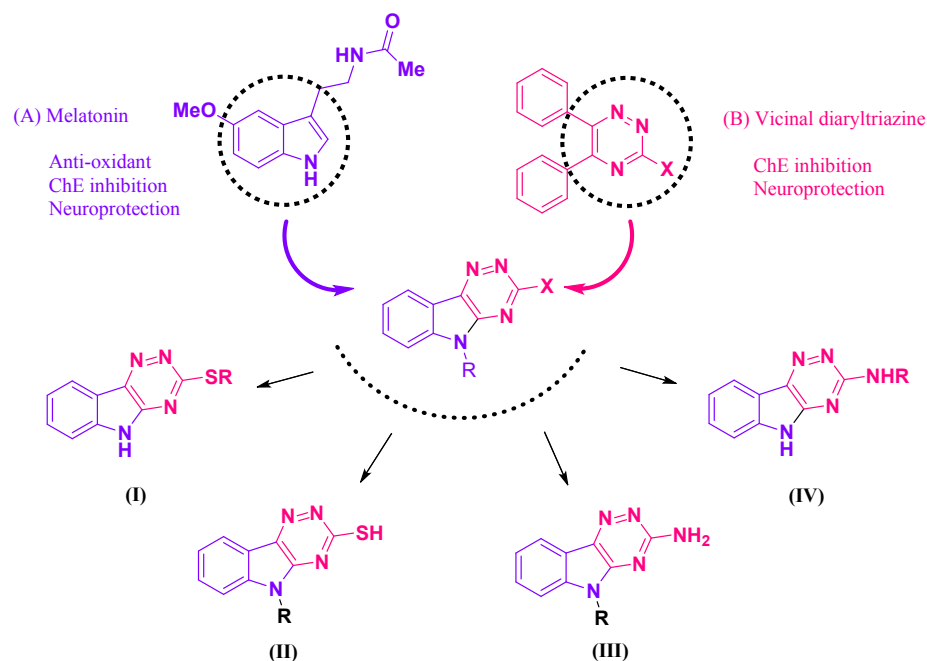
Figure 1. Molecular hybridization approach to design triazinoindole derivatives.

Different 5*H*-[1,2,4]triazino[5,6-*b*]indole-3-thiol and 5*H*-[1,2,4]triazino[5,6-*b*]indol-3-

amine derivatives were designed by following a rational hybridization approach (**Figure 1**). The

molecular interactions of the designed derivatives were evaluated theoretically by means of

docking the designed compounds within the active site of AChE and BuChE. Both the designed

scaffolds showed promising binding affinities within the active sites of AChE as well as BuChE

(**Figure 2**). The 5*H*-[1,2,4]triazino[5,6-*b*]indole-3-thiol scaffold showed stability within the CAS

of AChE (docking score: -7.96) by forming π-π interactions with Trp84 and Phe330 and hydrogen

bonding with His440. While, the same scaffold in the active site of BuChE (docking score: -7.21)

exhibited π-π interactions with Trp82, Trp430 and His438 along with hydrogen bonding with

His438. Another designed scaffold 5*H*-[1,2,4]triazino[5,6-*b*]indol-3-amine showed similar π-π

interactions but offering higher binding affinities with AChE (docking score: -8.89) and BuChE

(docking score: -7.22) enzymes due to additional strong hydrogen bonding caused by the 3-amino

group. During the in vitro enzyme inhibition study, 5*H*-[1,2,4]triazino[5,6-*b*]indole-3-thiol showed

11.26 µM and 55.81 µM inhibitory activity (IC$_{50}$) against AChE and BuChE respectively, whereas

5*H*-[1,2,4]triazino[5,6-*b*]indol-3-amine was found to possess IC$_{50}$ values of 9.76 µM and 51.25

µM against AChE and BuChE, respectively. On the basis of these moderately promising activities

of the designed scaffolds, modifications were carried out by incorporating various alkyl/benzyl

substituents to understand the SAR and to come up with some potential leads. Accordingly,

compounds of the four series (**I-IV**) as shown in **Figure 1**, were synthesized and discussed here in
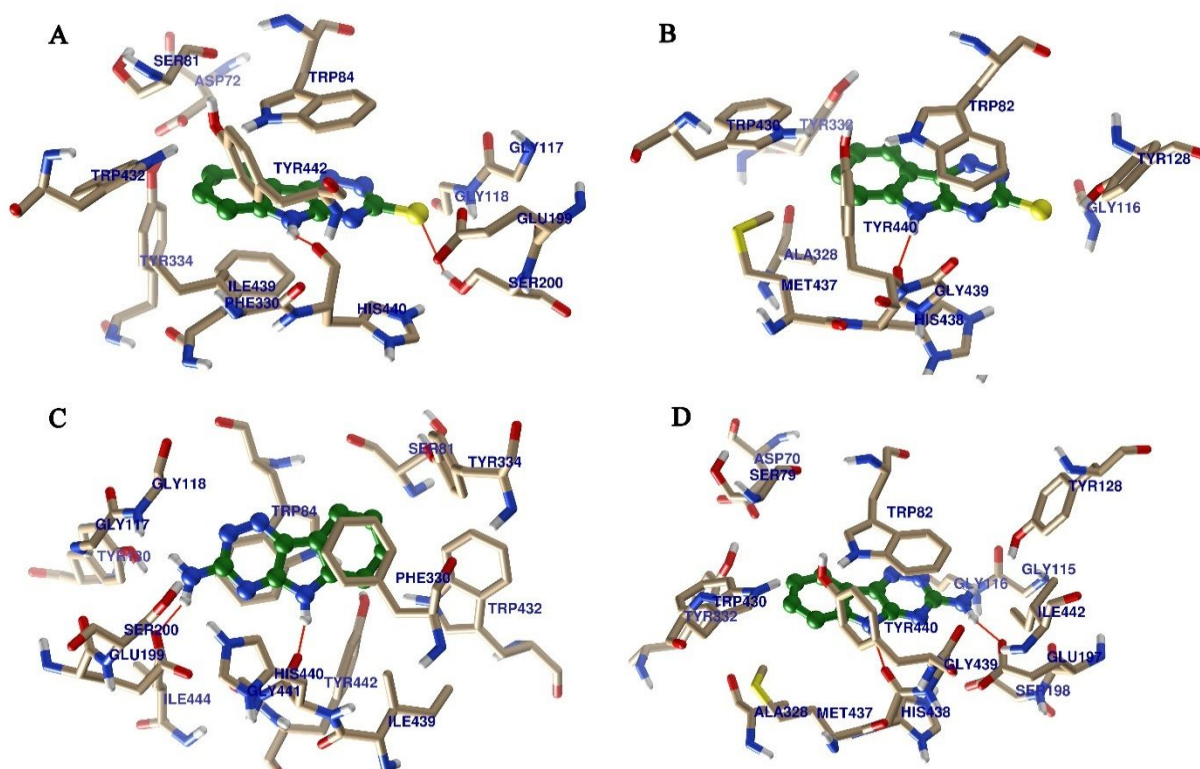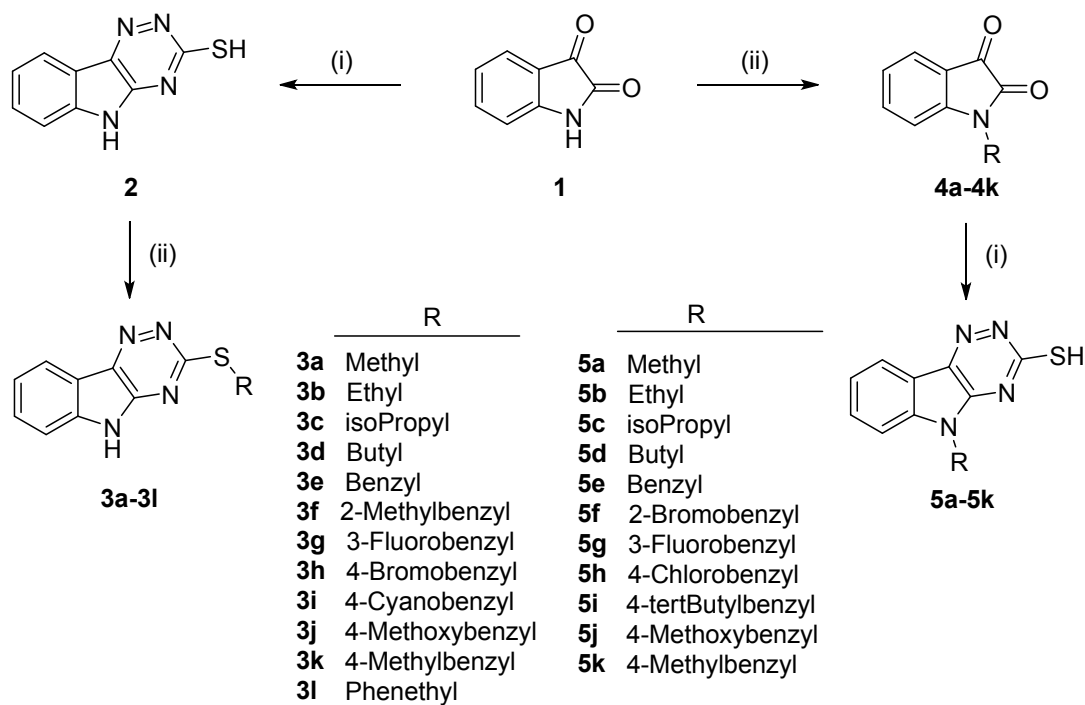
this work.

Figure 2. Interaction of 5*H*-[1,2,4]triazino[5,6-*b*]indole-3-thiol with (A) AChE, (B) BuChE, and 5*H* [1,2,4]triazino[5,6-*b*]indol-3-amine with (C) AChE and (D) BuChE.

RESULTS AND DISCUSSION

Chemistry

Compounds **2**, **3a-3l** and **5a-5k** were synthesized as depicted in **Scheme 1**. Compound **2** was obtained by condensation of commercially available isatin (**1**) with thiosemicarbazide in aqueous potassium carbonate solution at reflux conditions. The clear liquid obtained was acidified by glacial acetic acid to get the condensed product **2**. Alkylation or benzylation of compound **2** with the corresponding alkyl/benzyl halides gave thio-substituted compounds **3a-3l**. Similarly, *N*-substituted 1,2,4-triazino-[5,6-*b*]indole-3-thiol derivatives **5a-5k** were synthesized by condensation of the *N*-substituted isatins **4a-4k** with thiosemicarbazide. *N*-Alkylation or *N*-benzylation of the isatins were achieved with the corresponding alkyl/benzyl halides in the presence of potassium carbonate in DMF.

Scheme 1. Synthesis of compounds 2, 3a-3l and 5a-5k.

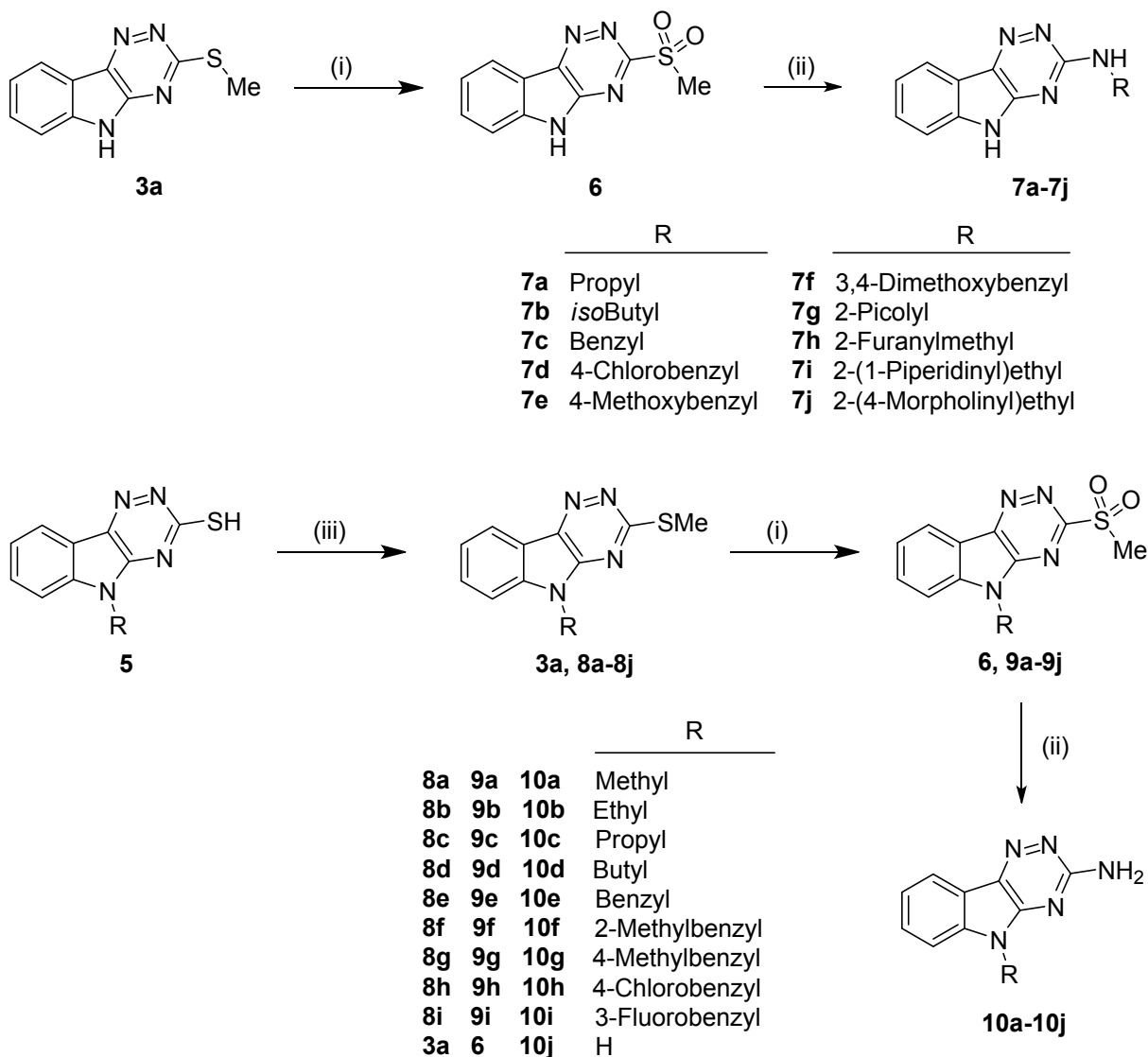|	R			R
3a	Methyl		**5a**	Methyl
3b	Ethyl		**5b**	Ethyl
3c	isoPropyl		**5c**	isoPropyl
3d	Butyl		**5d**	Butyl
3e	Benzyl		**5e**	Benzyl
3f	2-Methylbenzyl		**5f**	2-Bromobenzyl
3g	3-Fluorobenzyl		**5g**	3-Fluorobenzyl
3h	4-Bromobenzyl		**5h**	4-Chlorobenzyl
3i	4-Cyanobenzyl		**5i**	4-tertButylbenzyl
3j	4-Methoxybenzyl		**5j**	4-Methoxybenzyl
3k	4-Methylbenzyl		**5k**	4-Methylbenzyl
3l	Phenethyl			

Reagents and conditions. (i) Thiosemicarbazide, K_2CO_3, H_2O, reflux, overnight; (ii) alkyl/substituted benzyl halides, K_2CO_3, DMF.

When the substituted isatins were subjected to cyclization reaction with aminoguanidine instead of thiosemicarbazide, uncyclized *N*-substituted isatin-3-aminoguanylhydrazones were obtained instead of the 5-substituted [1,2,4]triazino[5,6-*b*]indol-3-amine derivatives. All efforts made to cyclize these *N*-substituted isatin-3-aminoguanylhydrazones to get 5-substituted [1,2,4]triazino[5,6-*b*]indol-3-amine derivatives failed and only the non-cyclized starting compounds were obtained. In one attempt, cyclization of *N*-benzylisatin-3-aminoguanylhydrazone in the presence of a strong base and diethylene glycol as a polar protic solvent, the hydrolyzed product, i.e. 2-(benzylamino)benzoic acid was isolated.

In an alternative approach, the desired amino derivatives were synthesized from the thiol derivatives. The thiol derivatives were first methylated and the methylthio derivatives were treated with various amines.[60] Unfortunately the thiomethyl derivatives failed to react with the amines. So the thiomethyl group at the C-3 position was converted to sulfone, as it has more electron withdrawing ability compared to the parent thiomethyl group. This was achieved by oxidizing the thiomethyl group by *m*CPBA to sulfone. When these sulfone derivatives were reacted with amines in THF under refluxing conditions, the sulfone group was substituted by the amino group offering the desired substituted [1,2,4]triazino[5,6-*b*]indol-3-amine derivatives **7a-7j**. Similarly, compounds **5** were methylated and further oxidized to the corresponding sulfone compounds **9a-9j**. These sulfone compounds were reacted with ammonia to obtain the desired 5-substituted [1,2,4]triazino[5,6-*b*]indol-3-amine derivatives **10a-10j** (**Scheme 2**).
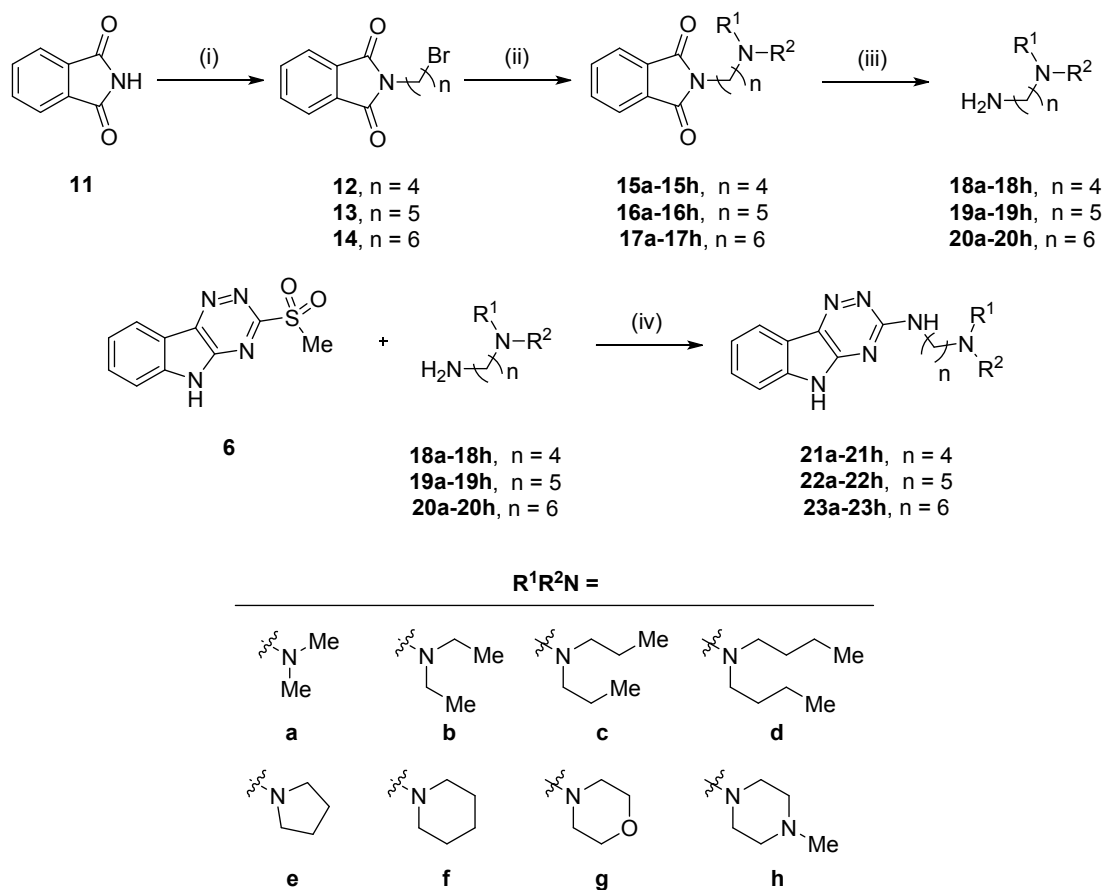
Scheme 2. Synthesis of compounds 7a-7j and 10a-10j.

	R		R
7a	Propyl	**7f**	3,4-Dimethoxybenzyl
7b	*iso*Butyl	**7g**	2-Picolyl
7c	Benzyl	**7h**	2-Furanylmethyl
7d	4-Chlorobenzyl	**7i**	2-(1-Piperidinyl)ethyl
7e	4-Methoxybenzyl	**7j**	2-(4-Morpholinyl)ethyl

8a	**9a**	**10a**	Methyl
8b	**9b**	**10b**	Ethyl
8c	**9c**	**10c**	Propyl
8d	**9d**	**10d**	Butyl
8e	**9e**	**10e**	Benzyl
8f	**9f**	**10f**	2-Methylbenzyl
8g	**9g**	**10g**	4-Methylbenzyl
8h	**9h**	**10h**	4-Chlorobenzyl
8i	**9i**	**10i**	3-Fluorobenzyl
3a	**6**	**10j**	H

Reagents and conditions. (i) *m*CPBA, DCM, 0 ℃ to RT; (ii) Amines/ammonia, THF, reflux; (iii) MeI, K_2CO_3, DMF.

The aminoalkylamines **18a-20h** required for the synthesis of compounds **21a-23h** were prepared through Gabriel synthesis using phthalimide as the starting material. Phthalimide (**11**) was reacted with dibromoalkanes to form *N*-(bromoalkyl)phthalimides **12-14**. The desired basic amines (**a-h**; R^1R^2NH) were reacted with *N*-(bromoalkyl)phthalimides **12-14** to yield compounds **15a-17h**. Hydrazinolysis of compounds **15a-17h** in methanol offered the desired aminoalkyl-

10

amines **18a-20h** in 67–87 % yields. These aminoalkylamines **18a-20h** were reacted with

compound **6** as discussed previously to obtain the desired final products **21a-23h** (**Scheme 3**).

Scheme 3. Synthesis of compounds 21a-23h.

11

12, n = 4
13, n = 5
14, n = 6

15a-15h, n = 4
16a-16h, n = 5
17a-17h, n = 6

18a-18h, n = 4
19a-19h, n = 5
20a-20h, n = 6

6

18a-18h, n = 4
19a-19h, n = 5
20a-20h, n = 6

21a-21h, n = 4
22a-22h, n = 5
23a-23h, n = 6

$R^1R^2N =$

a   **b**   **c**   **d**

e   **f**   **g**   **h**

Reagents and conditions. (i) Br(CH$_2$)$_n$Br, K$_2$CO$_3$, TEBAC, acetone, RT; (ii) HNR^{1}R^2, TEA, MeOH, reflux; (iii) NH$_2$NH$_2$.H$_2$O, MeOH, reflux; (iv) THF, reflux.

Biological evaluation

Inhibition studies on AChE and BuChE

The potential of the synthesized compounds to inhibit cholinesterases (ChEs) was

evaluated in vitro using a spectrophotometric method of Ellman et al. using donepezil and tacrine

as reference drugs as previously reported by our group.[59,61,62] The obtained IC$_{50}$ values of the

11

compounds for the two enzymes and their selectivity over each other were summarized in **Table 1-3**. All the tested compounds showed IC_{50} values for both the enzymes in micromolar to submicromolar ranges. Compounds **23e** and **23f** exhibited the highest inhibition of AChE (IC_{50} values of 0.56 µM and 0.67 µM, respectively) and BuChE (IC_{50} values of 1.17 µM and 0.84 µM, respectively).

12

Table 1. *In vitro* Inhibition of AChE, BuChE and Selectivity Index (SI) of compounds 2, 3a-3l and 5a-5k.
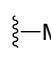

(2, 3a-3l)　　　　　　　(5a-5k)
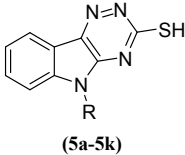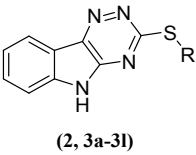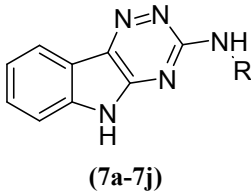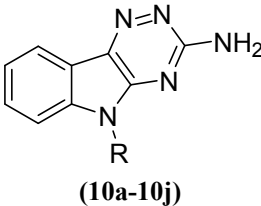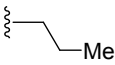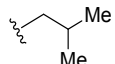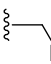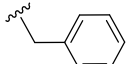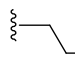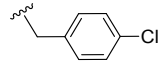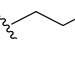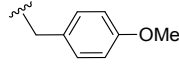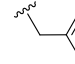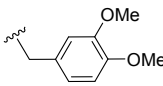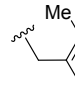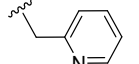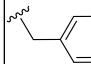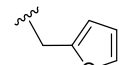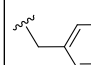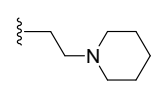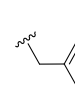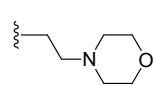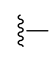
Compd	R	IC$_{50}$ ± SEM (μM)		SI[c]	Compd	R	IC$_{50}$ ± SEM (μM)		SI[c]
		AChE[a]	BuChE[b]				AChE[a]	BuChE[b]	
2	—H	11.26 ± 1.24	55.81 ± 2.12	4.96	5a	—Me	7.33 ± 0.82	58.61 ± 1.23	7.99
3a	—Me	12.62 ± 1.45	55.24 ± 2.04	4.37	5b	—CH$_2$CH$_2$Me	8.50 ± 0.77	91.62 ± 2.76	10.9
3b	—CH$_2$Me	16.01 ± 1.42	48.40 ± 1.93	3.02	5c	—CH(Me)Me	6.16 ± 0.53	35.28 ± 3.01	5.72
3c	—CH(Me)Me	10.03 ± 0.83	33.69 ± 1.76	3.35	5d	—(CH$_2$)$_3$Me	5.36 ± 0.46	14.26 ± 1.29	2.66
3d	—(CH$_2$)$_3$Me	12.28 ± 1.66	40.08 ± 1.51	3.26	5e	benzyl	8.05 ± 0.78	75.29 ± 2.82	9.35
3e	benzyl	20.33 ± 1.47	42.05 ± 1.68	2.07	5f	2-Br-benzyl	15.35 ± 1.02	22.01 ± 1.34	1.43
3f	2-Me-benzyl	9.88 ± 0.75	76.50 ± 2.51	7.74	5g	3-F-benzyl	5.52 ± 0.40	70.22 ± 2.56	12.7
3g	3-F-benzyl	19.16 ± 1.43	84.96 ± 2.02	4.43	5h	4-Cl-benzyl	15.73 ± 0.98	23.47 ± 1.76	1.49
3h	4-Br-benzyl	17.49 ± 1.32	51.93 ± 2.95	2.97	5i	4-(C(Me)$_3$)-benzyl	13.97 ± 0.93	18.24 ± 1.11	1.30
3i	4-CN-benzyl	19.02 ± 1.65	75.99 ± 2.77	3.99	5j	4-OMe-benzyl	13.21 ± 1.52	19.02 ± 1.34	1.44
3j	4-OMe-benzyl	9.64 ± 0.87	46.74 ± 2.69	4.84	5k	4-Me-benzyl	5.73 ± 0.51	2.97 ± 0.90	0.52
3k	4-Me-benzyl	15.52 ± 1.37	49.34 ± 2.85	3.18	Tacrine		0.056 ± 0.01	0.008 ± 0.00	0.14
3l	phenethyl	9.93 ± 0.92	61.42 ± 2.13	6.18	Donepezil		0.023 ± 0.01	1.87 ± 0.08	81.3

[a] AChE from human erythrocytes; IC$_{50}$, 50% inhibitory concentration (means ± SEM of three experiments).
[b] BuChE from equine serum.
[c] Selectivity Index = IC$_{50}$ (BuChE)/IC$_{50}$ (AChE).

13

Table 2. *In vitro* Inhibition of AChE, BuChE and Selectivity Index (SI) of compounds 7a-7j and 10a-10j.
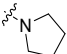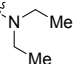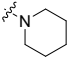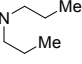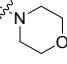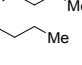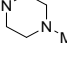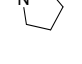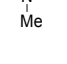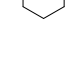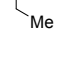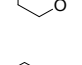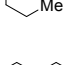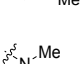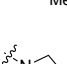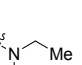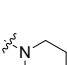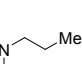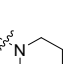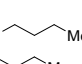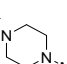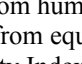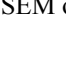
(7a-7j)

(10a-10j)

Compd	R	IC$_{50}$± SEM (µM)		SI	Compd	R	IC$_{50}$± SEM (µM)		SI
		AChE[a]	BuChE[b]				AChE[a]	BuChE[b]	
7a	—Me (propyl)	11.07 ± 0.86	52.19 ± 2.01	4.71	10a	—Me	7.81 ± 1.01	52.23 ± 1.76	6.69
7b	CH(Me)Me	9.21 ± 0.54	61.23 ± 1.12	6.64	10b	—Me (ethyl)	8.13 ± 1.32	29.42 ± 1.21	3.62
7c	benzyl	8.06 ± 0.75	56.41 ± 1.65	6.99	10c	—Me (propyl)	10.12 ± 1.16	32.78 ± 1.47	3.24
7d	4-Cl-benzyl	41.22 ± 1.83	9.09 ± 0.65	0.22	10d	—Me (butyl)	9.26 ± 0.82	16.02 ± 1.10	1.73
7e	4-OMe-benzyl	36.63 ± 1.22	67.32 ± 1.32	1.84	10e	benzyl	20.57 ± 1.34	24.87 ± 1.38	1.21
7f	3,4-diOMe-benzyl	10.75 ± 0.62	13.12 ± 1.02	1.22	10f	2-Me-benzyl	17.23 ± 1.22	32.72 ± 1.32	1.90
7g	pyridin-2-yl-methyl	14.71 ± 1.37	26.08 ± 1.21	1.77	10g	4-Me-benzyl	22.09 ± 1.78	22.64 ± 1.49	1.02
7h	furan-2-yl-methyl	20.22 ± 1.21	33.02 ± 1.65	1.63	10h	4-Cl-benzyl	24.63 ± 2.01	29.45 ± 1.62	1.20
7i	piperidin-ethyl	6.16 ± 0.53	20.53 ± 2.01	3.33	10i	3-F-benzyl	20.22 ± 1.25	25.32 ± 1.23	1.25
7j	morpholin-ethyl	6.61 ± 0.69	9.14 ± 0.54	1.38	10j	—H	9.76 ± 1.25	51.25 ± 1.32	5.25

[a] AChE from human erythrocytes; IC$_{50}$, 50% inhibitory concentration (means ± SEM of three experiments).
[b] BuChE from equine serum.
[c] Selectivity Index = IC$_{50}$ (BuChE)/IC$_{50}$ (AChE).

Table 3. *In vitro* Inhibition of AChE, BuChE and Selectivity Index (SI) of compounds 21a-23h.

(21a-23h)

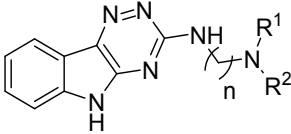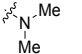| Compd	n	R¹R²N	IC$_{50}$± SEM (µM) AChE[a]	IC$_{50}$± SEM (µM) BuChE[b]	SI	Compd	n	R¹R²N	IC$_{50}$± SEM (µM) AChE[a]	IC$_{50}$± SEM (µM) BuChE[b]	SI
21a	4	N(Me)Me	33.70 ± 1.12	6.39 ± 0.22	0.19	**22e**	5	pyrrolidine	0.85 ± 0.05	17.01 ± 0.40	20.0
21b	4	N(Me)(Et)	6.31 ± 0.43	11.09 ± 0.27	1.75	**22f**	5	piperidine	0.96 ± 0.04	2.77 ± 0.05	2.89
21c	4	N(Et)(Me)	2.47 ± 0.11	8.05 ± 0.51	3.26	**22g**	5	morpholine	18.58 ± 0.41	6.74 ± 0.21	0.36
21d	4	N(Pr)(Me)	20.70 ± 0.76	0.47 ± 0.03	0.02	**22h**	5	4-methylpiperazine	1.65 ± 0.11	29.19 ± 1.10	17.7
21e	4	pyrrolidine	2.69 ± 0.08	5.89 ± 0.70	2.19	**23a**	6	N(Me)Me	1.25 ± 0.09	4.43 ± 0.27	3.54
21f	4	piperidine	3.17 ± 0.10	18.01± 1.31	5.68	**23b**	6	N(Me)(Et)	2.40 ± 0.11	12.70 ± 0.42	5.29
21g	4	morpholine	15.01 ± 0.54	1.92 ± 0.15	0.13	**23c**	6	N(Et)(Me)	1.48 ± 0.08	3.43 ± 0.24	2.32
21h	4	4-methylpiperazine	2.61 ± 0.07	32.19 ± 1.02	12.3	**23d**	6	N(Pr)(Me)	1.43 ± 0.07	4.01 ± 0.32	2.80
22a	5	N(Me)Me	3.58 ± 0.28	23.24 ± 0.67	6.49	**23e**	**6**	pyrrolidine	**0.56 ± 0.02**	**1.17 ± 0.09**	**2.09**
22b	5	N(Me)(Et)	6.79 ± 0.22	0.34 ± 0.03	0.05	**23f**	6	piperidine	0.67 ± 0.02	0.84 ± 0.03	1.25
22c	5	N(Et)(Me)	2.77 ± 0.07	0.48 ± 0.03	0.17	**23g**	6	morpholine	4.16 ± 0.15	23.65 ± 1.38	5.69
22d	5	N(Pr)(Me)	2.76 ± 0.18	0.38 ± 0.05	0.14	**23h**	6	4-methylpiperazine	0.79 ± 0.04	3.92 ± 0.21	4.96

[a] AChE from human erythrocytes; IC$_{50}$, 50% inhibitory concentration (means ± SEM of three experiments).
[b] BuChE from equine serum.
[c] Selectivity Index = IC$_{50}$ (BuChE)/IC$_{50}$ (AChE).

15

Structure-activity relationships

To validate our design rationale, initially compound **2** was prepared and evaluated initially for its cholinesterase inhibitory potential. To our delight, as shown in **Table 1.** Compound **2** exhibited good inhibitory activity (AChE, IC_{50} = 11.26 µM; BuChE, IC_{50} = 55.81 µM). This encouraging result of the lead scaffold prompted us to explore various substituents on thiol sulphur and the nitrogen of the indole ring to frame a structure-activity relationship. Introducing alkyl substituents on the indole ring as in compounds **5a-5d** increased the inhibitory activity. Among them, compound **5d** with the butyl chain showed the most potent inhibitory activity (AChE, IC_{50} = 5.36 µM; BuChE, IC_{50} = 14.26 µM). Incorporation of benzyl and substituted benzyls at NH of indole ring decreased the AChE inhibitory activity except for compounds **5g** and **5k**. Compound **5g** and **5k** having 3-fluorobenzyl and 4-methylbenzyl groups, respectively showed potent inhibitory activities. The thio-substituted compounds **3a-3l** offered IC_{50} values for AChE in the range of 9-20 µM. Presence of various substituents on thiol group did not influence the activity significantly in comparison to the lead compound **2**. The inhibitory activity was retained as such when thiol group was replaced with amino group (**Table 2**). When the *N*-propyl moiety in compound **7a** was replaced with 2-(1-piperidinyl)ethyl (compound **7i**) and 2-(4-morpholinyl)ethyl (compound **7j**) moieties, inhibitory activities against both the enzymes got increased notably. Compounds **7i** and **7j** showed inhibitory activities (AChE; IC_{50}=6.16 µM, 6.61 µM, respectively) and (BuChE; IC_{50} = 20.53 µM, 9.14 µM, respectively).

Joining of the tricyclic triazinoindole moiety with cyclic amines like piperidine and morpholine through two carbon atom spacers improved AChE inhibition dramatically compared to the simple alkyl/benzyl substituted triazinoindole derivatives. Based on this observation, we planned to study the effect of the attached basic amines and the length of the linker on the

16

cholinesterase inhibitory activity of the resulting compounds. As indicated in **Table 3**, all the compounds **21a-23h** exhibited good inhibitory activity against both the enzymes ranging from IC_{50} values of 0.564 to 36.7 μM for AChE and from 0.341 to 32.19 μM for BuChE. These results suggested that the presence of a heterocyclic amines is particularly important for the ChE inhibitory activity as all the compounds bearing pyrrolidino, piperidino, morpholino and *N*-methylpiperazino moieties exhibited strong ChE inhibition. Pyrrolidino moiety appeared to be a better choice over other amines, as compounds **21e**, **22e** and **23e** bearing pyrrolidino moiety exhibited higher activity than the rest of the compounds having other amines as attachments **(Figure 3)**.

It has been observed that changing the length of the carbon chain also potentially affected the inhibitory activity. A comparative analysis of the inhibitory potential of compounds **21e, 22e** and **23e** having a pyrrolidine ring as heterocyclic amine, revealed that compound **23e** (n = 6, IC_{50} value of 0.564 μM) exhibited the highest AChE inhibitory activity while compound **21e** (n = 4, IC_{50} value of 2.690 μM) and compound **22e** (n = 5, IC_{50} value of 0.853 ± 0.02 μM) showed 5-fold and 1.5-fold decrease in AChE inhibitory activities in comparison to compound **23e (Figure 3)**. However, their inhibitory activity against BuChE was slightly lower than that against AChE, which might be due to the conformational differences between the structures of these two enzymes.[63] Compound **23e** (IC_{50} value of 1.178 μM) exhibited an acceptable level of BuChE inhibitory activity while compound **21e** (IC_{50} value of 5.893 μM) and compound **22e** (IC_{50} value of 17.01 μM) showed 5-fold and 14-fold decrease in BuChE inhibitory activities. Compounds **23e** (SI value of 2.09) and **23f** (SI value of 1.25) have more balanced activity on both the cholinesterase enzymes than donepezil (SI value of 81.3) and tacrine (SI value of 0.14).
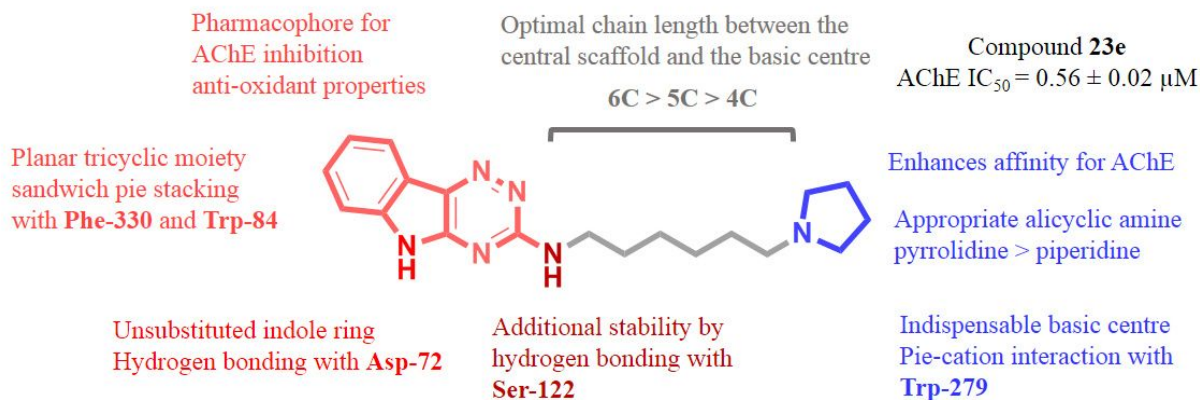
Figure 3. Important structural features of compound **23e**.

Antioxidant activity [1,1-diphenyl-2-picrylhydrazyl (DPPH) radical scavenging activity]

The DPPH radical scavenging assay is commonly used as a rapid and reliable method to assess the antioxidant/free radical scavenging potential of compounds.[64] DPPH is a stable free radical that can accept a hydrogen radical or an electron to become a stable molecule. The antioxidant activity of the selected compounds was estimated by their ability to reduce DPPH· radical (purple color) to DPPHH (yellow) and the corresponding radical-scavenging potential was evaluated by the decrease in the absorbance at 517 nm.[65] Only those compounds having IC_{50} values (AChE) less than 5 μM were selected for this study. Ascorbic acid was used as the positive control in this assay. All the test compounds exhibited notable free radical scavenging activity ranging from 40−55 % and 56-70 % at 10 μM and 20 μM concentrations respectively (**Table 4**).

Compound **23e** showed better free radical scavenging activity (54.9 %, 64.3 % at 10 μM and 20 μM concentrations, respectively) compared to ascorbic acid (36.5 %, 61.8 % at 10 μM and 20 μM concentrations, respectively) where as tacrine and donepezil were found to be devoid of significant free radical scavenging activity at these concentrations.

Table 4. DPPH Radical Scavenging Activity of the Compounds.[a]

Compd	RP of DPPH (%)[b]		Compd	RP of DPPH (%)[b]	
	10 μM	20 μM		10 μM	20 μM
21c	45.5 ± 3.1	57.3 ± 2.9	23b	43.7 ± 2.5	60.3 ± 3.4
21e	52.1 ± 2.4	63.1 ± 2.3	23c	42.7 ± 3.7	58.4 ± 3.1
21f	51.5 ± 1.6	62.7 ± 1.7	23d	47.3 ± 2.0	59.6 ± 2.2
21h	53.7 ± 2.7	65.4 ± 1.3	23e	**54.9 ± 1.8**	**64.3 ± 2.8**
22a	43.2 ± 3.3	60.2 ± 2.7	23f	54.3 ± 2.1	66.4 ± 2.4
22c	44.3 ± 2.4	59.4 ± 3.1	23g	56.7 ± 1.6	67.3 ± 1.7
22d	46.7 ± 1.9	60.7 ± 3.3	23h	55.1 ± 3.4	64.2 ± 1.9
22e	53.2 ± 2.4	62.4 ± 2.5	Tacrine	3.4 ± 0.4	6.4 ± 0.3
22f	52.8 ± 2.9	60.7 ± 2.9	Done.	4.5 ± 0.6	4.9 ± 1.2
22h	54.1 ± 1.7	65.1 ± 2.1	Ascorbic acid	36.5 ± 2.9	61.8 ± 3.2
23a	44.1 ± 3.4	61.3 ± 2.3			

[a]Data are expressed as Mean ± SE (three independent experiments)
[b]RP of DPPH (%) = reduction percentage of DPPH.

Assessment of Cytotoxicity and Neuroprotection offered by the synthesized compounds

To ascertain the therapeutic potential of the synthesized compounds, their effect on cell viability and neuroprotective ability against oxidative stress were assessed using the human neuroblastoma SH-SY5Y cell line. Only those compounds having IC_{50} values (AChE) less than 5 μM were selected for these studies. For the assessment of cytotoxicity of the test compounds, cells were exposed to significantly high concentrations of the test compounds (40 μM and 80 μM) for 24 hours, followed by determination of the cell viability using MTT assay. Even at such high concentrations, all the test compounds caused negligible cell death (**Table 5**).

Table 5. Cell viability, and neuroprotective action of the selected test compounds against H$_2$O$_2$ and Aβ$_{1-42}$ induced toxicity in the human neuroblastoma SH-SY5Y cell line.[a]

Compd	Cell viability (%)		Neuroprotection (%) (against H$_2$O$_2$)		Neuroprotection (%) (against Aβ$_{1-42}$)	
	40 μM	80 μM	10 μM	20 μM	10 μM	20 μM
21c	92.4 ± 2.2	90.3 ± 1.8	34.4 ± 2.7	48.9 ± 2.3	37.5 ± 2.1	56.2 ± 1.9
21e	93.0 ± 1.5	91.2 ± 2.1	39.8 ± 1.9	53.2 ± 3.2	40.3 ± 2.5	57.5 ± 2.2
21f	91.9 ± 2.4	87.1 ± 3.3	41.7 ± 1.3	55.4 ± 1.9	42.1 ± 1.9	60.7 ± 1.4
21h	91.3 ± 3.2	85.7 ± 2.4	37.2 ± 2.8	50.3 ± 2.9	41.5 ± 2.7	59.0 ± 1.5
22a	92.2 ± 3.1	90.5 ± 1.9	30.4 ± 3.6	46.5 ± 2.3	39.4 ± 3.1	57.3 ± 2.2
22c	92.4 ± 2.5	89.8 ± 3.1	31.8 ± 3.5	48.4 ± 2.2	38.1 ± 2.8	56.2 ± 2.9
22d	90.4 ± 3.3	87.1 ± 2.2	33.5 ± 2.9.	48.7 ± 3.1	38.5 ± 2.5	59.5 ± 2.3
22e	93.1 ± 2.7	90.6 ± 1.5	41.8 ± 3.5	54.3 ± 1.7	43.7 ± 3.1	60.1 ± 3.4
22f	93.9 ± 3.2	92.2 ± 1.9	43.4 ± 2.2	55.6 ± 2.1	41.4 ± 2.4	62.4 ± 1.9
22h	90.5 ± 3.7	86.4 ± 2.9	41.2 ± 2.7.	50.2 ± 2.8	40.3 ± 1.9	58.7 ± 2.1
23a	92.4 ± 3.2	89.3 ± 2.5	32.7 ± 3.4	43.5 ± 2.6	37.1 ± 2.3	59.3 ± 3.3
23b	93.2 ± 2.1	91.7 ± 1.9	31.2 ± 2.5	40.4 ± 3.6	37.7 ± 3.1	57.2 ± 3.4
23c	94.3 ± 2.2	91.1 ± 3.2	35.3 ± 1.4	46.1 ± 2.0	39.1 ± 2.6	57.5 ± 2.3
23d	91.4 ± 2.8	87.4 ± 2.3	34.2 ± 3.5	49.5 ± 2.7	38.8 ± 1.9	58.3 ± 2.9
23e	**94.9 ± 3.2**	**92.3 ± 1.5**	**42.5 ± 2.1**	**53.7 ± 1.3**	**44.5 ± 2.1**	**62.6 ± 1.9**
23f	94.5 ± 2.1	91.8 ± 2.8	44.8 ± 1.7	54.5 ± 2.4	43.2 ± 2.5	63.6 ± 2.2
23g	92.1 ± 2.7	89.7 ± 1.9	40.3 ± 1.8	52.3 ± 2.2	45.3 ± 2.2	61.4 ± 3.3
23h	91.4 ± 3.2	85.4 ± 2.7	41.2 ± 1.4	51.6 ± 2.5	42.7 ± 3.1	62.5 ± 2.5
Tacrine	90.1 ± 1.8	88.1 ± 2.4	51.0 ± 3.4	70.4 ± 3.2	40.5 ± 2.3	58.7 ± 2.7
Donep.	92.4 ± 2.5	90.7 ± 1.2	53.4 ± 3.1	72.1 ± 2.7	47.2 ± 2.1	65.1 ± 1.8

[a]Data are expressed as Mean ± SE (three independent experiments)

20

The neuroprotective potential of the selected compounds against the oxidative stress induced by exogenous toxins (H_2O_2 or $A\beta_{1-42}$) was evaluated. H_2O_2-induced toxicity is due to the oxidative damage to the neuronal cells[66] while the $A\beta$-induced toxicity is more complex, involving generation of reactive oxygen species, interleukin-1, interleukin-6, TNF-α like damaging cytokines' release, and mitochondrial dysfunction.[33,67]

In this study, when the cells were exposed to H_2O_2 (100 μM) and $A\beta_{1-42}$ (25 μM) separately, notable toxicities to cells were observed and the cell viability got declined to nearly 55% and 52%, respectively. To assess the neuroprotective potential of the test compounds against these toxic insults, the cells were pretreated with the test compounds (10 μM, and 20 μM) for 2 h followed by treatment with the insults for 24 h. The selected derivatives exhibited a significant neuroprotective effect at 10 μM and 20 μM concentrations. For comparison, the cells were co-incubated with compound **23e**, **23f**, donepezil and tacrine at different concentrations. Compound **23e** offered significant protection to the cells against the toxic insults (**Figure 4**). The results suggested that these compounds possessed the ability to protect neuronal cells against oxidative-stress-associated cell death.
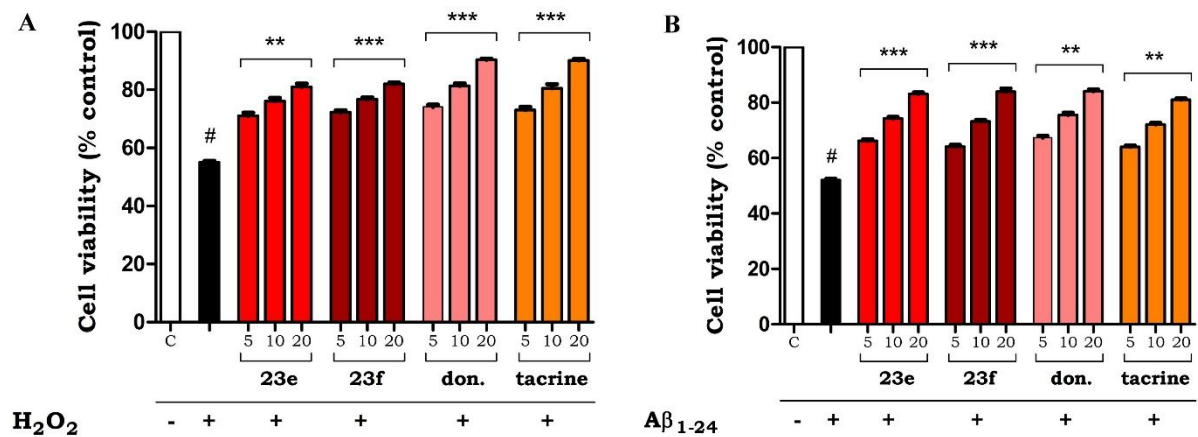
Figure 4. Protective effects of compounds **23e**, **23f**, donepezil and tacrine against H_2O_2 and $A\beta_{1-42}$-induced cytotoxicity in SH-SY5Y cells. Determination of the viability of SH-SY5Y cells by the MTT assay after treatment with (A) H_2O_2 (100 μM) and (B) $A\beta_{1-42}$ (25 μM) in the absence or presence of the indicated concentrations of

compounds **23e**, **23f** and the standard drugs. All the data were expressed as mean ± SD of three experiments and each included triplicate sets. #p < 0.05 vs control; **p < 0.01, ***p < 0.001 vs $H_2O_2/A\beta_{1-42}$ alone.

In vitro Blood-Brain Barrier Permeation Assay

The BBB permeability is a primary criterion for the development of novel CNS active agents. The ability of triazinoindole derivatives to penetrate into the brain was assessed using a parallel artificial membrane permeation assay (PAMPA), in a similar manner as described by Di *et al.*[68,69] This assay is used to predict the passive diffusion of a molecule through the BBB. The BBB permeability (P_e) of the most active compounds **23e** and **23f** was determined through a porcine brain lipid. The assay was validated by comparing the experimental permeability values [P_e(exp)] of seven commercial drugs with the reported permeability values [P_e(ref)], offering a linear relationship i.e., P_e(exp.) = 1.16 P_e(ref.) + 0.1668 (R^2 = 0.9781) (see the Supporting Information, **Figure S1**). From this equation and considering the limits for BBB permeation established by Di *et al.*,[68] it was concluded that compounds with P_e(exp) greater than 4.8×10^{-6} cm s^{-1} (see the Supporting Information, **Table S2**) were capable of crossing the BBB. Both the compounds **23e** and **23f** showed permeability values above this limit (**Table 6**). Therefore, P_e(exp) suggested a high potential of the compounds to cross the BBB by passive diffusion.

Table 6. **Permeability (P_e 10^{-6} cm s^{-1}) of compounds 23e, 23f and donepezil in the PAMPA-BBB permeation assay with their predicted penetration into the CNS.**

Compd.	(P_e 10^{-6} cm s^{-1})	Prediction
23e	11.3 ± 1.8	CNS+
23f	12.5 ± 1.2	CNS+
Donepezil	14.3 ± 1.7	CNS+

Data are expressed as mean ± SEM of three independent experiments.

Computational studies

Docking studies

To have an idea of the binding mode of compound **23e** with the cholinesterase enzymes, docking studies were performed within the active sites of Torpedo Californica AChE (*Tc*AChE) and Human BuChE (*h*BuChE). To validate the generated grids for docking studies, the co-crystallized molecules in the 3D structures of *Tc*AChE and *h*BuChE (PDB Code: **2CKM** and **4BDS** respectively) were initially knocked out of the binding sites. The knocked out molecules were constructed a fresh, energy minimized and re-docked into the active sites of the grids. Very similar interactions were observed between the re-docked molecules and the enzymes as was the case with the original co-crystallized ligands. The RMSD values of the re-docked ligands with those of the original orientations in co-crystallized forms in 2CKM and 4BDS were observed to be 0.40 Å and 0.26 Å, respectively.

It is well known that AChE has a dumbbell shaped active site gorge composed of two active sites: the CAS at the bottom and the PAS at the lip. The CAS pocket looks like a vessel on its bottom lies Trp84 which is crucial for binding of both the substrates to the inhibitors. Moreover, halfway up the gorge is a narrow tunnel where some crucial amino acid residues such as Phe330 and Tyr-334 stabilize the enzyme-inhibitor complex. At the entrance of the gorge exists the PAS, which is mainly built up by Trp279 and Tyr70 residues. The docking interactions of compound **23e** were studied in the active site of the AChE of *Tc*AChE, and then *Tc*AChE was humanized with *h*AChE to know the human sequence interacting with compound **23e**.
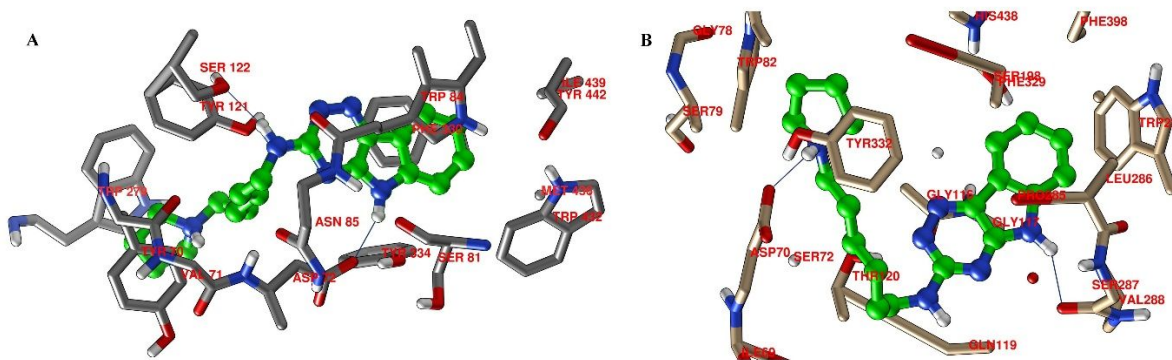
Figure 5. Docking interactions of compound **23e** in the active sites of (A) AChE and (B) BuChE.

The interaction view of compound **23e** with AChE is represented in **Figure 5A**. As presented, compound **23e** was stacked well in the groove formed by Trp84, Trp279 and Phe330 (*h*AChE: Trp86, Trp284 and Tyr337) amino acid residues. It has orientation along the active site gorge similar to the reference compound donepezil, extending from the active site amino acid residue Trp84 to the peripheral site amino acid residue Trp279. Ligand interactions with these two amino acids are important to elicit a strong inhibitory effect by the dual binding site inhibitors. Hydrophobic planar nature of the tricyclic scaffold allows making of a more favorable sandwich type π-π stacking with Trp84 and Phe330 (*h*AChE: Trp86 and Tyr337). The -NH group of the indole ring exhibited hydrogen bonding with Gly80 (*h*AChE: Gly82). The -NH group at the 3rd position of the triazine ring showed hydrogen bonding with Ser122 (*h*AChE: Ser125). The nitrogen atom of pyrrolidine ring could be protonated at physiological *p*H. The protonated nitrogen showed strong cation-π interaction with Trp279 (*h*AChE Trp284). This interaction is particularly important as Trp279 plays a prominent role in deposition of beta-amyloid plaques.[24]

The binding mode of the compound **23e** with BuChE revealed that it also occupied the large catalytic cavity of BuChE (**Figure 5B**). The aromatic ring of the tricyclic moiety was observed to be interacting with Trp231 and Phe329 residues by π-π stacking. π-Alkyl interaction

was observed between the aromatic ring of the scaffold and Leu286. Further, the -NH group on 3rd

position added stability to the ligand-receptor complex by forming hydrogen bond with Ser287.

Additionally, salt bridge between -NH of the pyrrolidine and Asp70, and cation-π interaction

between the nitrogen of pyrrolidine and Trp82 provided stability to the ligand-receptor complex.

Molecular dynamics simulations

In the molecular docking studies, compound **23e** exhibited very good interactions within

the active sites of the AChE and BuChE enzymes. Thus to confirm, validate and understand the

time dependent interactions of the active compound **23e** with the AChE and BuChE enzymes and

stability of ligand-receptor complex, molecular dynamics study was performed. The binding

stability of the ligand-receptor complex was studied for a period of 20 ns duration to check its time

dependent stability. In order to observe the binding stability of the complex over a period of time,

certain parameters like RMSD-P, RMSF-P and RMSD-L (P = Protein; L = Ligand) were

scrutinized to support the results of docking study. Initial pose of the ligand-receptor complex was

considered as the reference frame to calculate these values. The RMSD-P is essentially studied to

understand the level of movements of various atoms/groups in the enzyme when the ligand is

present in the active site of the receptor. This provides insight into the structural conformations of

the enzyme over a given period of simulation. The RMSD-P for AChE in the ligand -receptor

complex was found to be in the range of 0.7 to 2.0 Å. This finding explained that the presence of

23e in the active site of the AChE has not prejudiced the stability of the protein backbone all the

way throughout the simulation period. To recognize the stability of the ligand with respect to the

receptor and its active binding site, the RMSD-L of **23e** was determined. The 'Lig fit' on Prot

RMSD-L for ligand was observed in the range of 0.8 to 3.2 Å. The 'Lig fit Prot' is the RMSD of

a ligand when the protein-ligand complex is first aligned on the reference protein backbone and

then the RMSD of the ligand heavy atoms is determined. Here, despite having a large number of rotatable bonds in the ligand, the RMSD value is not observed to be significantly higher than the protein RMSD, suggesting that the compound **23e** is stable within the binding site and it does not diffuse away from the active site during the entire course of simulation period. Additionally the Lig fit on Lig RMSD was calculated to comprehend the internal fluctuation of the ligand atoms, and it was observed in the acceptable range of 0.4 to 2.4 Å (**Figure 6A**).

The structural integrity of the receptor and the residual mobility of the ligand were quantified in terms of RMSF-P (**Figure 6B**). For all the residues, including the loop as well as the terminal residues of the protein, with the compound **23e** in the active site, the RMSF-P was below 3.2 Å. The protein-ligand stability interaction study was also performed over a period of time to evaluate the interaction stability. In the docking studies, the H-bond was observed between –NH of indole and –NH of 3-amino group of compound **23e** with Gly80 and Ser122 (*h*AChE: Gly82 and Ser125) residues respectively. From the MD simulation study it was established that the two –NH groups of the compound **23e** formed H-bonds with Gly80 and Ser122. These were observed to be stable over 54 % and 91 % of the simulation time with Gly80 and Ser122 respectively. Further, the salt bridge between the protonated pyrrolidine and Asp72 (*h*AChE: Asp74) was observed to be stable for around 24 % of the simulation time. All these H-bond strengths were with H-bond distance of 2.5 Å or less and donor angle of $\geq 120°$ and acceptor angle of $\geq 90°$. The cation-π interactions between the protonated pyrrolidine and Trp279 and Tyr334 (*h*AChE: Trp284 and Tyr341) were also found to be stable over 76 % and 29 % of entire simulation time respectively. Further, strong hydrophobic interactions of the compound **23e** with Trp-84, Trp-279 and Phe-330 played a vital role in providing stability to the ligand-receptor complex where all these hydrophobic interactions were observed for more than 60 % of the total simulation time

26

(**Figure 6C**). The other ligand parameters like rGyr, MolSA, SASA and PSA were observed in the

acceptable range as shown in **Figure 6D**.
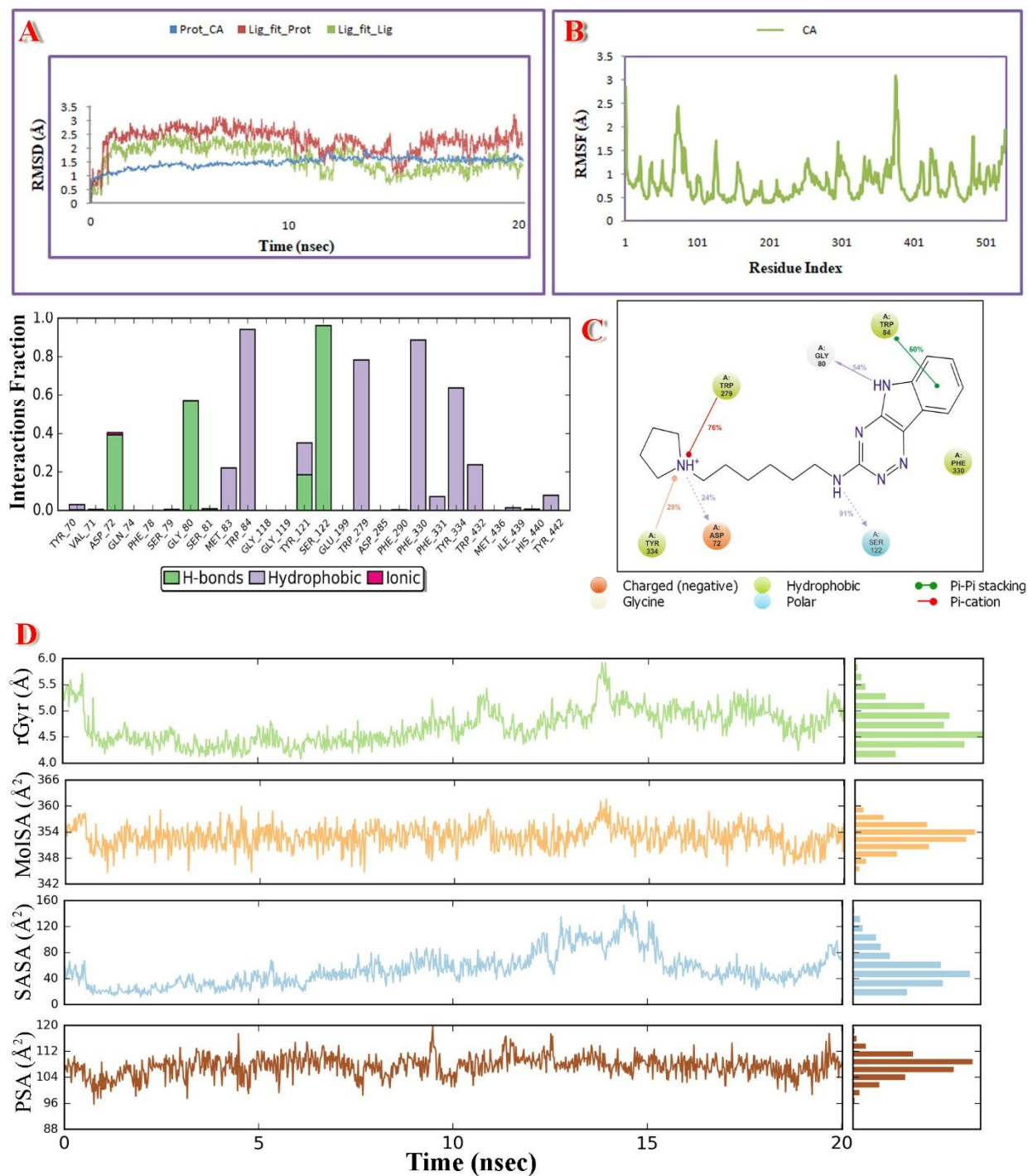
Figure 6. (A) RMSD-P and RMSD-L plots for AChE with **23e**; (B) RMSF-P plot for AChE with **23e**; (C) Ligand and receptor residue contact diagram for AChE with **23e**; (D) rGyr; MolSA; SASA and PSA for **23e** with AChE.

Similarly, the molecular dynamics study of compound **23e** with BuChE was also performed and this also indicated good stability of ligand-receptor complex. The RMSD-P was in the range of 0.8 to 1.9 Å. Whereas the RMSD-L 'Lig fit' on Prot was observed in between 1.2 to 3.2 Å which was not alarmingly higher than the RMSD-P. The 'Lig fit' on the ligand was observed in 0.4 to 1.8 Å range (**Figure 7A**). The protein fluctuation value RMSF-P was observed below 3.6 Å (**Figure 7B**). The ligand-receptor interaction analysis elucidated the stability of ligand-receptor complex by supporting the H-bonding between -NH of indole and -NH at 3rd position of the compound **23e** with protein residues Leu286 and Ser287, respectively. These were observed to be stable over 34 % and 87 % of simulation time respectively. The protonated pyrrolidine formed a stable salt bridge with Asp70 over 96 % of the simulation time period. The residues Trp82, Trp231, Leu286, Phe329 and Tyr332 were positively contributing towards the stability of the complex by hydrophobic interactions (**Figure 7C**). The other ligand parameters like rGyr, MolSA, SASA and PSA were also observed in the acceptable range (**Figure 7D**). These observations from the molecular dynamics study strongly supported the observations made in the docking studies.
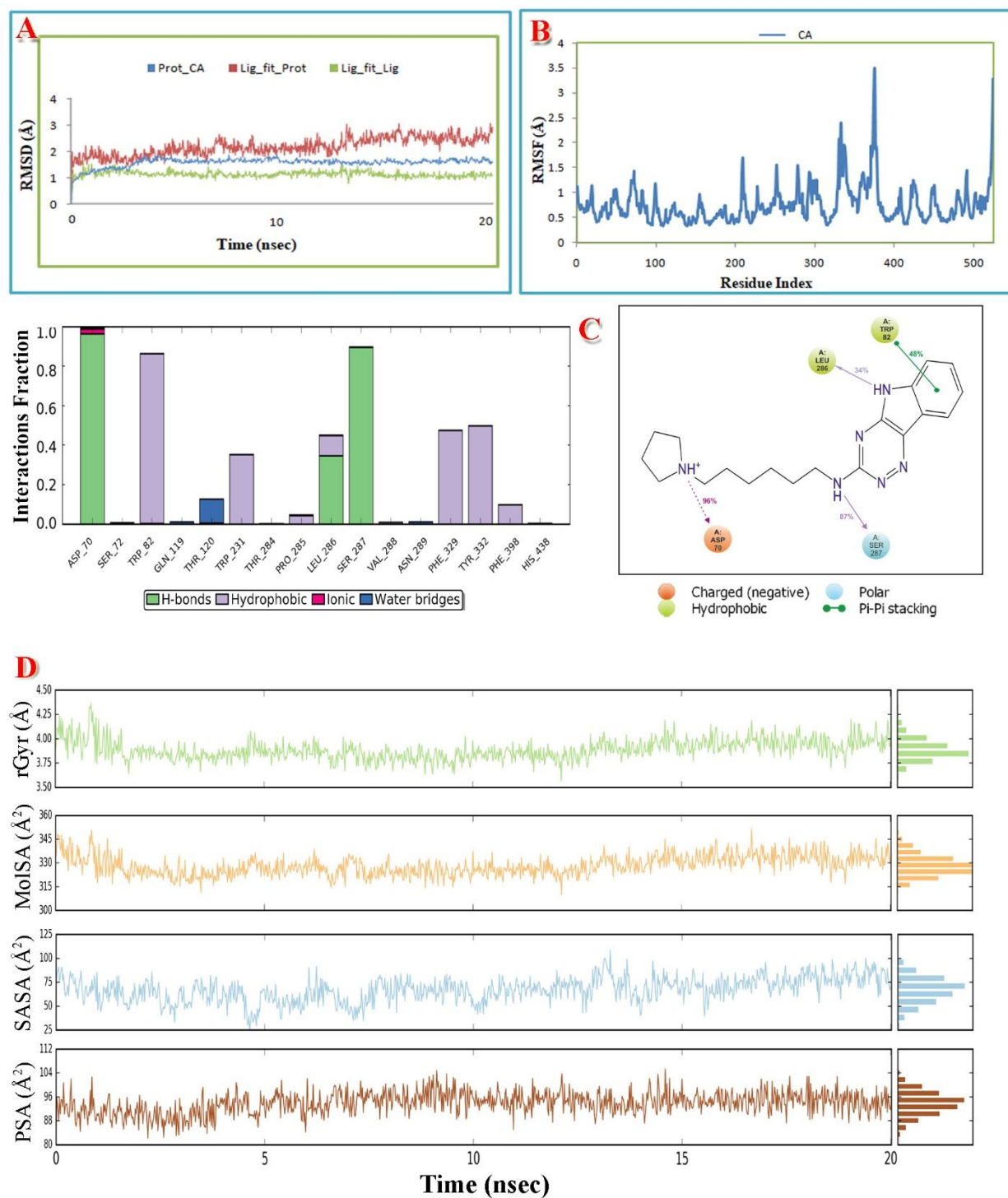
Figure 7. (A) RMSD-P and RMSD-L plots for BuChE with **23e**; (B) RMSF-P plot for BuChE with **23e**; (C) Ligand and receptor residue contact diagram for BuChE with **23e**; (D) rGyr; MolSA; SASA and PSA for **23e** with BuChE.

1
2
3
4
5
6
7
8
9
10
11
12
13
14
15
16
17
18
19
20
21
22
23
24
25
26
27
28
29
30
31
32
33
34
35
36
37
38
39
40
41
42
43
44
45
46
47
48
49
50
51
52
53
54
55
56
57
58
59
60

In-silico prediction of physicochemical and pharmacokinetics parameters.

On account of poor ADME (absorption, distribution, metabolism, and excretion) properties, approximately four drug candidates out of ten flunk in clinical trials. These late-stage failures significantly contribute to the enhancement of development cost for the new drugs. Hence, we need to resort to ADME predictions as a part of the drug development process to have an idea of the ADME properties during clinical trials.[70] Due to significant developments in the field of computational chemistry in recent times, virtual prediction of ADME properties becomes relatively easy and also reliable. For the most active compounds **23e** and **23f** along with donepezil and tacrine as reference drugs, pharmacokinetics profile indicators like Lipinski's parameters, QPlogP$_{o/w}$, PSA, QPPMDCK, QPlogBB, QPPCaco, QPLogKhsa, etc. were predicted with QikProp module **(Table 7)**.[71]

30

Table 7. Predicted ADMET indicators of compound 23e, 23f, donepezil and tacrine.

Parameter	Limit	23e	23f	Donepezil	Tacrine
MW	130-725	338.455	352.481	379.498	198.267
HBA	2-20	5.5	5.5	5.5	2
HBD	0-6	2	2	0	1.5
NRB	0-8	8	8	6	1
QPlogP$_{o/w}$	-2 to 6.5	3.196	3.455	4.242	2.536
PSA	7 to 200	69.799	71.149	46.234	33.825
Volume	500-2000	1180.047	1225.635	1248.451	701.299
ReFG	0-2	0	0	0	0
SASA	300 to 1000	679.568	701.805	681.675	425.06
Rule of Five (violation)	0-1	0	0	0	0
CNS	-	1	1	1	1
QPPMDCK	-	122.099	111.307	589.289	1602.036
QPlogBB	-3 to 1.2	-0.628	-0.686	0.223	0.047
QPPCaco	-	249.594	229.114	1070.771	2965.755
QPlogKhSa	-1.5 to 1.5	0.36	0.476	0.516	0.049
QPlogS	-6.5 to 0.5	-4.034	-4.419	-4.059	-3.036
% HOA	0-100	88.567	89.416	100	100
#star	0-5	0	0	0	0

MW: molecular weight, HBA: hydrogen-bond acceptor atoms, HBD: hydrogen-bond donor atoms, QPlogPo/w: predicted octanol/water partition coefficient, PSA: polar surface area, ReFG: number of reactive functional groups, SASA: total solvent accessible surface area, CNS: predicted central nervous system activity on a -2 (inactive) to +2 (active) scale, QPPMDCK: predicted apparent MDCK cell permeability in nm/s, QPPCaco: caco-2 cell permeability in nm/s, QPlogBB: brain/blood partition coefficient, QPlogKhsa: binding to human serum albumin, QPlogS: predicted aqueous solubility, % HOA: human oral absorption on 0–100% scale, #star: number of parameters' values that fall outside the 95 % range of similar values for known drugs.

According to Lipinski's rule-of-five[72], most "drug-like" molecules have LogP $\leq$ 5, molecular weight $\leq$ 500, number of hydrogen bond acceptors $\leq$ 10, and number of hydrogen bond donors $\leq$ 5. According to this rule, poor absorption or permeation is more likely when molecules violate more than one of these rules. Compounds **23e** and **23f** do not break Lipinski's rule of five at all, predicting them to be promising drug candidates. Number of rotatable bonds and topological Polar Surface Area (TPSA) are the two other important parameters introduced by Veber and co-workers.[73] Number of rotatable bonds is the simple topological parameter for molecular flexibility. It has been shown to be a very good descriptor for oral bioavailability of drugs. For oral bioavailability, a molecule should have less than 7 atoms in linear chains outside the rings or 8 rotatable bonds. TPSA value is another key descriptor that was shown to equate well with passive molecular diffusion through membranes and therefore, allows prediction of drug absorption, including intestinal absorption, bioavailability and blood-brain barrier (BBB) penetration.[74] The mean TPSA value for the marketed CNS drugs is 40.5 $Å^2$ with a range of 4.63– 108 $Å^2$.[75] Compounds **23e** and **23f** possess 8 rotatable bonds each and TPSA values of 69.8 $Å^2$ and 71.2 $Å^2$ respectively. QPCaco-2 is indicative of the oral absorption of a drug. It assesses the apparent gut-blood barrier permeability. Values above 500 predict high oral absorption which is obtained for both the compound **23e** and **23f**. Similarly, human oral absorption percent (% HOA) values also support prediction of good oral bioavailability of the test compounds. Brain/blood partition coefficient (QPlogBB), *n*-octanol–water partition coefficient (QPlogP$_{o/w}$), apparent MDCK cell permeability (QPPMDCK), and CNS predict the ability of a compound to cross the blood–brain barrier (BBB), a mandatory criterion for CNS active drugs. Typically, drugs which penetrate the BBB through passive diffusion should have *n*-octanol–water partition coefficient (logP$_{o/w}$) values of ~3.[76] The QPPMDCK predicts the apparent MDCK cell permeability in nm/s. MDCK (Madin-

Darby canine kidney) cell permeability is considered to be a good mimic for the blood–brain barrier.[77] A value of QPPMDCK above 25 is considered as good and almost all the test ligands have shown considerably high values. The test ligands are predicted to be CNS active as they have a value of CNS as 1. The QPlogKhsa value predicts the binding of CNS active drug with human serum albumin. Compound **23e** and **23f** showed compliance with the recommended values, indicating that these compounds would have low serum albumin binding and the unbound fraction would have access to the putative receptor drug target. #star denotes the number of parameters' values that fall outside the 95 % range of similar values for known drugs. A large number of #stars indicates that the molecule is less drug-like than the molecule with few #stars. Values of #star for compound **23e** and **23f** indicate their drug-likeness. Additionally, a compound possessing tertiary nitrogen containing moiety which is a common feature in many CNS acting drugs, shows a higher degree of brain permeation.[75] Thus, it can be claimed that compounds **23e** and **23f** are predicted to possess good pharmacokinetics profile, which would enhance their biological significance.

Assessment of Cognitive Improvement in Animal Model of AD

Morris Water Maze Test

To determine the effect of compound **23e** on cognitive improvement, an animal model of scopolamine-induced amnesia in the rodents was adopted.[78-80] Scopolamine blocks the cholinergic pathway distinctly by antagonizing the muscarinic receptors, offering a typical AD model to explore the role of cholinergic system in cognition.

Morris water maze learning test was utilized to assess the hippocampal-dependent spatial learning ability of the animals. This test assesses the reference or long-term memory by observing the escape latency.[81] During the last 5 days of the treatment period, escape latency time (ELT) was recorded for the animals of the experimental groups. The ELT was significantly prolonged (**Figure**

33

8A) by scopolamine treatment (1.4 mg/kg, ip). In donepezil (5 mg/kg, po) treated group, ELT was considerably shortened as compared to the scopolamine-treated control group. Compound **23e** (5 mg/kg and 10 mg/kg, po) significantly reduced ELT as compared to the scopolamine-treated control group. This result revealed that the animals retained the previous memory in the Morris water maze test, showing spatial memory improvement.
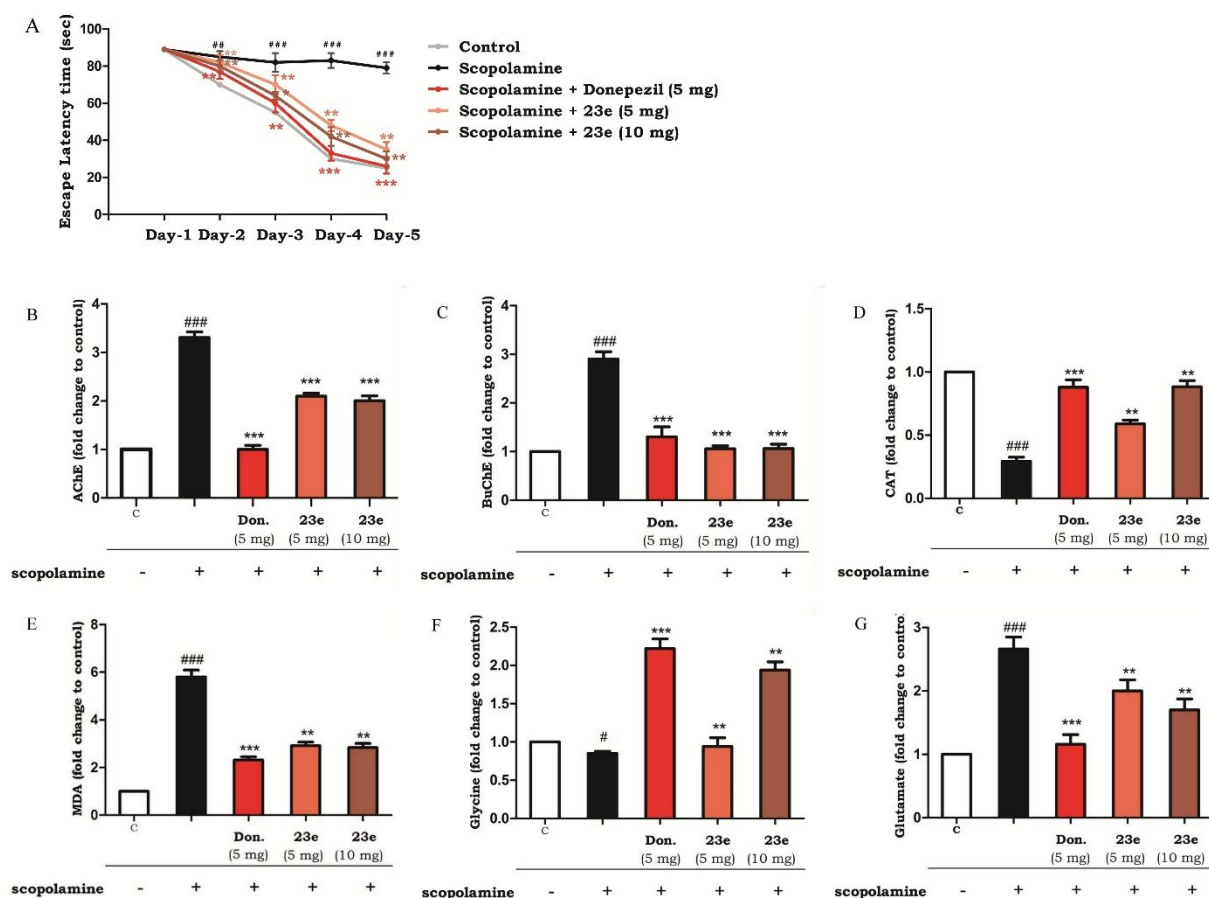
Figure 8. MWM test, ex vivo anticholinesterase and antioxidant activities, neurotransmitters' level in scopolamine-induced amnesic brain. Data are expressed as mean ± SEM (n = 7): (###) $p < 0.001$, (#) $p < 0.05$ vs vehicle-treated control group; (***) $p < 0.001$, (**) $p < 0.01$, vs scopolamine-treated control group. C = vehicle-treated control group.

Neurochemical analysis

After completion of the MWM test, the effects of the scopolamine and compound **23e** on cholinesterase levels and oxidant stress parameters in brain were assessed. Scopolamine treatment

significantly increases the cholinesterase levels in the brain. The effect of compound **23e** on the brain cholinesterase levels was assessed in mice using Ellman's method. The inflated levels of AChE (**Figure 8B**) and BuChE (**Figure 8C**) were significantly attenuated by compound **23e** at a dose equivalent to donepezil. Malondialdehyde (MDA), catalase (CAT), glutamate and glycine levels in the brain were assessed in order to further perceive the anti-amnesic effects of compound **23e**. Estimation of the lipid peroxidation products in the brain homogenate samples was carried out by thiobarbituric acid reactive substances (TBARS) assay, which estimates the MDA, a byproduct of lipid peroxidation by measuring the absorbance at 532 nm. Scopolamine- treated group showed elevated MDA levels (**Figure 8C**) in comparison to the vehicle-treated control group. Treatment of compound **23e** to the amnesic mice appreciably attenuated the increase in MDA levels in the brain (**Figure 8C**) as compared to the scopolamine-treated group. CAT is an important antioxidant defense system responsible for the decomposition of hydrogen peroxide to water and oxygen. Scopolamine treatment significantly reduced the CAT levels (**Figure 8D**) in the brains of the treated animals compared to the vehicle-treated control group animals. However, treatment of the amnesic mice with compound **23e** elevated the CAT levels considerably (**Figure 8D**). These results revealed the anti-oxidant potential of the test compound **23e**.

Disturbances in the balance between glutamate (excitatory neurotransmitter) and glycine (inhibitory neurotransmitter) system leads to the development of pathological features observed in AD.[82] Apart from the role in signal transmission and plasticity, glutamate also takes part in the regulation of survival or apoptosis induction of brain cells. This system is counter balanced by glycine signaling to assure normal brain functioning by maintaining equilibrium between these inhibitory and excitatory activities. Scopolamine-treated group showed reduced levels of glycine (**Figure 8F**) compared to the vehicle-treated control group. The reduced level of glycine

35

is also associated with impairment in the cognitive functions.[83-84] Treatment of the amnesic mice with compound **23e** increased the glycine levels (**Figure 8F**) as compared to the scopolamine-treated group. The elevated levels of glycine could improve the NMDA receptor hypofunction which is helpful in reviving the cognitive function and memory. Furthermore, the scopolamine-treated group showed elevated levels of glutamate (**Figure 8G**) compared to the vehicle-treated control group. The elevated level of glutamate is alarming to the neuronal cells.[85-86] It causes the triggering of calcium-dependent intracellular pathways, generating highly reactive free radical species, surging the oxidative stress which ultimately leads to cell death.[87] Treatment of the amnesic mice with compound **23e** decreased the glutamate levels (**Figure 8G**) as compared to the scopolamine-treated group. This might provide protection against excitotoxicity induced by elevated levels of glutamate.

Y-Maze Test

The animal model of $A\beta_{1-42}$-induced AD in rodents was used to assess the effect of compound **23e** on learning and memory. In this model, animals were subjected to intracerebroventricular (icv) injection of $A\beta_{1-42}$ in the hippocampal region of the brain. Impairment of the working memory in the animals was assessed using Y-maze test.[59, 88] The spontaneous alteration in the behavior of the animals was considered to reflect short-term or spatial working memory. As shown in **Figure 9**, spontaneous alternations in $A\beta_{1-42}$-treated mice were significantly lowered over the vehicle treated control mice. Donepezil, used as a reference standard, could considerably increase spontaneous alternation behavior compared to the $A\beta_{1-42}$-treated group. Further, the lowered spontaneous alternations induced by $A\beta_{1-42}$ were significantly reversed by compound **23e** at both 5 mg/kg and 10 mg/kg dose levels (**Figure 9**).
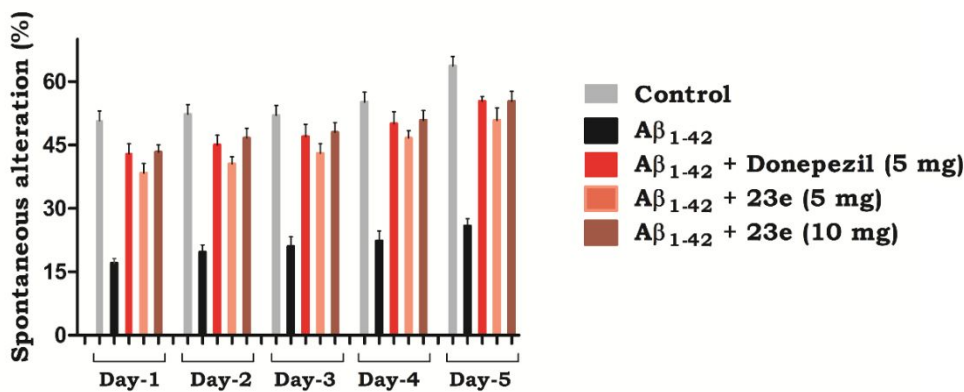
Figure 9. Compound **23e** improved immediate working memory in rats which received icv injection of $A\beta_{1-42}$ in the Y-maze test.

Results of these behavioral studies and neurochemical analysis in scopolamine-induced amnesia and Aβ-induced AD models revealed that compound **23e** possessed the ability to reverse the reference and working memory-deficit as well as manage the oxidative stress-induced dementia.

Acute Toxicity Study

For the development of a NCE as a drug, determination of its acute toxicity is considered to be an important criterion. Acute toxicity of compound **23e**, the most promising candidate of the current study, was determined according to OECD 423 guidelines.[89] Wistar female rats were dosed with compound **23e** at a dose of 2000 mg/kg (n = 3 per group) by oral administration. After administration of the compound, the animals were monitored continuously for the first 4 hrs for any abnormal behavior and mortality. Later on the animals were intermittently observed for the next 24 hrs and occasionally for 14 days for any sign of delayed effects. All the animals survived in the duration of the study period and appeared healthy in terms of fur sleekness, water and food consumption, and body weight. On the 15th day, all the animals were sacrificed for macroscopic examination of the heart, liver, and kidneys for any damage. No damage was observed in these

organs. The results from the study showed that mice treated with compound **23e** did not produce any acute toxicity or mortality immediately or during the post-treatment period. Therefore, compound **23e** can be considered to be nontoxic and well tolerated at doses up to 2000 mg/kg.

Conclusion

Encouraged by the therapeutic potential of the MTDLs as anti-AD agents, we intended to amalgamate two different activities, cholinesterase inhibition and anti-oxidant activity in a single scaffold to enhance the potential of anti-AD drug therapy. Combination of the indole ring and the 1,2,4-triazine nucleus by molecular hybridization approach resulted into triazinoindole scaffold. Incorporation of various substituents in the triazinoindole scaffold resulted in a novel series of anti-AD agents showing good in vitro cholinesterase inhibitory and anti-oxidant activities. Among these compounds, the most active compound **23e** showed IC_{50} values of 0.56 µM for AChE and 1.17 µM for BuChE (SI value of 2.09). Molecular modelling studies indicated significant interactions between the most potent compound **23e** with PAS as well as CAS sites of both the enzymes. Results from the docking studies were further validated by time dependent molecular dynamics study. Compound **23e** displayed excellent neuroprotective activity against H_2O_2 as well as Aβ-induced toxicity in SH-SY5Y cells in a concentration dependent manner. Further, it did not show any significant toxicity in neuronal SH-SY5Y cells in the cytotoxicity assay. Compound **23e** showed high permeability in PAMPA-BBB assay. The overall ideology to develop efficacious MTDLs is to have the proof of concept by performing in vivo studies, which would provide relevance to the results obtained in in vitro studies. Keeping in mind the excellent in vitro profile of compound **23e**, it was selected for further in vivo evaluation of its anti-AD efficacy in animal models. Compound **23e** was able to successfully reverse the cognitive impairment in both MWM and Y-Maze tests. Restoration of CAT and MDA levels to their

38

normal values supports the anti-oxidant potential of compound **23e**. Additionally compound **23e** is endowed with the capability to restore the memory deficit through increasing glycine levels and decreasing glutamate levels in scopolamine-treated animals.   It did not show any acute toxicity in mice at a dose of 2000 mg/kg. In addition, compound **23e** was predicted in silico to possess notable ADMET properties. Taken together, these findings project compound **23e** as a well-balanced potential MTDL for further development as a novel anti-AD drug.

EXPERIMENTAL SECTION

General: All the commercial reagents and solvents required for synthesis of the compounds were purchased from Spectrochem, Sigma-Aldrich, S. d. fine chemicals and Avra chemicals and were purified by general laboratory techniques whenever needed. Reaction monitoring was assessed by thin layer chromatography (TLC), using silica gel precoated plates ($60F_{254}$, Merck, 0.25 mm thickness) visualizing in ultraviolet (UV) light (λ=254 nm) or in iodine chamber. Chromatographic purification was performed by flash column chromatography with a Teledyne ISCO CombiFlash Rf system using RediSep Rf columns. Yields reported here are unoptimized. Melting points were determined in glass capillary tubes using silicon oil-bath type melting point apparatus (Veego) or by Differential Scanning Calorimetry (DSC) using Shimadzu DSC-60 and are uncorrected. Purity of the compound was accessed by HPLC, with all the compounds exhibiting $\geq$95% purity level. HPLC purity determination methods are described in the Supporting Information. The IR spectra were recorded on a Bruker ALPHA-T (Germany) FT-IR spectrophotometer for all the reported compounds and are consistent with the assigned structures. ^{1}H NMR and ^{13}C NMR spectra were recorded on Bruker Advance-II 400 MHz spectrometer in $CDCl_3$ or DMSO-d_6 solvents. Chemical shifts (δ) have been expressed in parts per million (ppm) relative to the standard TMS, and the peak patterns were indicated as s (singlet), d (doublet), t (triplet), m (multiplet), and br (broad

39

signal). Mass spectra were recorded using Thermo Fisher mass spectrometer with EI ion source. Elemental analyses were performed on a Thermo Fisher FLASH 2000 organic elemental analyzer. The elemental composition of the compounds were within ±0.4% range of the calculated values. All the procedures performed on the animals during this work were in accordance with CPCSEA established guidelines and regulations, and were reviewed and approved by IAEC (Institutional Animal Ethics Committee) **(Approval No. MSU/IAEC/2016-17/1636).**

Chemistry

5*H*-[1,2,4]Triazino[5,6-*b*]indole-3-thiol (2).

General Procedure A: To a stirred suspension of isatin (**1**) (1 g, 6.5 mmol) in aqueous potassium carbonate (1.34 g in 50 mL water) was added thiosemicarbazide (592 mg, 6.5 mmol). The mixture was refluxed for 16 h. After cooling down to room temperature the solution was acidified with glacial acetic acid and left overnight. The obtained precipitate was filtered, washed with a mixture of water/acetic acid (24:1 v/v). The resulting solid was triturated with hot DMF, filtered and dried to yield compound **2** as a pale yellow solid. Yield 92 %; m.p. > 350 °C (lit.[90] m.p. > 350 °C); IR (KBr, cm^{-1}): 3410, 3038, 1609, 1427, 1345, 1160; ^{1}H NMR (CDCl$_3$): δ 14.58 (br, 1H, -S*H*), 12.35 (br, 1H, -N*H*), 7.98 (d, 1H, Ar*H*), 7.62-7.58 (m, 1H, Ar*H*), 7.43 (d, 1H, Ar*H*), 7.35-7.31 (m, 1H, Ar*H*); MS (m/z): 203 (M+H)$^+$; RP-HPLC (Method-A) purity: 98.6%, t_R = 3.58 min.

Synthesis of 3-(substituted-thio)-5*H*-[1,2,4]triazino[5,6-*b*]indole (3a-3l)

General Procedure B: To a suspension of 5*H*-[1,2,4]triazino[5,6-*b*]indole-3-thiol (**2**) (1g, 4.95 mmol) in DMF (20 mL), potassium carbonate (1.02 g, 7.42 mmol) and alkyl/aryl-alkyl bromide (4.95 mmol) were added. The reaction mixture was allowed to stir at 60 °C for 6-8 hours. After completion of the reaction, the reaction mixture was poured into crushed ice. The precipitated

product so formed was filtered, washed with water and recrystallized to yield the titled compounds

3a-3l.

3-Methylthio-5*H*-[1,2,4]triazino[5,6-*b*]indole (3a). Greenish yellow solid; yield 69 %; m.p. 306.73 °C (DSC); IR (KBr, cm^{-1}): 3204, 3056, 2801, 1604, 1342, 1184; ^{1}H NMR (DMSO-d_6): δ 12.62 (br, 1H, -N*H*), 8.28 (d, 1H, Ar*H*), 7.67-7.64 (m, 1H, Ar*H*), 7.55 (d, 1H, Ar*H*), 7.42-7.39 (m, 1H, Ar*H*), 2.66 (s, 3H, -C*H₃*); ^{13}C NMR (DMSO-d_6): δ 168.1, 147.2, 141.3, 140.8, 131.3, 122.9, 121.9, 118.2, 113.2, 13.9; MS (m/z): 216 (M)$^+$; RP-HPLC (Method-A) purity: 99.5%, t_R = 8.23 min.

3-Ethylthio-5*H*-[1,2,4]triazino[5,6-*b*]indole (3b). Yellow solid, yield 69 %; m.p. 287.45 °C (DSC); IR (KBr, cm^{-1}): 3210, 3059, 2802, 1606, 1336, 1187; ^{1}H NMR (DMSO-d_6): δ 12.57 (br, 1H, -N*H*), 8.28 (d, 1H, Ar*H*), 7.68-7.64 (m, 1H, Ar*H*), 7.55 (d, 1H, Ar*H*), 7.42-7.39 (m, 1H, Ar*H*), 3.27 (q, *J* = 7.3 Hz, 2H, -SC*H₂*), 1.43 (t, *J* = 7.3 Hz, 3H, -CH$_2$C*H₃*); ^{13}C NMR (DMSO-d_6): δ 167.7, 147.2, 141.3, 140.8, 131.3, 122.9, 121.9, 118.2, 113.2, 24.3, 15.1; MS (m/z): 230 (M)$^+$; RP-HPLC (Method-A) purity: 98.8%, t_R = 5.92 min.

3-*iso*Propylthio-5*H*-[1,2,4]triazino[5,6-*b*]indole (3c). Light yellow solid; yield 67 %; m.p. 282.63 °C (DSC); IR (KBr, cm^{-1}): 3200, 3058, 2865, 2800, 1603, 1339, 1182; ^{1}H NMR (DMSO-d_6): δ 12.53 (br, 1H, -N*H*), 8.28 (d, 1H, Ar*H*), 7.66-7.62 (m, 1H, Ar*H*), 7.54 (d, 1H, Ar*H*), 7.42-7.38 (m, 1H, Ar*H*), 4.13-4.06 (m, 1H, -SC*H*), 1.47 (d, 6H, -C*H₃*); ^{13}C NMR (DMSO-d_6): δ 167.8, 147.2, 141.3, 140.8, 131.3, 122.9, 121.9, 118.2, 113.2, 35.7, 23.3; MS (m/z): 244 (M)$^+$; RP-HPLC (Method-A) purity: 97.4%, t_R = 4.72 min.

3-Butylthio-5*H*-[1,2,4]triazino[5,6-*b*]indole (3d). Light yellow solid; yield 68 %; m.p. 262.83 °C (DSC); IR (KBr, cm^{-1}): 3209, 3057, 2867, 2800, 1606, 1336, 1187; ^{1}H NMR (DMSO-d_6): δ 12.57

(br, 1H, -N*H*), 8.27 (d, 1H, Ar*H*), 7.66-7.62 (m, 1H, Ar*H*), 7.54 (d, 1H, Ar*H*), 7.41-7.37 (m, 1H, Ar*H*), 3.27 (t, 2H, -SC*H*$_2$), 1.80-1.72 (m, 2H, -SCH$_2$C*H*$_2$), 1.55-1.45 (m, 2H, -C*H*$_2$CH$_3$), 0.97 (t, 3H, -CH$_2$C*H*$_3$); ^{13}C NMR (DMSO-d_6): δ 167.8, 147.2, 141.4, 140.7, 131.3, 122.9, 121.9, 118.2, 113.2, 31.4, 30.1, 22.0, 14.1; MS (m/z): 258 (M)$^+$; RP-HPLC (Method-B) purity: 98.5%, t_R = 13.32 min.

3-Benzylthio-5*H*-[1,2,4]triazino[5,6-*b*]indole (3e). Yellow solid; yield 70 %; m.p. 275.15 °C (DSC); IR (KBr, cm^{-1}): 3203, 3055, 2930, 2797, 1600, 1338, 1180, 752; ^{1}H NMR (DMSO-d_6): δ 12.54 (br, 1H, -N*H*), 8.29 (d, 1H, Ar*H*), 7.67-7.63 (m, 1H, Ar*H*), 7.56 (d, 1H, Ar*H*), 7.50 (d, 2H, Ar*H*), 7.43-7.39 (m, 1H, Ar*H*), 7.33-7.29 (m, 2H, Ar*H*), 7.26-7.22 (m, 1H, Ar*H*), 4.56 (s, 2H, -C*H*$_2$); ^{13}C NMR (DMSO-d_6): δ 167.2, 147.1, 141.6, 140.8, 138.1, 131.4, 129.6, 128.9, 127.7, 123.1, 122.0, 118.2, 113.2, 34.6; MS (m/z): 292 (M)$^+$; RP-HPLC (Method-B) purity: 99.2%, t_R = 14.23 min.

3-(2-Methylbenzylthio)-5*H*-[1,2,4]triazino[5,6-*b*]indole (3f). Yellow solid; yield 66 %; m.p. 254.96 °C (DSC); IR (KBr, cm^{-1}): 3201, 3059, 2969, 2801, 1600, 1340, 1175, 771, 747; ^{1}H NMR (DMSO-d_6): δ 12.53 (br, 1H, -N*H*), 8.27 (d, 1H, Ar*H*), 7.66-7.61 (m, 1H, Ar*H*), 7.53-7.51 (m, 1H, Ar*H*), 7.47-7.45 (m, 1H, Ar*H*), 7.41-7.37 (m, 1H, Ar*H*), 7.19-7.10 (m, 3H, Ar*H*), 4.54 (s, 2H, -SC*H*$_2$), 2.42 (s, 3H, ArC*H*$_3$); MS (m/z): 306.09 (M)$^+$; RP-HPLC (Method-B) purity: 98.8%, t_R = 20.89 min.

3-(3-Fluorobenzylthio)-5*H*-[1,2,4]triazino[5,6-*b*]indole (3g). Light yellow solid; yield 71 %; m.p. 262.80 °C; IR (KBr, cm^{-1}): 3210, 3059, 2944, 2802, 1606, 1335, 1182, 884, 755; ^{1}H NMR (DMSO-d_6): δ 12.55 (br, 1H, -N*H*), 8.29 (d, 1H, Ar*H*), 7.67-7.63 (m, 1H, Ar*H*), 7.56 (d, 1H, Ar*H*), 7.43-7.39 (m, 1H, Ar*H*), 7.35-7.29 (m, 3H, Ar*H*), 7.03-6.98 (m, 1H, Ar*H*), 4.57 (s, 2H, -SC*H*$_2$); ^{13}C NMR (DMSO-d_6): δ 166.9, 163.5, 161.6, 147.1, 141.7, 140.9, 131.5, 130.9, 125.7, 123.0,

42

122.0, 118.1, 116.4, 114.6, 113.3, 33.9; MS (m/z): 309.99 (M)$^+$; RP-HPLC (Method-B) purity: 97.5%, t_R = 16.89 min.

3-(4-Bromobenzylthio)-5*H*-[1,2,4]triazino[5,6-*b*]indole (3h). Yellow solid; yield 74 %; m.p. 294.73 °C (DSC); IR (KBr, cm^{-1}): 3203, 3054, 2965, 2798, 1603, 1340, 1180, 752; ^{1}H NMR (DMSO-d_6): δ 12.62 (br, 1H, -N*H*), 8.30 (d, 1H, Ar*H*), 7.71-7.67 (m, 1H, Ar*H*), 7.58 (d, 1H, Ar*H*), 7.45-7.38 (m, 3H, Ar*H*), 7.14-7.12 (m, 2H, Ar*H*), 4.51 (s, 2H, -SC*H*$_2$), 2.26 (s, 3H, -C*H*$_3$); ^{13}C NMR (DMSO-d_6): δ 166.4, 146.6, 141.2, 140.3, 137.4, 131.2, 130.9, 122.5, 121.5, 120.2, 117.6, 112.7, 33.2; MS (m/z): 371 (M)$^+$; RP-HPLC (Method-B) purity: 98.3%, t_R = 24.1 min.

3-(4-Cyanobenzylthio)-5*H*-[1,2,4]triazino[5,6-*b*]indole (3i). Brownish solid; yield 76 %; m.p. 288.48 °C (DSC); IR (KBr, cm^{-1}): 3200, 3151, 2978, 2226, 1599, 1179, 743; ^{1}H NMR (DMSO-d_6): δ 12.62 (br, 1H, -N*H*), 8.29 (d, 1H, Ar*H*), 7.78-7.66 (m, 5H, Ar*H*), 7.57 (d, 1H, Ar*H*), 7.44-7.40 (m, 1H, Ar*H*), 4.63 (s, 2H, -SC*H*$_2$); ^{13}C NMR (DMSO-d_6): δ 166.6, 147.1, 144.6, 141.8, 140.9, 132.8, 131.5, 130.6, 123.0, 122.0, 119.3, 118.0, 113.3, 110.3, 34.0; MS (m/z): 317.09 (M)$^+$; RP-HPLC (Method-B) purity: 99.8%, t_R = 11.0 min.

3-(4-Methoxybenzylthio)-5*H*-[1,2,4]triazino[5,6-*b*]indole (3j). Light yellow solid; yield 64 %; m.p. 254.93 °C (DSC); IR (KBr, cm^{-1}): 3054, 2961, 2931, 2834, 1609, 1250, 1178, 753; ^{1}H NMR (DMSO-d_6): δ 12.57 (br, 1H, -N*H*), 8.29 (d, 1H, Ar*H*), 7.68-7.64 (m, 1H, Ar*H*), 7.56 (d, 1H, Ar*H*), 7.46-7.38 (m, 3H, Ar*H*), 6.87-6.82 (m, 2H, Ar*H*), 4.50 (s, 2H, -SC*H*$_2$), 3.73 (s, 3H, -OC*H*$_3$); MS (m/z): 322.09 (M)$^+$; RP-HPLC (Method-B) purity: 98.4%, t_R = 15.17 min.

3-(4-Methylbenzylthio)-5*H*-[1,2,4]triazino[5,6-*b*]indole (3k). Yellow solid; yield 72 %; m.p. 290.38 °C (DSC); IR (KBr, cm^{-1}): 3202, 3052, 2964, 2798, 1604, 1340, 1181, 751; ^{1}H NMR (DMSO-d_6): δ 12.62 (br, 1H, -N*H*), 8.30 (d, 1H, Ar*H*),7.71-7.67 (m, 1H, Ar*H*), 7.58 (d, 1H, Ar*H*),

7.45-7.38 (m, 3H, Ar*H*), 7.14-7.12 (m, 2H, Ar*H*), 4.51 (s, 2H, -SC*H*₂), 2.26 (s, 3H, -C*H*₃); ¹³C

NMR (DMSO-*d*₆): δ 166.8, 146.6, 141.0, 140.3, 136.4, 134.3, 130.8, 128.9, 122.4, 121.4, 117.6,

112.7, 33.8, 20.7; MS (m/z): 306.19 (M)⁺; RP-HPLC (Method-B) purity: 98.5%, t_R = 20.69 min.

3-Phenethylthio-5*H*-[1,2,4]triazino[5,6-*b*]indole (3l). Yellow solid; yield 74 %; m.p. 246.05 °C

(DSC); IR (KBr, cm⁻¹): 3204, 3058, 2965, 2801, 1606, 1334, 1186, 751, 695; ¹H NMR (DMSO-

*d*₆): δ 12.55 (br, 1H, -N*H*), 8.30 (d, 1H, Ar*H*), 7.69-7.64 (m, 1H, Ar*H*), 7.57 (d, 1H, Ar*H*), 7.44-

7.40 (m, 1H, Ar*H*), 7.36-7.30 (m, 4H, Ar*H*), 7.26-7.20 (m, 1H, Ar*H*), 3.53-3.49 (m, 2H, -

SC*H*₂CH₂), 3.10-3.06 (m, 2H, -SCH₂C*H*₂); ¹³C NMR (DMSO-*d*₆): δ 167.5, 147.2, 141.4, 140.7,

131.3, 129.2, 128.9, 126.9, 122.9, 121.9, 118.2, 113.2, 35.5, 31.9; MS (m/z): 306.19 (M)⁺; RP-

HPLC (Method-B) purity: 98.3%, t_R = 17.89 min.

Synthesis of 5-substituted 5*H*-[1,2,4]triazino[5,6-*b*]indole-3-thiol derivatives (5a-5k)

Following the **General Procedure A**, 5-substituted 5*H*-[1,2,4]triazino[5,6-*b*]indole-3-thiol

derivatives **5a-5k** were synthesized by condensation of N_1-substituted isatins with

thiosemicarbazide. The obtained solids were recrystallized to yield the titled compounds.

5-Methyl[1,2,4]triazino[5,6-*b*]indole-3-thiol (5a). Pale yellow solid; yield 68 %; m.p. 290.34 °C

(DSC); IR (KBr, cm⁻¹): 2975, 1601, 1566, 1362, 1139, 750; ¹H NMR (DMSO-*d*₆): δ 14.61 (bs,

1H, -S*H*), 8.02 (d, 1H, Ar*H*), 7.71-7.67 (m, 1H, Ar*H*), 7.59 (d, 1H, Ar*H*), 7.41-7.37 (m, 1H, Ar*H*),

3.70 (s, 3H,-C*H*₃); MS (m/z): 217.20 (M+H)⁺; RP-HPLC (Method-A) purity: 99.8%, t_R = 6.69

min.

5-Ethyl[1,2,4]triazino[5,6-*b*]indole-3-thiol (5b). Yellow solid; yield 73 %; m.p. 304.17 °C

(DSC); IR (KBr, cm⁻¹): 2855, 1574, 1347, 1143, 743; ¹H NMR (DMSO-*d*₆): δ 14.61 (bs, 1H, -S*H*),

8.03 (d, 1H, Ar*H*), 7.71-7.63 (m, 2H, Ar*H*), 7.41-7.37 (m, 1H, Ar*H*), 4.27 (q, *J* = 7.2 Hz, 2H, -

44

NCH_2CH_3), 1.37 (t, J = 7.2 Hz, 3H, -NCH_2CH_3); ^{13}C NMR (DMSO-d_6): δ 179.0, 147.6, 143.2, 135.3, 131.8, 123.5, 121.8, 117.5, 111.6, 35.9, 12.9; MS (m/z): 231.10 (M+H)[+]; RP-HPLC (Method-A) purity: 99.6%, t_R = 4.50 min.

5-*iso*Propyl[1,2,4]triazino[5,6-*b*]indole-3-thiol (5c). Yellow solid; yield 66 %; m.p. 307.01 °C (DSC); IR (KBr, cm^{-1}): 2941, 1602, 1559, 1349, 1146, 742; ^{1}H NMR (DMSO-d_6): δ 14.73 (bs, 1H*, -*S*H*), 8.05 (d, 1H, Ar*H*), 7.80 (d, 1H, Ar*H*), 7.70-7.65 (m, 1H, Ar*H*), 7.41-7.37 (m, 1H, Ar*H*), 5.08-5.05 (m, 1H, -NC*H*), 1.60 (d, 6H, -C*H*$_3$); ^{13}C NMR (DMSO-d_6): δ 178.8, 147.7, 142.6, 135.3, 131.7, 123.8, 121.9, 117.9, 112.9, 45.8, 19.5; MS (m/z): 245.20 (M+H)[+]; RP-HPLC (Method-A) purity: 98.9%, t_R = 9.74 min.

5-Butyl[1,2,4]triazino[5,6-*b*]indole-3-thiol (5d). Yellow solid; yield 71 %; m.p. 274.32 °C (DSC); IR (KBr, cm^{-1}): 2925, 1603, 1561, 1330, 1137, 757; ^{1}H NMR (DMSO-d_6): δ 14.42 (bs, 1H*, -*S*H*), 7.86 (d, 1H, Ar*H*), 7.53-7.52 (m, 2H, Ar*H*), 7.24-7.20 (m, 1H, Ar*H*), 4.01 (t, 2H, -NC*H*$_2$), 1.59-1.53 (m, 2H, -NCH$_2$C*H*$_2$), 1.20-1.14 (m, 2H, -C*H*$_2$CH$_3$), 0.74 (t, 3H, -CH$_2$C*H*$_3$); ^{13}C NMR (DMSO-d_6): δ 179.0, 147.9, 143.6, 135.2, 131.8, 123.4, 121.8, 117.4, 111.8, 42.9, 29.6, 19.6, 13.7; MS (m/z): 259.20 (M+H)[+]; RP-HPLC (Method-B) purity: 99.8%, t_R = 14.49 min.

5-Benzyl[1,2,4]triazino[5,6-*b*]indole-3-thiol (5e). Light yellow solid; yield 69 %; m.p. 293.24 °C (DSC); IR (KBr, cm^{-1}): 2841, 1599, 1569, 1163, 744; ^{1}H NMR (DMSO-d_6): δ 14.73 (bs, 1H*,-*S*H*), 8.02 (d, 1H, Ar*H*), 7.60-7.56 (m, 1H, Ar*H*), 7.43 (d, 1H, Ar*H*), 7.38-7.25 (m, 6H, Ar*H*), 5.47 (s, 2H, -NC*H*$_2$); ^{13}C NMR (DMSO-d_6): δ 179.3, 148.4, 143.3, 135.4, 131.8, 128.8, 127.8, 127.3, 123.7, 121.9, 117.6, 111.9, 44.0; MS (m/z): 291.68 (M)[+]; RP-HPLC (Method-A) purity: 98.6%, t_R = 6.46 min.

5-(2-Bromobenzyl)[1,2,4]triazino[5,6-*b*]indole-3-thiol (5f). Yellow solid; yield 84 %; m.p. 298.92 °C (DSC); IR (KBr, cm⁻¹): 2980, 2889, 1575, 1180, 748; ¹H NMR (DMSO-d_6): δ 14.72 (bs, 1H, -S*H*), 8.09 (d, 1H, Ar*H*), 7.72-7.70 (m, 1H, Ar*H*), 7.63-7.59 (m, 1H, Ar*H*), 7.43-7.39 (m, 1H, Ar*H*), 7.35 (d, 1H, Ar*H*), 7.27-7.22 (m, 2H, Ar*H*), 6.93-6.91 (m, 1H, Ar*H*), 5.45 (s, 2H, -NC*H₂*); MS (m/z): 370.09 (M)⁺, 372 (M+2)⁺; RP-HPLC (Method-B) purity: 99.8%, t_R = 17.49 min.

5-(3-Fluorobenzyl)[1,2,4]triazino[5,6-*b*]indole-3-thiol (5g). Yellow solid; yield 64 %; m.p. 282.15 °C (DSC); IR (KBr, cm⁻¹): 2925, 1597, 1571, 1349, 1146, 745; ¹H NMR (DMSO-d_6): δ 14.71 (bs, 1H, -S*H*), 8.19 (s, 1H, Ar*H*), 8.04 (d, 1H, Ar*H*), 7.62-7.58 (m, 1H, Ar*H*), 7.46 (d, 1H, Ar*H*), 7.40-7.33 (m, 1H, Ar*H*), 7.19 (d, 2H, Ar*H*), 7.08-7.03 (m, 2H, Ar*H*), 5.48 (s, 2H, -NC*H₂*); MS (m/z): 311.20 (M+H)⁺; RP-HPLC (Method-A) purity: 95.7%, t_R = 3.84 min.

5-(4-Chlorobenzyl)[1,2,4]triazino[5,6-*b*]indole-3-thiol (5h) Yellow solid; yield 76 %; m.p. 300.43 °C (DSC); IR (KBr, cm⁻¹): 2980, 2885, 1571, 1377, 1141, 754; ¹H NMR (DMSO-d_6): δ 14.69 (bs, 1H, -S*H*), 8.04 (d, 1H, Ar-*H*), 7.63-7.59 (m, 1H, Ar-*H*), 7.48 (d, 1H, Ar-*H*), 7.41-7.35 (m, 5H, Ar-*H*), 5.45 (s, 2H, -NC*H₂*); MS (m/z): 325.99 (M)⁺, 328 (M+2)⁺ ; RP-HPLC (Method-B) purity: 98.3%, t_R = 13.65 min.

5-(4-*tert*-Butylbenzyl)[1,2,4]triazino[5,6-*b*]indole-3-thiol (5i). Yellow solid; yield 81 %; m.p. 249.58 °C (DSC); IR (KBr, cm⁻¹): 3236, 3145, 2970, 2900, 1606, 1465, 1334, 1140; ¹H NMR (DMSO-d_6): δ 12.46 (bs, 1H, -S*H*), 7.73-7.72 (m, 1H, Ar*H*), 7.34-7.27 (m, 5H, Ar*H*), 7.12-7.08 (m, 1H, Ar*H*), 7.02-7.00 (m, 1H, Ar*H*), 4.91 (s, 2H, -NC*H₂*), 1.26 (s, 9H, -C*H₃*); MS (m/z): 350.09 (M+H)⁺ ; RP-HPLC (Method-A) purity: 99.6%, t_R = 4.31 min.

5-(4-Methoxybenzyl)[1,2,4]triazino[5,6-*b*]indole-3-thiol (5j). Yellow solid; yield 78 %; m.p. >250 °C (decomposition); IR (KBr, cm^{-1}): 2980, 1608, 1346, 1246, 759; ^{1}H NMR (DMSO-d_6): δ 14.63 (bs, 1H, -S*H*), 7.57-7.53 (m, 2H, Ar*H*), 7.34-7.32 (m, 2H, Ar*H*), 7.12-7.08 (m, 1H, Ar*H*), 6.98-6.96 (m, 1H, Ar*H*), 6.88-6.86 (m, 2H, Ar*H*), 4.84 (s, 2H, -NC*H*$_2$), 3.73 (s, 3H, -OC*H*$_3$); MS (m/z): 321.09 (M)$^+$; RP-HPLC (Method-B) purity: 97.0%, t_R = 18.95 min.

5-(4-Methylbenzyl)[1,2,4]triazino[5,6-*b*]indole-3-thiol (5k). Yellow solid; yield 72%; m.p. 292.88 °C (DSC); IR (KBr, cm^{-1}): 2924, 1599, 1572, 1347, 1145, 752; ^{1}H NMR (DMSO-d_6): δ 14.69 (bs, 1H, -S*H*), 8.03 (d, 1H, Ar*H*), 7.61-7.57 (m, 1H, Ar*H*), 7.45 (d, 1H, Ar*H*), 7.38-7.34 (m, 1H, Ar*H*), 7.25 (d, 2H, Ar*H*), 7.12 (d, 2H, Ar*H*), 5.41 (s, 2H, -NC*H*$_2$), 2.27 (s, 3H, -C*H*$_3$); ^{13}C NMR (DMSO-d_6): δ 179.3, 148.3, 143.3, 137.1, 135.4, 132.4, 132.8, 129.3, 127.3, 123.7, 121.9, 117.6, 112.0, 43.9, 20.7; MS (m/z): 307.20 (M+H)$^+$; RP-HPLC (Method-A) purity: 99.3%, t_R = 5.89 min.

3-(Methylsulfonyl)-5*H*-[1,2,4]triazino[5,6-*b*]indole (6).

General procedure C: To a stirred solution of 3-(methythio)-5*H*-[1,2,4]triazino[5,6-*b*]indole (**5a**) (1 g, 4.62 mmol) in anhydrous methylene chloride (20 mL) at 0 °C, *m*CPBA (80-85% tech solid, 1.79 g, 10.40 mmol) was added as a solid in small portions over a period of a few minutes. The resulting reaction mixture was stirred at room temperature with the exclusion of moisture for 24 hrs. The progress of the reaction was monitored by TLC. After completion of the reaction, the organic phase was washed several times with saturated sodium bicarbonate solution and then with the brine solution. The collected organic phase was dried over anhydrous magnesium sulfate, filtered, and evaporated to give light yellowish solid. Yield 72 %; m.p. 232-234 °C; IR (KBr, cm^{-1}): 3447, 3307, 1621, 1591, 1297, 1090, 758; ^{1}H NMR (DMSO-d_6): δ 13.25 (bs, 1H, N*H*), 8.45 (d,

47

1H, Ar*H*), 7.77-7.81 (m, 1H, Ar*H*), 7.68 (d, 1H, Ar*H*), 7.49-7.53 (m, 1H, Ar*H*), 3.50 (s, 3H, SO$_2$C*H$_3$*); MS (m/z): 249 [M+H]$^+$.

Synthetic of *N*-substituted-5*H*-[1,2,4]triazino[5,6-*b*]indol-3-amine derivatives (7a-7j)

General procedure D: To 3-(methylsulfonyl)-5*H*-[1,2,4]triazino[5,6-*b*]indole (**6**) (0.5 g, 2.014 mmol) in THF (20 mL), an appropriate amine (10 mmol) was added and refluxed on a water-bath for approximately 4 hrs. Progress of the reaction was monitored by TLC. After completion of the reaction, the reaction mixture was poured into ice cold water (20 mL). The aqueous phase was extracted with ethyl acetate (3×30 mL), the organic layer was combined and washed with sodium bicarbonate solution (5 %) and brine, the collected organic layer was dried over anhydrous sodium sulphate and evaporated to give a crude product which was further purified by flash chromatography.

***N*-Propyl-5*H*-[1,2,4]triazino[5,6-*b*]indol-3-amine (7a).** Yellow solid; yield 70 %; m.p. 252-253 °C; IR (KBr, cm^{-1}): 3447, 3060, 2963, 1614, 1533, 1459, 1393, 749; ^{1}H NMR (DMSO-*d$_6$*): δ 11.73 (bs, 1H, N*H*), 8.07 (d, 1H, Ar-*H*), 7.44-7.22 (m, 3H, Ar-*H,* 1H, -N*H*), 3.40-3.37 (m, 2H, -NHC*H$_2$*), 1.69-1.64 (m, 2H, -C*H$_2$*CH$_3$), 0.97 (t, 3H, -CH$_2$C*H$_3$*); ^{13}C NMR (DMSO-*d$_6$*): δ 161.7, 149.0, 139.5, 128.5, 121.9, 119.9, 119.7, 116.2, 112.3, 43.0, 22.6, 11.9; MS (m/z): 228.1 [M+H]$^+$; RP-HPLC (Method-C) purity: 96.1%, t_R = 4.65 min.

***N-iso*Butyl-5*H*-[1,2,4]triazino[5,6-*b*]indol-3-amine (7b).** Yellow solid; yield 82 %; m.p. 243-245 °C; IR (KBr, cm^{-1}): 3429, 3069, 2960, 1609, 1524, 1467, 750; ^{1}H NMR (DMSO-*d$_6$*): δ 11.81 (bs, 1H, N*H*), 8.08 (d, 1H, Ar-*H*), 7.45-7.25 (m, 3H, Ar-*H*), 3.24 (m, 2H, -NHC*H$_2$*), 2.02-1.95 (m, 1H, -C*H*), 0.94 (d, 6H, C*H$_3$*); ^{13}C NMR (DMSO-*d$_6$*): δ 161.7, 149.0, 139.5, 128.5, 121.9, 119.9, 119.7, 116.2, 112.3, 49.4, 28.1, 20.8; MS (m/z): 242.1 [M+H]$^+$; RP-HPLC (Method-C) purity: 96.7%, t_R = 3.39 min.

48

N-Benzyl-5H-[1,2,4]triazino[5,6-b]indol-3-amine (7c). Yellow solid; yield 81 %; m.p. 294 °C (DSC); IR (KBr, cm^{-1}): 3440, 3076, 2966, 1606, 1528, 694; ^{1}H NMR (DMSO-d_6): δ 11.79 (bs, 1H, N*H*), 8.08 (d, 1H, Ar-*H*), 7.45-7.18 (m, 8H, Ar-*H*), 4.67 (d, 2H, -NHC*H*$_2$); ^{13}C NMR (DMSO-d_6): δ 161.7, 148.9, 140.5, 139.6, 128.9, 128.7, 127.5, 127.2, 122.0, 120.0, 119.6, 116.2, 112.3, 44.4; MS (m/z): 276.1 [M+H]$^+$; RP-HPLC (Method-C) purity: 96.9%, t_R = 7.32 min.

N-(4-Chlorobenzyl)-5H-[1,2,4]triazino[5,6-b]indol-3-amine (7d). Yellow solid; yield 68 %, m.p. 218-220 °C; IR (KBr, cm^{-1}): 3414, 3062, 2921, 1620, 1592, 1092, 758; ^{1}H NMR (DMSO-d_6): δ 11.82 (bs, 1H, -N*H*), 8.07 (d, 1H, Ar-*H*), 7.46-7.24 (m, 7H, Ar-*H*, 1H, -N*H*), 4.63 (d, 2H, -NHC*H*$_2$); ^{13}C NMR (DMSO-d_6): δ 161.5, 149.0, 139.6, 139.0, 131.6, 129.3, 128.8, 128.7, 122.4, 120.1, 119.5, 116.0, 112.4, 43.9; MS (m/z): 310.1 [M+H]$^+$; RP-HPLC (Method-C) purity: 96.4%, t_R = 5.94 min.

N-(4-Methoxybenzyl)-5H-[1,2,4]triazino[5,6-b]indol-3-amine (7e). Yellow solid; yield 75 %; m.p. 241-243 °C; IR (KBr, cm^{-1}): 3371, 3058, 2961, 1610, 756; ^{1}H NMR (DMSO-d_6): δ 11.83 (bs, 1H, -N*H*), 8.06 (d, 1H, Ar-*H*), 7.96 (bs, 1H, -N*H*), 7.46-7.24 (m, 5H, Ar-*H*), 6.86-6.82 (m, 2H, Ar-*H*), 4.57 (d, 2H, -NHC*H*$_2$), 3.73 (s, 3H, OC*H*$_3$); MS (m/z): 306.1 [M+H]$^+$; RP-HPLC (Method-C) purity: 97.3%, t_R = 4.11 min.

N-(3,4-Dimethoxybenzyl)-5H-[1,2,4]triazino[5,6-b]indol-3-amine (7f). Yellow solid; yield 70 %; m.p. 201-203 °C; IR (KBr, cm^{-1}): 3374, 1615, 1518, 806; ^{1}H NMR (DMSO-d_6): δ 8.07 (d, 1H, Ar-*H*), 7.46-6.82 (m, 6H, Ar-*H*, 1H, -N*H*), 4.57 (d, 2H, -NHC*H*$_2$), 3.76 (s, 3H, -OC*H*$_3$), 3.74 (s, 3H, -OC*H*$_3$); ^{13}C NMR (DMSO-d_6): δ 161.2, 149.1, 148.9, 148.2, 139.7, 132.9, 128.7, 122.0, 120.1, 119.7, 116.0, 112.4, 112.5, 111.9; MS (m/z): 336.1 [M+H]$^+$; RP-HPLC (Method-C) purity: 97.7%, t_R = 3.63 min.

49

N-(2-Picolyl)-5H-[1,2,4]triazino[5,6-b]indol-3-amine (7g). Brownish yellow solid; yield 82 %; m.p. 241-243 °C; IR (KBr, cm^{-1}): 3396, 3069, 2972, 1615, 1562, 750; ^{1}H NMR (DMSO-d_6): δ 11.79 (bs, 1H, -N*H*), 8.52 (d, 1H, Ar-*H*), 8.13-7.18 (m, 7H, Ar-*H*, 1H, -N*H*), 4.77 (d, 2H, -NHC*H*$_2$); ^{13}C NMR (DMSO-d_6): δ 159.8, 149.3, 148.9, 139.6, 137.2, 137.1, 128.8, 122.5, 121.1, 120.9, 120.2, 119.5, 116.0, 112.4, 46.5; MS (m/z): 277.1 [M+H]$^{+}$; RP-HPLC (Method-C) purity: 98.3%, t_R = 3.36 min.

N-((Furan-2-yl)methyl)-5H-[1,2,4]triazino[5,6-b]indol-3-amine (7h). Yellow solid; yield 63 %; m.p. 234-236 °C. IR (KBr, cm^{-1}): 3406, 3118, 2967, 1615, 1559, 751; ^{1}H NMR (DMSO-d_6): δ 11.83 (bs, 1H, -N*H*), 8.12-8.08 (m, 1H, Ar-*H*), 7.92-6.26 (m, 6H, Ar-*H*, 1H, -N*H*), 4.64 (d, 2H, -NHC*H*$_2$); ^{13}C NMR (DMSO-d_6): δ 155.8, 153.5, 148.9, 142.5, 139.7, 128.8, 122.1, 120.9, 120.2, 119.5, 116.0, 110.9, 107.3, 38.3; MS (m/z): 266.1 [M+H]$^{+}$; RP-HPLC (Method-C) purity: 98.0%, t_R = 3.55 min.

N-(2-(Piperidin-1-yl)ethyl)-5H-[1,2,4]triazino[5,6-b]indol-3-amine (7i). Yellow solid; yield 69 %; m.p. 217-219 °C; IR (KBr, cm^{-1}): 3399, 3231, 3113, 1618, 1524, 1126, 1092, 754; ^{1}H NMR (DMSO-d_6): δ 11.84 (bs, 1H, -N*H*), 8.07 (d, 1H, Ar-*H*), 7.46-7.24 (m, 3H, Ar-*H*, 1H, -N*H*), 3.52-3.50 (m, 2H, -NHC*H*$_2$CH$_3$), 2.55-2.52 (m, 2H, C*H*$_2$), 2.43-2.40 (m, 4H, -NC*H*$_2$), 1.55-1.51 (m, 4H, -C*H*$_2$), 1.42-1.41 (m, 2H, -C*H*$_2$); ^{13}C NMR (DMSO-d_6): δ 155.8, 149.0, 139.5, 128.4, 122.0, 120.0, 119.7, 116.0, 112.3, 57.9, 54.6, 41.4, 26.0, 24.5; MS (m/z): 297.1 [M+H]$^{+}$; RP-HPLC (Method-D) purity: 98.5%, t_R = 5.33 min.

N-(2-Morpholinoethyl)-5H-[1,2,4]triazino[5,6-b]indol-3-amine (7j). Yellow solid, yield 68 %; m.p. >270 °C; IR (KBr, cm^{-1}): 3337, 3070, 2967, 1607, 1526, 1132, 757; ^{1}H NMR (DMSO-d_6): δ 11.74 (s, 1H, -N*H*), 8.08 (d, 1H, Ar-*H*), 7.45-7.03 (m, 3H, Ar-*H*, 1H, -N*H*), 3.64-3.62 (m, 4H, -OC*H*$_2$), 3.57-3.55 (m, 2H, -NHC*H*$_2$), 2.62-2.59 (m, 2H, -NC*H*$_2$), 2.49-2.47 (m, 4H, -NC*H*$_2$); ^{13}C

NMR (DMSO-d_6): δ 161.7, 149.0, 139.5, 128.6, 122.0, 120.0, 119.6, 116.2, 112.4, 66.7, 57.7, 53.8,

38.3; MS (m/z): 299.2 [M+H]$^+$; RP-HPLC (Method-D) purity: 99.1%, t_R = 4.55 min.

Synthesis of 5-substituted-3-(methylthio)-5*H*-[1,2,4]triazino[5,6-*b*]indole derivatives (8a-8i)

Following the **General Procedure B**, 5-substituted 3-(methylthio)-5*H*-[1,2,4]triazino[5,6-*b*]indole derivatives **8a-8i** were synthesized by methylation of the respective thiol derivatives **7**

with methyl iodide.

5-Methyl-3-(methylthio)-5*H*-[1,2,4]triazino[5,6-*b*]indole (8a). Greenish yellow solid; yield 85

%; m.p. 160-162 ˚C; IR (KBr, cm^{-1}): 3052, 3022, 2968, 2925, 1578, 1179, 1072, 762; MS (m/z):

231 [M+H]$^+$.

5-Ethyl-3-(methylthio)-5*H*-[1,2,4]triazino[5,6-*b*]indole (8b). Yellow solid; yield 82 %; m.p.

148-150 ˚C; IR (KBr, cm^{-1}): 3054, 2970, 2928, 2872, 1580, 1188, 1078, 749; MS (m/z): 245

[M+H]$^+$.

5-Propyl-3-(methylthio)-5*H*-[1,2,4]triazino[5,6-*b*]indole (8c). Light yellow solid; yield 80 %;

m.p. 128-130 ˚C; IR (KBr, cm^{-1}): 3053, 3026, 2966, 2924, 1575, 1190, 1073, 746; MS (m/z): 259

[M+H]$^+$.

5-Butyl-3-(methylthio)-5*H*-[1,2,4]triazino[5,6-*b*]indole (8d). Light yellow solid; yield 84 %;

m.p. 140-142 ˚C; IR (KBr, cm^{-1}): 3054, 2953, 2925, 1578, 1187, 1075, 742; MS (m/z): 273

[M+H]$^+$.

5-Benzyl-3-(methylthio)-5*H*-[1,2,4]triazino[5,6-*b*]indole (8e). Yellow solid; yield 87 %; m.p.

168-170 ˚C; IR (KBr, cm^{-1}): 3058, 3028, 2955, 2923, 1578, 1186, 1074, 745, 694; MS (m/z): 307

[M+H]$^+$.

51

5-(2-Methylbenzyl)-3-(methylthio)-5*H*-[1,2,4]triazino[5,6-*b*]indole (8f). Light yellow solid; yield 82 %; m.p. 161-163 ˚C; IR (KBr, cm^{-1}): 3059, 3029, 2974, 2924, 1574, 1181, 1073, 748; MS (m/z): 321 [M+H]$^+$.

5-(4-Methylbenzyl)-3-(methylthio)-5*H*-[1,2,4]triazino[5,6-*b*]indole (8g). Light yellow solid; yield 81 %; m.p. 195-197 ˚C; IR (KBr, cm^{-1}): 3056, 2922, 1581, 1182, 1083, 749; MS (m/z): 321 [M+H]$^+$.

5-(4-Chlorobenzyl)-3-(methylthio)-5*H*-[1,2,4]triazino[5,6-*b*]indole (8h). Light yellow solid; yield 79 %; m.p. 181-183 ˚C; IR (KBr, cm^{-1}): 3059, 3026, 2927, 1583, 1184, 1088, 748; MS (m/z): 341 [M+H]$^+$.

5-(4-Fluorobenzyl)-3-(methylthio)-5*H*-[1,2,4]triazino[5,6-*b*]indole (8i). Light yellow solid; yield 85 %; m.p. 176-178 ˚C; IR (KBr, cm^{-1}): 3055, 2924, 1581, 1185, 1078, 751; MS (m/z): 325 [M+H]$^+$.

Synthesis of 5-substituted-3-(methylsulfonyl)-5*H*-[1,2,4]triazino[5,6-*b*]indole derivatives (9a-9i)

Following the **General Procedure C**, 5-substituted-3-(methylsulfonyl)-5*H*-[1,2,4]triazino[5,6-*b*]indole derivatives **9a-9i** were synthesized by oxidation of respective thiomethyl derivatives **8a-8i** with *m*CPBA. The obtained product was used in next step without further purification.

Synthesis of 5-substituted-5*H*-[1,2,4]triazino[5,6-*b*]indol-3-amine derivatives (10a-10j)

Following the **General Procedure D**, 5-substituted-5*H*-[1,2,4]triazino[5,6-*b*]indol-3-amine derivatives **10a-10j** were synthesized by reaction of respective sulfone derivatives **9a-9f, 6** with aqueous ammonia. The obtained solids were purified by flash chromatography to yield the titled compounds **10a-10j**.

5-Methyl-5*H*-[1,2,4]triazino[5,6-*b*]indol-3-amine (10a). Light brown solid; yield 64 %; m.p. >270 ˚C; IR (KBr, cm^{-1}): 3383, 3307, 3212, 1549,1106,770; ^{1}H NMR (DMSO-d_6): δ 8.09 (d, 1H, Ar*H*), 7.60 (d, 1H, Ar*H*), 7.54-7.50 (m, 1H, Ar*H*), 7.35-7.31 (m, 1H, Ar*H*), 7.26 (bs, 2H, -N*H*$_2$), 3.72 (s, 3H, -NC*H*$_3$), MS (m/z): 200 [M+H]$^+$; RP-HPLC (Method-C) purity: 95.2%, t_R = 4.32 min.

5-Ethyl-5*H*-[1,2,4]triazino[5,6-*b*]indol-3-amine (10b). Brown solid; yield 67 %; m.p. >270 ˚C; IR (KBr, cm^{-1}): 3384, 3308, 3211, 2937, 1549, 1019, 755; ^{1}H NMR (DMSO-d_6): δ 8.02 (d, 1H, Ar*H*), 7.71-7.62 (m, 2H, Ar*H*), 7.41-7.37 (m, 1H, Ar*H*), 6.84 (bs, 2H, -N*H*$_2$), 4.30-4.24 (m, 2H, -NC*H*$_2$CH$_3$), 1.82-1.76 (m, 3H, - NCH$_2$C*H*$_3$), MS (m/z): 214.2 [M+H]$^+$; RP-HPLC (Method-C) purity: 99.0%, t_R = 4.68 min.

5-Propyl-5*H*-[1,2,4]triazino[5,6-*b*]indol-3-amine (10c). Greenish yellow solid; yield 67 %; m.p. 265-267 ˚C; IR (KBr, cm^{-1}): 3384,3308, 3212, 2938, 1588, 1105, 755; ^{1}H NMR (DMSO-d_6): δ 8.11 (d, 1H, Ar*H*), 7.65 (d, 1H, Ar*H*), 7.52-7.48 (m, 1H, Ar*H*), 7.34-7.30 (m, 1H, Ar*H*), 7.27 (bs, 2H, -N*H*$_2$), 4.21 (t, 2H, -NC*H*$_2$), 1.85-1.78 (m, 2H, -C*H*$_2$CH$_3$), 0.90 (t, 3H, -CH$_2$C*H*$_3$); MS (m/z): 229 [M+H]$^+$; RP-HPLC (Method-C) purity: 99.1%, t_R = 4.88 min.

5-Butyl-5*H*-[1,2,4]triazino[5,6-*b*]indol-3-amine (10d). Light brown solid; yield 70%; m.p. 208-210 ˚C; IR (KBr, cm^{-1}): 3377, 3298, 3210, 2961, 1525, 1035, 741; ^{1}H NMR (DMSO-d_6): δ 8.10 (d, 1H, Ar*H*), 7.52-7.51 (m, 2H, Ar*H*), 7.31-7.27 (m, 1H, Ar*H*), 6.90 (bs, 2H, -N*H*$_2$), 4.22-4.19 (m, 2H, -NC*H*$_2$), 1.81-1.74 (m, 2H, -NCH$_2$C*H*$_2$), 1.36-1.30 (m, 2H, -C*H*$_2$CH$_3$), 0.92 (t, 3H, -CH$_2$C*H*$_3$); MS (m/z): 242.3 [M+H]$^+$; RP-HPLC (Method-C) purity: 98.0%, t_R = 5.65 min.

5-Benzyl-5*H*-[1,2,4]triazino[5,6-*b*]indol-3-amine (10e). Reddish brown solid; yield 68 %; m.p. 265-267 ˚C; IR (KBr, cm^{-1}): 3396, 3329, 3029, 2929, 1542, 1030, 746; ^{1}H NMR (DMSO-d_6): δ 8.14-7.93 (m, 1H, Ar*H*), 7.49-7.22 (m, 8H, Ar*H*), 5.45 (s, 2H, -NC*H*$_2$); MS (m/z): 276.2 [M+H]$^+$; RP-HPLC (Method-C) purity: 99.1%, t_R = 8.92 min.

53

5-(2-Methylbenzyl)-5*H*-[1,2,4]triazino[5,6-*b*]indol-3-amine (10f). Yellow solid; yield 71 %; m.p. 253-254°C; IR (KBr, cm^{-1}): 3462, 3334, 3009, 2922, 1553, 1107, 744; ^{1}H NMR (CDCl$_3$): δ 8.40 (d, 1H, Ar*H*), 7.44-7.35 (m, 2H, Ar*H*), 7.28-7.20 (m, 2H, Ar*H*), 7.13 (d, 1H, Ar*H*), 7.09-7.06 (m, 1H, Ar*H*), 6.72 (d, 1H, Ar*H*), 5.44 (bs, 2H, -N*H*$_2$), 5.21 (s, 2H, -NC*H*$_2$), 2.44 (s, 3H, -C*H*$_3$); MS (m/z): 290 [M+H]$^+$; RP-HPLC (Method-C) purity: 95.9%, t_R = 5.54 min.

5-(4-Methylbenzyl)-5*H*-[1,2,4]triazino[5,6-*b*]indol-3-amine (10g). Yellow solid; yield 64 %; m.p. 245-247 °C; IR (KBr, cm^{-1}): 3471, 3271, 3057, 2963, 1536, 1098, 743; ^{1}H NMR (DMSO-d_6) δ 7.95-7.93 (m, 1H, Ar*H*), 7.55-7.14 (m, 5H, Ar*H*), 6.90-6.88 (m, 2H, Ar*H*), 5.27 (s, 2H, -NC*H*$_2$), 3.72 (s, 3H, -C*H*$_3$); MS (m/z): 290.2 [M+H]$^+$; RP-HPLC (Method-C) purity: 96.6%, t_R = 5.73 min.

5-(4-Chlorobenzyl)-5*H*-[1,2,4]triazino[5,6-*b*]indol-3-amine (10h). Light brown solid; yield 67 %; m.p. 215-217 °C; IR (KBr, cm^{-1}): 3417, 3298, 2925, 1540, 1039, 746; ^{1}H NMR (CDCl$_3$) δ 8.39 (d, 1H, Ar*H*), 7.47-7.43 (m, 1H, Ar*H*), 7.39-7.26 (m, 6H, Ar*H*), 5.47 (s, 2H, -NC*H*$_2$), 5.16 (bs, 2H, -N*H*$_2$);; MS (m/z): 310 [M+H]$^+$; RP-HPLC (Method-C) purity: 97.4%, t_R = 5.99 min.

5-(3-Fluorobenzyl)-5*H*-[1,2,4]triazino[5,6-*b*]indol-3-amine (10i). Brown solid; yield 59 %; m.p. 230-232 °C; IR (KBr, cm^{-1}): 3418, 3299, 2924, 1550, 1039, 748; ^{1}H NMR (DMSO-d_6): δ 7.96-7.94 (m, 1H, Ar*H*), 7.55-7.46 (m, 4H, Ar*H*), 7.32-7.30 (m, 1H, Ar*H*), 7.18-7.16 (m, 2H, Ar*H*), 5.33 (s, 2H, -NC*H*$_2$); MS (m/z): 294 [M+H]$^+$; RP-HPLC (Method-C) purity: 97.4%, t_R = 6.93 min.

5*H*-[1,2,4]Triazino[5,6-*b*]indol-3-amine (10j). Light brown solid; yield 52 %; m.p. > 270°C; IR (KBr, cm^{-1}): 3383, 3307, 3212, 1558, 1021,755; ^{1}H NMR (DMSO-d_6) δ 8.30 (d, 1H, Ar*H*), 7.67-7.63 (m, 1H, Ar*H*), 7.56 (d, 1H, Ar*H*), 7.43-7.39 (m, 1H, Ar*H*), 6.90 (bs, 2H, -N*H*$_2$), MS (m/z): 186.09 [M+H]$^+$; RP-HPLC (Method-C) purity: 98.7%, t_R = 3.45 min.

General Procedure for the synthesis of *N*-(bromoalkyl)phthalimides (12-14): Phthalimide (1 g, 6.80 mmol), potassium carbonate (3.76 g, 27.2 mmol), and benzyltriethylammonium chloride

(154 mg, 0.68 mmol) were suspended in acetone (50 mL). Dibromoalkane (27.2 mmol) was added to the suspension and the reaction mixture was stirred at room temperature for 24 hrs. The solvent was evaporated under vacuum and the residue was dissolved in water (50 mL) and dichloromethane (50 mL). The organic layer was separated and the aqueous solution was further extracted with dichloromethane (50 mL × 2). The combined organic solution was dried over sodium sulphate, filtered, and concentrated. The crude product was purified by column chromatography to provide *N*-(bromoalkyl)phthalimides as colourless solid. Melting points data for **12-14** were in accordance with the literature values.[91]

N-**(Bromobutyl)phthalimides (12)**. White solid; yield 95%, m.p. 75-78 °C; IR (KBr, cm^{-1}): 2988, 2862, 1768, 1712, 1610, 717.

N-**(Bromopentyl)phthalimides (13)**. White solid; yield 96%, m.p. 61-63 °C; IR (KBr, cm^{-1}): 2932, 2862, 1769, 1710, 1613, 717.

N-**(Bromohexyl)phthalimides (14)** White solid; yield 94%, mp 57-59 °C; IR (KBr, cm^{-1}): 2983, 2927, 2860, 1764, 1704, 1610, 720.

General Procedure for the synthesis of *N,N*-(disubstitutedamino)alkylamines (18a-20h): To a solution of *N*-(bromoalkyl)phthalimide (4 mmol) in methanol (50 mL), secondary amines (4.8 mmol) and triethylamine (0.7 mL, 4.8 mmol) were added. The reaction mixture was refluxed overnight. After completion of the reaction, the solvent was removed under reduced pressure. The residue was dissolved in chloroform and washed with water and brine. The collected organic layer was dried over magnesium sulfate, filtered and evaporated under reduced pressure to give yellowish brown oil which were used in next step without further purification. The phthalimides thus obtained were dissolved in methanol and hydrazine monohydrate (0.8 mL, 16 mmol) was added dropwise. The mixture was refluxed for about 4 hours. The reaction mixture was cooled to

room temperature, the insoluble phthalhydrazide filtered off and the filtrate evaporated under reduced pressure. The obtained oil was dissolved in chloroform and filtered to remove some more phthalhydrazide (this procedure was repeated until complete disappearance of phthalhydrazide was observed). The filtrate was concentrated to give pure product as viscous yellowish oil which was used as such without further purification.

Synthesis of *N*-substituted-5*H*-[1,2,4]triazino[5,6-*b*]indol-3-amine derivatives (21a-23h)

Following the **General Procedure D**, *N*-substituted-5*H*-[1,2,4]triazino[5,6-*b*]indol-3-amine derivatives **21a-23h** were synthesized by reacting compound **6** with the respective amines **18a-20h**. The obtained solids were purified by flash chromatography to yield the titled compounds **21a-23h**.

N-(4-(Dimethylamino)butyl)-5*H*-[1,2,4]triazino[5,6-*b*]indol-3-amine (21a). Yellow solid; yield 67 %; m.p. 161-163 ˚C; IR (KBr, cm^{-1}): 3443, 3327, 3048, 2944, 1615, 1463, 1393, 742; ^{1}H NMR (DMSO-d_6): δ 11.75 (bs, 1H, N*H*), 8.09-8.07 (m, 1H, Ar*H*), 7.46-7.39 (m, 2H, Ar*H*), 7.27-7.23 (m, 1H, Ar*H*), 3.50-3.49 (m, 2H, -NHC*H*$_2$), 2.80-2.78 (m, 2H, -NC*H*$_2$), 2.563 (s, 6H, -NC*H*$_3$), 1.80-1.82 (m, 2H, -NHCH$_2$C*H*$_2$), 1.68-1.75 (m, 2H, -C*H*$_2$); ^{13}C-NMR (DMSO-d_6): δ 155.9, 149.0, 139.6, 128.6, 122.1, 120.03, 119.6, 116.1, 112.4, 56.9, 46.1, 42.6, 26.3, 26.2; MS (m/z): 285.1 [M+H]$^+$; RP-HPLC (Method-D) purity: 98.1%, t_R = 3.45 min.

N-(4-(Diethylamino)butyl)-5*H*-[1,2,4]triazino[5,6-*b*]indol-3-amine (21b). Yellow solid; yield 69 %; m.p. 190-192 ˚C; IR (KBr, cm^{-1}): 3442, 3336, 2966, 1616, 1461, 1391, 748; ^{1}H NMR (CDCl$_3$): δ 8.24 (d, 1H, Ar*H*), 7.48-7.44 (m, 1H, Ar*H*), 7.36 (d, 1H, Ar*H*), 7.33-7.29 (m, 1H, Ar*H*), 6.04 (bs, 1H, -N*H*), 3.55-3.50 (m, 2H, -NHC*H*$_2$), 2.51-2.42 (m, 6H, -NC*H*$_2$), 1.74-1.54 (m, 4H, -C*H*$_2$C*H*$_2$), 1.05 (t, 6H, C*H*$_3$); MS (m/z): 313.3 [M+H]$^+$; RP-HPLC (Method-D) purity: 97.4%, t_R = 3.43 min.

56

N-(4-(Dipropylamino)butyl)-5H-[1,2,4]triazino[5,6-b]indol-3-amine (21c). Yellow solid; yield 69 %; m.p. 198-200 ˚C; IR (KBr, cm^{-1}): 3444, 3333, 3003, 2956, 1615, 1461, 1390, 746; ^{1}H NMR (DMSO-d_6): δ 11.72 (bs, 1H, N*H*), 8.06 (d, 1H, Ar*H*), 7.44-7.36 (m, 2H, Ar*H*), 7.26-7.22 (m, 1H, Ar*H*)**,** 2.55-2.54 (m, 2H, -NHC*H$_2$*), 2.41-2.38 (m, 2H, -NC*H$_2$*), 2.32 (t, 4H, -NC*H$_2$*), 1.66-1.62 (m, 2H, -NHCH$_2$C*H$_2$*), 1.51-1.48 (m, 2H, -C*H$_2$*), 1.44-1.35 (m, 4H, -C*H$_2$*CH$_3$), 0.84 (t, *J* = 7.3 Hz, 6H, -C*H$_3$*); ^{13}C-NMR (DMSO-d_6): δ 155.8, 149.1, 139.5, 128.5, 121.9, 119.9, 119.7, 116.2, 112.3, 56.0, 53.8, 41.1, 27.3, 24.8, 20., 12.3; MS (m/z): 341.1 [M+H]$^+$; RP-HPLC (Method-D) purity: 97.6%, t_R = 3.72 min.

N-(4-(Dibutylamino)butyl)-5H-[1,2,4]triazino[5,6-b]indol-3-amine (21d). Yellow solid; yield 64 %; m.p. 180-182 ˚C; IR (KBr, cm^{-1}): 3442, 3222, 3003, 2955, 1614, 1460, 1388, 743; ^{1}H NMR (CDCl$_3$): δ 8.25 (d, 1H, Ar*H*), 7.48-7.44 (m, 1H, Ar*H*), 7.39 (d, 1H, Ar*H*), 7.33-7.29 (m, 1H, Ar*H*), 5.89 (bs, 1H, N*H*), 3.55-3.50 (m, 2H, -NHC*H$_2$*), 2.54-2.50 (m, 2H, -NC*H$_2$*), 2.48-2.40 (m, 4H, -NC*H$_2$*), 1.73-1.66 (m, 2H, -NHCH$_2$C*H$_2$*), 1.63-1.56 (m, 2H, -NCH$_2$C*H$_2$*), 1.47-1.40 (m, 4H, -NCH$_2$C*H$_2$*), 1.33-1.24 (m, 4H, -C*H$_2$*CH$_3$), 0.89 (t, 6H, -C*H$_3$*); ^{13}C-NMR (DMSO-d_6): δ155.9, 149.1, 139.5, 128.4, 121.9, 119.9, 119.7, 116.2, 112.3, 53.6, 53.8, 41.1, 29.4, 27.3, 24.8, 20.5, 14.3; MS (m/z): 369.2 [M+H]$^+$; RP-HPLC (Method-D) purity: 96.2%, t_R = 3.51 min.

N-(4-(Pyrrolidin-1-yl)butyl)-5H-[1,2,4]triazino[5,6-b]indol-3-amine (21e). Yellow solid; yield 71 %; m.p. 220-222 ˚C; IR (KBr, cm^{-1}): 3434, 3219, 3000, 2934, 1617, 1459, 1382, 745; ^{1}H NMR (DMSO-d_6): δ 8.06 (d, 1H, Ar*H*), 7.44-7.36 (m, 2H, Ar*H*), 7.26-7.22 (m, 1H, Ar*H*), 3.41-3.34 (m, 2H, -NHC*H$_2$*), 2.47-2.43 (m, 6H, -NC*H$_2$*), 1.71-1.64 (m, 6H, -NCH$_2$C*H$_2$*), 1.59-1.54 (m, 2H, C*H$_2$*); MS (m/z): 311.3 [M+H]$^+$; RP-HPLC (Method-D) purity: 97.6%, t_R = 3.42 min.

N-(4-(Piperidin-1-yl)butyl)-5H-[1,2,4]triazino[5,6-b]indol-3-amine (21f). Yellow solid; yield 66 %; m.p. 199-201˚C; IR (KBr, cm^{-1}): 3445, 3326, 3061, 2933, 1660, 1460, 1393, 748; ^{1}H NMR

(DMSO-d_6): δ 11.74 (bs, 1H, NH), 8.06 (d, 1H, ArH), 7.44-7.22 (m, 3H, ArH), 3.41-3.40 (m, 2H, -NHCH_2), 2.32-2.26 (m, 6H, -NCH_2), 1.66-1.59 (m, 2H, -NHCH$_2$CH_2), 1.58-1.49 (m, 6H, -NCH$_2$CH_2), 1.40-1.39 (m, 2H, -CH_2); ^{13}C-NMR (DMSO-d_6): δ 155.78, 149.05, 139.54, 128.44, 121.9, 119.9, 119.7, 116.1, 112.3, 58.8, 54.5, 41.2, 27.4, 26.0, 24.7, 24.4; MS (m/z): 325.1 [M+H]$^+$; RP-HPLC (Method-D) purity: 98.2%, t_R = 3.43 min.

N-(4-Morpholinobutyl)-5H-[1,2,4]triazino[5,6-b]indol-3-amine (21g). Yellow solid; yield, 63 %; m.p. 191-193 ˚C; IR (KBr, cm^{-1}): 3430, 3222, 3007, 2944, 1612, 1457, 1387, 747; ^{1}H NMR (DMSO-d_6): δ 11.63 (bs, 1H, NH), 8.07 (d, 1H, ArH), 7.447.36 (m, 2H, ArH), 7.26-7.22 (m, 1H, ArH), 3.65-3.62 (m, 4H, -OCH_2), 3.46-3.44 (m, 2H, -NHCH_2), 2.39-2.32 (m, 6H, -NCH_2), 1.71-1.62 (m, 2H, -CH_2), 1.71-1.54 (m, 4H, -CH_2); ^{13}C-NMR (DMSO-d_6): δ155.8, 149.1, 139.5, 128.5, 121.9, 119.9, 119.7, 116.2, 112.3, 66.7, 58.5, 53.8, 41.1, 27.2, 24.0; MS (m/z): 327.3 [M+H]$^+$; RP-HPLC (Method-D) purity: 97.2%, t_R = 3.49 min.

N-(4-(4-Methylpiperazin-1-yl)butyl)-5H-[1,2,4]triazino[5,6-b]indol-3-amine (21h). Yellow solid; yield 65 %; m.p. 175-177 ˚C; IR (KBr, cm^{-1}): 3425, 3222, 3052, 2935, 1615, 1457, 1389, 741; ^{1}H NMR (DMSO-d_6): δ 11.68 (bs, 1H, -NH), 8.03 (d, 1H, ArH), 7.41-7.32 (m, 2H, ArH), 7.23-7.19 (m, 1H, ArH), 3.39-3.38 (m, 2H, -NHCH_2), 2.31-2.27 (m, 10H, -NCH_2), 2.15 (s, 3H, -NCH_3), 1.64-1.59 (m, 2H, -NHCH$_2$CH_2), 1.55-1.48 (m, 2H, -CH_2); ^{13}C-NMR (DMSO-d_6): δ 155.9, 149.1, 139.6, 128.5, 121.9, 119.9, 119.7, 116.2, 112.3, 58.0, 55.2, 53.2, 46.2, 41.2, 27.2, 24.4; MS (m/z): 340.3 [M+H]$^+$; RP-HPLC (Method-D) purity: 99.5%, t_R = 3.45 min.

N-(5-(Dimethylamino)pentyl)-5H-[1,2,4]triazino[5,6-b]indol-3-amine (22a). Yellow solid; yield 62 %; m.p. 198-200 ˚C; IR (KBr, cm^{-1}): 3222, 3111, 3007, 2945, 1612, 1457, 748; ^{1}H NMR (DMSO-d_6): δ 8.10-8.05 (m, 1H, ArH), 7.44-7.35 (m, 2H, ArH), 7.26-7.21 (m, 1H, ArH), 3.35-3.30 (m, 2H, -NHCH_2), 2.20 (t, 2H, -NCH_2), 2.135 (s, 6H, -NCH_3), 1.68-1.60 (m, 2H, -

58

NHCH$_2$CH_2), 1.46-1.34 (m, 4H, -CH_2); ^{13}C-NMR (DMSO-d_6): δ 155.9, 149.0, 139.5, 128.4, 121.9, 119.9, 119.7, 116.2, 112.3, 59.6, 45.7, 41.2, 29.2, 27.4, 24.9; MS (m/z): 299.3 [M+H]$^+$; RP-HPLC (Method-D) purity: 97.8%, t_R = 3.20 min.

N-(5-(Diethylamino)pentyl)-5H-[1,2,4]triazino[5,6-b]indol-3-amine (22b). Yellow solid; yield 70 %; m.p. 191-193 ˚C; IR (KBr, cm^{-1}): 3442, 3333, 3059, 2967, 1615, 1460, 1370, 745; ^{1}H NMR (DMSO-d_6): δ 11.62 (bs, 1H, NH), 8.06-8.02 (m, 1H, ArH), 7.37-7.32 (m, 2H, ArH), 7.23-7.19 (m, 1H, ArH), 3.36-3.29 (m, 2H, -NHCH_2), 2.44-2.39 (m, 4H, -NCH_2), 2.34 (t, 2H, -NCH_2), 1.63-1.57 (m, 2H, -NHCH$_2$CH_2), 1.41-1.30 (m, 4H, -CH_2), 0.92 (t, 6H, -CH_3); ^{13}C-NMR (DMSO-d_6): δ 155.9, 149.0, 139.5, 128.4, 121.9, 119.9, 119.7, 116.2, 112.3, 52.7, 46.7, 41.2, 29.3, 26.9, 24.9, 12.2; MS (m/z): 327.1 [M+H]$^+$; RP-HPLC (Method-D) purity: 98.40%, t_R = 4.18 min.

N-(5-(Dipropylamino)pentyl)-5H-[1,2,4]triazino[5,6-b]indol-3-amine (22c). Yellow solid; yield 66 %; m.p. 200-202 ˚C; IR (KBr, cm^{-1}): 3443, 3329, 3057, 2956, 1614, 1461, 1390, 747; ^{1}H NMR (CDCl$_3$): δ 8.25 (d, 1H, ArH), 7.49-7.45 (m, 1H, ArH), 7.37 (d, 1H, ArH), 7.33-7.30 (m, 1H, ArH), 5.54 (bs, 1H, -NH), 3.54-3.49 (m, 2H, -NHCH_2), 2.47-2.38 (m, 6H, -NCH_2), 1.71-1.66 (m, 2H, -NHCH$_2$CH_2), 1.55-1.39 (m, 8H, -CH_2), 0.86 (t, 6H, -CH_3); ^{13}C-NMR (DMSO-d_6): δ 155.9, 149.1, 139.6, 128.4, 121.9, 119.9, 119.7, 116.2, 112.3, 56.1 53.9, 41.1, 29.2, 27.1, 24.9, 20.4, 12.2; MS (m/z): 355.3 [M+H]$^+$; RP-HPLC (Method-D) purity: 99.2%, t_R = 5.0 min.

N-(5-(Dibutylamino)pentyl)-5H-[1,2,4]triazino[5,6-b]indol-3-amine (22d). Yellow solid; yield 72 %; m.p. 184-186 ˚C; IR (KBr, cm^{-1}): 3444, 3332, 3059, 2931, 1614, 1460, 1390, 746; ^{1}H NMR (CDCl$_3$): δ 8.18 (d, 1H, ArH), 7.41-7.37 (m, 1H, ArH), 7.31-7.29 (m, 1H, ArH), 7.25-7.22 (m, 1H, ArH), 5.54 (bs, 1H, -NH), 3.40-3.36 (m, 2H, -NHCH_2), 2.41-2.36 (m, 6H, -NCH_2), 1.63-1.54 (m, 2H, -NHCH$_2$CH_2), 1.48-1.44 (m, 2H, -CH_2), 1.39-1.33 (m, 6H, -NCH$_2$CH_2), 1.25-1.20 (m, 4H, -CH_2), 0.82 (t, 7.3 Hz, 6H, -CH_3); ^{13}C-NMR (DMSO-d_6): δ 155.8, 149.0, 139.5, 128.4, 121.9,

59

119.9, 119.7, 116.1, 112.3, 53.9, 53.6, 41.2, 29.4, 29.2, 27.0, 24.9, 20.5, 14.4; MS (m/z): 383.2 [M+H]$^+$; RP-HPLC (Method-D) purity: 98.8%, t_R = 3.07 min.

N-(5-(Pyrrolidin-1-yl)pentyl)-5H-[1,2,4]triazino[5,6-b]indol-3-amine (22e). Yellow solid; yield 73 %; m.p. 191-193˚C; IR (KBr, cm^{-1}): 3459, 3306, 3059, 2937, 1615, 1456, 1383, 743; ^{1}H NMR (DMSO-d_6): δ 11.66 (bs, 1H, -NH), 8.06-8.02 (m, 1H, ArH), 7.37-7.32 (m, 2H, ArH), 7.22-7.18 (m, 1H, ArH), 3.38-3.37 (m, 2H, -NHCH_2), 2.39-2.34 (m, 6H, NCH_2), 1.68-1.57 (m, 6H, -NCH$_2$CH_2), 1.51-1.44 (m, 2H, -CH_2), 1.41-1.34 (m, 2H, -CH_2); ^{13}C-NMR (DMSO-d_6): δ 155.8, 149.1, 139.5, 128.5, 121.9, 119.7, 119.6, 116.2, 112.2, 53.2, 54.1, 41.1, 29.3, 28.7, 25.0, 23.5; MS (m/z): 325.4 [M+H]$^+$; RP-HPLC (Method-D) purity: 98.3%, t_R = 2.84 min.

N-(5-(Piperidin-1-yl)pentyl)-5H-[1,2,4]triazino[5,6-b]indol-3-amine (22f). Yellow solid; yield 63 %; m.p. 196-198˚C; IR (KBr, cm^{-1}): 3423, 3223, 3007, 2935, 1614, 1455, 1383, 741; ^{1}H NMR (DMSO-d_6): δ 11.58 (bs, 1H, -NH), 8.04 (d, 1H, ArH), 7.43-7.39 (m, 1H, ArH), 7.35 (d, 1H, ArH), 7.25-7.21 (m, 1H, ArH), 3.41-3.40 (m, 2H, -NHCH_2), 2.27-2.18 (m, 6H, -NCH_2), 1.64-1.59 (m, 2H, -NHCH$_2$CH_2), 1.49-1.41 (m, 6H, -NCH$_2$CH_2), 1.37-1.34 (m, 4H, -CH_2); ^{13}C-NMR (DMSO-d_6): δ 155.9, 149.1, 139.6, 128.5, 121.9, 119.9, 119.7, 116.2, 112.3, 59.2, 54.6, 41.2, 29.3, 26.7, 26.1, 25.0, 24.7; MS (m/z): 339.3 [M+H]$^+$; RP-HPLC (Method-D) purity: 96.8%, t_R = 5.43 min.

N-(5-Morpholinopentyl)-5H-[1,2,4]triazino[5,6-b]indol-3-amine (22g). Yellow solid; yield 62 %; m.p. 199-201 ˚C; IR (KBr, cm^{-1}): 3426, 3222, 3050, 2925, 1613, 1455, 1384, 749; ^{1}H NMR (DMSO-d_6): δ 11.41 (bs, 1H, -NH), 8.03 (d, 1H, ArH), 7.40-7.32 (m, 2H, ArH) 7.22-7.18 (m, 1H, ArH), 3.56-3.54 (m, 4H, -OCH_2), 3.39-3.37 (m, 2H, NHCH_2), 2.32-2.29 (m, 4H, -NCH_2), 2.27-2.24 (m, 2H, -NCH_2), 1.65-1.58 (m, 2H, -NHCH$_2$CH_2), 1.50-1.43 (m, 2H, -CH_2), 1.40-1.32 (m, 2H, -CH_2); ^{13}C-NMR (DMSO-d_6): δ 155.8, 149.1, 139.5, 128.4, 122.0, 119.9, 119.7, 116.1, 112.3,

60

66.7, 58.8, 53.9, 41.1, 29.2, 26.2, 24.9; MS (m/z): 341.1 [M+H]$^+$; RP-HPLC (Method-D) purity:

98.5%, t_R = 3.20 min.

N-(5-(4-Methylpiperazin-1-yl)pentyl)-5H-[1,2,4]triazino[5,6-b]indol-3-amine (22h). Yellow

solid; yield 68 %; m.p. 162-164 ˚C; IR (KBr, cm^{-1}): 3439, 3234, 3061, 2931, 1614, 1460, 1389,

745; ^{1}H NMR (CDCl$_3$): δ 9.76 (bs, 1H, -N*H*), 8.25 (d, 1H, Ar*H*), 7.49-7.44 (m, 2H, Ar*H*), 7.37-

7.31 (m, 1H, Ar*H*), 5.57 (bs, 1H, -NH), 3.53-3.47 (m, 2H, -NHC*H$_2$*), 2.60-2.42 (m, 6H, -NC*H$_2$*),

2.39-2.35 (m, 4H, -NC*H$_2$*), 2.29 (s, 3H, -NC*H$_3$*), 1.72-1.65 (m, 2H, -NHCH$_2$C*H$_2$*), 1.62-1.53 (m,

2H, -NCH$_2$C*H$_2$*), 1.46-1.37 (m, 2H, -C*H$_2$*); ^{13}C-NMR (DMSO-d_6): δ 155.6, 149.1, 139.7, 128.5,

121.9, 119.9, 119.3, 116.2, 112.3, 58.4, 55.2, 53.2, 46.2, 41.1, 29.2, 26.6, 24.9; MS (m/z): 354.3

[M+H]$^+$; RP-HPLC (Method-D) purity: 98.4%, t_R = 3.13 min.

N-(6-(Dimethylamino)hexyl)-5H-[1,2,4]triazino[5,6-b]indol-3-amine (23a). Yellow solid;

yield 69 %; m.p. 180-182 ˚C; IR (KBr, cm^{-1}): 3321, 3223, 3058, 2937, 1615, 1462, 1386, 744; ^{1}H

NMR (DMSO-d_6) δ 11.76 (bs, 1H, -N*H*), 8.06 (d, 1H, Ar*H*), 7.43-7.36 (m, 2H, Ar*H*), 7.27-7.25

(m, 1H, Ar*H*), 3.39-3.32 (m, 2H, -NHC*H$_2$*), 2.19 (t, 2H, -NC*H$_2$*), 2.11(s, 6H, -NC*H$_3$*), 1.62-1.61

(m, 2H, -NHCH$_2$C*H$_2$*), 1.43-1.32 (m, 6H, -C*H$_2$*); ^{13}C-NMR (DMSO-d_6): δ 155.7, 149.1, 139.5,

128.4, 121.9, 119.9, 119.7, 116.1, 112.3, 59.6, 45.6, 41.1, 29.3, 27.5, 27.1, 26.9; MS (m/z): 313.1

[M+H]$^+$; RP-HPLC (Method-D) purity: 99.8%, t_R = 3.52 min.

N-(6-(Diethylamino)hexyl)-5H-[1,2,4]triazino[5,6-b]indol-3-amine (23b). Yellow solid; yield

71 %; m.p. 170-172 ˚C; IR (KBr, cm^{-1}): 3443, 3333, 3060, 2929, 1614, 1461, 1374, 747; ^{1}H NMR

(CDCl$_3$): δ 8.25 (d, 1H, Ar*H*), 7.47-7.35 (m, 3H, Ar*H*), 5.75 (bs, 1H, -N*H*), 3.50-3.43 (m, 2H, -

NHC*H$_2$*), 2.65-2.59 (m, 4H, -NC*H$_2$*), 2.52-2.48 (m, 2H, NC*H$_2$*), 1.71-1.60 (m, 4H, -C*H$_2$*), 1.46-

1.37 (m, 4H, -C*H$_2$*), 1.07-1.03 (m, 6H, -C*H$_3$*); ^{13}C-NMR (DMSO-d_6): δ 155.9, 149.1, 139.6, 128.4,

121.9, 119.9, 119.7, 116.2, 112.3, 52.6, 46.7, 41.2, 29.3, 27.3, 27.2, 26.9, 12.04; MS (m/z): 341.1 [M+H]$^+$; RP-HPLC (Method-D) purity: 99.5%, t_R = 4.7 min.

N-(6-(Dipropylamino)hexyl)-5H-[1,2,4]triazino[5,6-b]indol-3-amine (23c). Yellow solid; yield 65%; m.p. 195-197˚C; IR (KBr, cm^{-1}): 3445, 3332, 3060, 2929, 1614, 1461, 1374, 747; ^{1}H NMR (DMSO-d_6): 11.669 (bs, 1H, -N*H*), 8.03 (d, 1H, Ar*H*), 7.40-7.38 (m, 1H, Ar*H*), 7.35-7.33 (m, 1H, Ar*H*)**,** 7.24-7.20 (m, 1H, Ar*H*)**,** 3.33-3.31 (m, 2H, -NHC*H*$_2$), 2.32-2.24 (m, 6H, -NC*H*$_2$), 1.62-1.58 (m, 2H, -NHCH$_2$C*H*$_2$), 1.39-1.29 (m, 10H, -C*H*$_2$), 0.80 (t, 6H, -C*H*$_3$); ^{13}C-NMR (DMSO-d_6): δ 155.8, 149.1, 139.6, 128.5, 121.9, 119.9, 119.7, 116.2, 112.3, 56.1, 53.9, 41.1, 29.3, 27.2, 27.1, 26.9, 20.4, 12.3; MS (m/z): 369.1 [M+H]$^+$; RP-HPLC (Method-D) purity: 99.1%, t_R = 9.72 min.

N-(6-(Dibutylamino)hexyl)-5H-[1,2,4]triazino[5,6-b]indol-3-amine (23d). Yellow solid; yield 68 %; m.p. 192-194˚C; IR (KBr, cm^{-1}): 3445, 3322, 3058, 2955, 1615, 1461, 1391, 747; ^{1}H NMR (DMSO-d_6): δ 11.74 (bs, 1H, N*H*), 8.09-8.07 (m, 1H, Ar*H*), 7.40-7.24 (m, 3H, Ar*H*), 3.42-3.40 (m, 2H, -NHC*H*$_2$), 2.54-2.33 (m, 6H, -NC*H*$_2$), 1.68-1.58 (m, 2H, -NHCH$_2$C*H*$_2$), 1.44-1.24 (m, 14H, -C*H*$_2$), 0.98-0.82 (m, 6H, -C*H*$_3$); ^{13}C-NMR (DMSO-d_6): δ 155.8, 149.1, 139.6, 128.4, 121.9, 119.9, 119.7, 116.1, 112.3, 53.9, 53.6, 41.2, 29.4, 29.3, 27.2, 26.9, 26.0, 20.5, 14.4; MS (m/z): 397.2 [M+H]$^+$; RP-HPLC (Method-D) purity: 98.6%, t_R = 8.67 min.

N-(6-(Pyrrolidin-1-yl)hexyl)-5H-[1,2,4]triazino[5,6-b]indol-3-amine (23e). Yellow solid; yield 73 %; m.p. 177-179 ˚C; IR (KBr, cm^{-1}): 3442, 3330, 3058, 2930, 1614, 1458, 743; ^{1}H NMR (DMSO-d_6): δ 11.66 (bs, 1H, -N*H*), 8.05-8.01 (m, 1H, Ar*H*), 7.37-7.32 (m, 2H, Ar*H*), 7.21-7.17 (m, 1H, Ar*H*), 3.36-3.34 (m, 2H, -NHC*H*$_2$), 2.38-2.32 (m, 6H, -NC*H*$_2$), 1.66-1.57 (m, 6H, -NCH$_2$C*H*$_2$), 1.45-1.40 (m, 2H, -NHCH$_2$C*H*$_2$), 1.38-1.30 (m, 4H, -C*H*$_2$); ^{13}C-NMR (DMSO-d_6): δ

155.8, 149.0, 139.6, 128.5, 121.9, 119.9, 119.7, 116.1, 112.3, 56.2, 54.1, 41.2, 29.3, 28.9, 27.4,

26.9, 23.5; MS (m/z): 339.1 [M+H]⁺; RP-HPLC (Method-D) purity: 97.5%, t_R = 4.35 min.

N-(6-(Piperidin-1-yl)hexyl)-5H-[1,2,4]triazino[5,6-b]indol-3-amine (23f). Yellow solid; yield

70 %; m.p. 178-180˚C; IR (KBr, cm⁻¹): 3445, 3322, 3058, 2955, 1615, 1461, 1391, 747; ¹H NMR

(DMSO-d_6): δ 11.68 (bs, 1H, -NH), 8.07 (d, 1H, ArH), 7.44-7.35 (m, 2H, ArH), 7.26-7.22 (m, 1H,

ArH), 3.42-3.32 (m, 2H, -NHCH₂), 2.31-2.21 (m, 6H, -NCH₂), 1.68-1.61 (m, 2H, -NHCH₂CH₂),

1.52-1.48 (m, 6H, -CH₂), 1.39-1.32 (m, 6H, -CH₂); ¹³C-NMR (DMSO-d_6): δ 155.8, 149.0, 139.5,

128.4, 121.9, 119.9, 119.7, 116.1, 112.3, 59.1, 54.6, 41.1, 29.3, 27.3, 26.9, 26.8, 26.1, 24.7; MS

(m/z): 353.1 [M+H]⁺; RP-HPLC (Method-D) purity: 97.1%, t_R = 4.66 min.

N-(6-Morpholinohexyl)-5H-[1,2,4]triazino[5,6-b]indol-3-amine (23g). Yellow solid; yield 65

%; m.p. 163-165 ˚C; IR (KBr, cm⁻¹): 3460, 3334, 3057, 2931, 1614, 1459, 1392, 748; ¹H NMR

(CDCl₃): δ 9.20 (bs, 1H, -NH), 8.25 (d, 1H, ArH), 7.49-7.46 (m, 1H, Ar-H), 7.41-7.38 (m, 1H,

ArH), 7.34-7.31 (m, 1H, ArH), 5.70 (bs, 1H, NH), 3.75-3.72 (m, 4H, -OCH₂), 3.50-3.53 (m, 2H, -

NHCH₂), 2.48-2.42 (m, 4H, -NCH₂), 2.36-2.33 (m, 2H, -NCH₂), 1.70-1.66 (m, 4H, -NHCH₂CH₂),

1.54-1.51 (m, 2H, -CH₂), 1.41-1.38 (m, 4H, -CH₂); ¹³C-NMR (DMSO-d_6): δ 155.9, 149.1, 139.6,

128.5, 121.9, 119.9, 119.7, 116.2, 112.3, 66.6, 58.7, 53.8, 41.1, 29.3, 27.1, 26.9, 26.8; MS (m/z):

355.1 [M+H]⁺; RP-HPLC (Method-D) purity: 98.9%, t_R = 3.7 min.

N-(6-(4-Methylpiperazin-1-yl)hexyl)-5H-[1,2,4]triazino[5,6-b]indol-3 amine (23h). Yellow

solid; yield 67 %; m.p. 160-162 ˚C; IR (KBr, cm⁻¹): 3460, 3336, 3056, 2928, 1614, 1459, 1391,

747; ¹H NMR (DMSO-d_6): δ 11.71(bs, 1H, -NH), 8.03 (d, 1H, ArH), 7.41-7.33 (m, 2H, ArH),

7.23-7.19 (m, 1H, ArH), 3.36-3.34 (m, 2H, -NHCH₂), 2.32-2.28 (m, 6H, -NCH₂), 2.24-2.20 (m,

2H, -NCH₂), 2.13 (s, 3H, -NCH₃), 1.62-1.56 (m, 2H, -NHCH₂CH₂), 1.42-1.29 (m, 6H, -CH₂); ¹³C-

NMR (DMSO-d_6): δ 155.1, 149.1, 139.6, 128.5, 121.9, 119.9, 119.7, 116.4, 112.3, 58.3, 55.2, 53.2,

46.2, 41.1, 29.3, 27.2, 26.9, 26.8; MS (m/z): 368.1 [M+H]$^+$; RP-HPLC (Method-D) purity: 99.1%,

t_R = 3.26 min.

Biology

Inhibition studies on AChE and BuChE

The potential of the test compounds to inhibit ChEs was assessed using the Ellman's

method as detailed in our earlier report.[59,61,62] Human AChE (product number C1682), equine

serum BuChE (product number C1057), 5,5′-dithiobis(2-nitrobenzoic acid) (DTNB, product

number D8130), acetylthiocholine iodide (ATCI, product number A5751), and butyrylthiocholine

iodide (BTCI, product number B3253) were purchased from Sigma-Aldrich. Donepezil

hydrochloride and tacrine hydrochloride hydrate were used as standard drugs. All the experiments

were carried out in 50 mM Tris-HCl buffer at pH 8. Five different concentrations (0.001−100 μM)

of each test compound were used to determine the enzyme inhibition activity. Briefly, 50 μL of

AChE (0.22 U/mL) or 50 μL of BuChE (0.06 U/mL) and 10 μL of the test or standard compounds

were incubated in 96-well plates at room temperature for 30 min. Further, 30 μL of the substrate,

viz. ATCI (15 mM) or BTCI (15 mM) was added, and the solution was incubated for additional

30 min. Finally, 160 μL of DTNB (1.5 mM) was added to it, and the absorbance was measured at

415 nm wavelength using microplate reader 680 XR (BIO-RAD, India). The IC$_{50}$ values were

determined from the absorbance obtained for various concentrations of the test and the standard

compounds. The IC$_{50}$ value recounts the concentration of the drug required to inhibit the enzyme

activity by 50%. All the determinations were performed in triplicate and at least in three

independent runs.

Antioxidant activity [1,1-diphenyl-2-picrylhydrazyl (DPPH) radical scavenging activity]

The spectrophotometric DPPH assay was carried out as described earlier.[61] Concentrations of the selected test compounds that exhibited promising neuroprotective effects against H_2O_2 insult were selected for the DPPH assay. In brief, 10 μL of a test compound (10 and 20 μM, in Tris-HCl buffer, pH 7.4) was mixed with 20 μL of DPPH (10 mM in methanol) in the 96 well plate. Finally, the volume was adjusted to 200 μL using methanol. After a 30 sec incubation at room temperature protected from light, the absorbance was noted at 520 nm wavelength using a microplate reader 680 XR (BIORAD, India). The free radical scavenging activity was determined as the reduction percentage (RP) of DPPH using the equation $RP = 100[(A_0 - A_C)/A_0]$, where A_0 is the untreated DPPH absorbance and A_C is the absorbance value for the added sample concentration C. Ascorbic acid was used as the standard antioxidant.

Cell Culture Studies.

The human neuroblastoma SH-SY5Y cell line was procured from National Centre for Cell Science (NCCS) (Pune, India). Cells were routinely cultured in Dulbecco's Modified Eagle Medium (DMEM) supplemented with 10% fetal bovine serum (FBS), 1 mM glutamine, 50 U/mL penicillin, and 50 μg/mL streptomycin (reagents from Gibco) at 37 °C in a humidified incubator at 5% CO_2. All the cells used in the study were of the low passage number (<15).

Determination of Cell Viability and Neuroprotection

To determine the cytotoxicity of the selected test compounds, 3-(4,5-dimethylthiazol-2-yl)-2,5-diphenyltetrazolium bromide (MTT) assay was performed. SH-SY5Y cells were seeded in 96-well plate at a density of 5×10^4 cells per well. After 24 h, the medium was replaced with relatively higher concentrations of test compounds (40 μM and 80 μM) for another 24 h at 37 °C.

65

After the incubation period, the cell viability was determined using MTT assay. In another set of experiments, the test compounds were assessed for their ability to protect SH-SY5Y cells against oxidative damage induced by H_2O_2 and $A\beta_{1-42}$. Cells were exposed to the test compounds at relatively low concentrations (5 μM, 10 μM, and 20 μM) and incubated for 2 hrs. After the incubation period, the test compounds were replaced with a medium containing cytotoxic insult, i.e., H_2O_2 (100 μM) or $A\beta_{1-42}$ (25 μM) and left for an additional 24 hrs period. Thereafter, the cell viability was assessed using MTT assay. Briefly, the medium was replaced with 80 μL of fresh medium and 20 μL of MTT (0.5 mg/mL, final concentration; Sigma) in PBS. After 4 hrs, MTT was removed and the crystals of formazan were dissolved in DMSO. Formazan concentrations were quantified at 570 nm with 630 nm reference wavelengths using a microplate reader 680 XR (BIO-RAD, India). Percentage protection against H_2O_2 and $A\beta_{1-42}$ insults was calculated by considering absorbance of the control cells as 100% of the cell viability.

In vitro Blood-Brain Barrier Permeation Assay

The PAMPA assay was performed to predict the BBB permeation of the most active compounds **23e** and **23f.** The donor microplates (PVDF membrane, pore size 0.45 μm) and the acceptor microplates were obtained from the Millipore. Porcine brain lipid (PBL) was purchased from Avanti Polar Lipids. The filter surface of the donor microplate was first impregnated with 4 μL of porcine brain lipid (20 mg in 1 mL dodecane). The acceptor microplate was filled with 200 μL of phosphate buffer saline (PBS)/ethanol (70:30). The test compounds (5 mg/mL) were dissolved in DMSO and diluted with PBS/ethanol (70:30) to get a final concentration of 100 μg/mL. 200 μL of the solution was filled in the donor well and the donor plate was carefully placed on the acceptor plate to form a sandwich and incubated for 120 min at 25 °C. After the incubation period, the donor plate was removed and the concentration of the test compounds in the acceptor

66

wells was determined using UV spectrophotometry. Each sample was analyzed at five different wavelengths, in four wells, and at least in three independent runs. The results are expressed as mean ± SEM. P_e was calculated using the following equation:

$$Pe = -\left(\frac{Vd \times Va}{(Vd + Va)A \times t}\right) \times \ln\left(1 - \frac{(drug)acceptor}{(drug)equilibrium}\right)$$

Where Vd and Va are the volumes in the donor well and acceptor well, respectively. A is the filter area, t is the permeation time, (drug)*acceptor* is the concentration of the test compound in the acceptor well, and (drug)*equilibrium* is the theoretical equilibrium concentration.

In the experiment, seven commercial drugs of known BBB permeability were included to validate the analysis set (Table S1, supporting information). A plot of the P_e(exp.) versus P_e(ref.) values gave a strong linear correlation, P_e(exp.) = 1.16 P_e(ref.) + 0.1668 (R^2 = 0.9781) (Figure S277, supporting information).

Assessment of Cognitive Improvement in Animal Model of AD

Morris Water Maze Test

Adult male Swiss Albino mice (20−25 g) were divided into five groups of seven animals each as per the given treatment (normal control, vehicle-treated control, donepezil at 5 mg/kg, compound **23e** at 5 mg/kg and 10 mg/kg). Scopolamine hydrochloride (1.4 mg/kg)[79,80] was dissolved in saline and administered intraperitoneally (ip) to the animals of all groups except the vehicle-treated control group, that received an equal volume of saline. Donepezil at 5 mg/kg and compound **23e** at 5 mg/kg and 10 mg/kg in 0.5% CMC were administered orally 30 min prior to administration of scopolamine to the respective experimental group animals. All these treatments were continued for 14 consecutive days. During the last 5 days of the treatment period, spatial learning and memory were assessed using Morris Water Maze (MWM) test.[59,79]

A maze consisting of a circular pool (65 cm diameter; 30 cm height) was filled with water (26 ± 1 °C) up to 20 cm depth. The inside walls of the pool were painted black. The pool was divided into four quadrants, and the escape platform was placed 1 cm below the water surface in the middle of any one quadrant. Experiments on the individual animals were carried out to determine the time required by the animal to reach the hidden platform (i.e., escape latency time, ELT) which assesses the spatial learning and memory. All the experiments were carried out in a soundproof room and supervised by a blind observer.

Neurochemical analysis

After completing the MWM test, the animals were sacrificed and the whole brain was isolated from the skull and homogenized in glass Teflon homogenizer in 12.5 mM sodium phosphate buffer (pH 7). The homogenates were centrifuged at 15000 rpm for 15 min at 4 °C. The supernatants were utilized for estimations of different biochemical parameters. The cholinergic biomarkers AChE and BuChE were estimated in the mice brain using Ellman's method. 100 μL of the supernatant was incubated with 2.7 mL of phosphate buffer and 100 μL of freshly prepared ATCI or BTCI (15 mM) for 5 min. Finally, 100 μL of DTNB (1.5 mM) was added, and the absorbance was noted at 415 nm wavelength spectrophotometrically.

MDA, an indicator of lipid peroxidation, was estimated using thiobarbituric acid reacting substance (TBARS) method as described earlier.[61] MDA reacted with thiobarbituric acid in acidic medium at high temperature and formed a red complex TBARS which was analyzed spectrophotometrically. Briefly, 200 μL of the supernatant was mixed with 1 mL of 50% trichloroacetic acid in 0.1 M HCl and 1 mL of 26 mM thiobarbituric acid. After vortex mixing, samples were heated at 95 °C for 20 min. Later on the samples were centrifuged at 15000 rpm for 10 min and the supernatants were read at 532 nm wavelength.

68

Catalase (CAT) is an enzyme mediating breakdown of H_2O_2, a toxic form of oxygen metabolite into oxygen and water. CAT activity was determined following the method described by Sinha.[59] Briefly, 100 μL of the supernatant was mixed with 150 μL of 0.01 M phosphate buffer (pH 7). Reaction was started by the addition of 250 μL of H_2O_2 (0.16 M) and the medium incubated at 37 °C for 1 min, and the reaction was stopped by the addition of 1 mL of dichromate-acetic acid reagent (5% $K_2Cr_2O_7$-glacial acetic acid; 1:3 v/v). The reaction mixture was immediately kept on a boiling water bath for 15 min that resulted in development of a green color. Finally, the mixture was analyzed at 570 nm wavelength spectrophotometrically.

In order to extract glycine and glutamate, 10 μL aliquots of hypothalamus homogenate were thawed, mixed with 0.17 M perchloric acid (10% w/v). The mixture was left for 20 min at 4 °C. Resulting supernatant was decanted in separate Eppendorf tube and centrifuged at 4 °C for 20 min at 15000 rpm. After centrifugation, supernatant fraction was separated and maintained at -70°C until determination of free amino acids by HPLC coupled with electrochemical detector (Model no. Waters 2465, Waters Corporation, Milford, USA). Mobile phase was prepared by dissolving monosodium phosphate (0.1 M), EDTA (0.5 mM) and potassium chloride (2 mM) in HPLC grade methanol (25% v/v), diluted with distilled water. The solution pH was adjusted to 4.5. The mobile phase was filtered twice degassed in an ultrasonic bath for 20 min, before circulation in HPLC system. Analysis was performed on Welchrom C18 column with 1.2 mL/min flow rate, 3000 psi pressure and 850 mV working potential of the detector. The internal standards were prepared by mixing 200 μL of 1 mM stock of glycine/glutamate in 200 μL of pooled supernatant and diluted with 600 μL with mobile phase. It was used with equimolar concentration of derivatizing agent [22 mg of o-phthalaldehyde dissolved in 500 μL of absolute ethanol, 500 μL of 1 M sodium sulfite and 900 μL of 0.1 M tetraborate buffer, adjusted to pH 10.4 with 5 M sodium

69

hydroxide] to make final concentrations of 2, 1, 0.5, 0.4, 0.2 and 0.1 µmoles/L, and 200 µL of which was injected into HPLC. The sample solutions were prepared by diluting 200 µL of homogenate in 800 µL mobile phase, 10 µL of it was mixed with 10 µL of derivatizing agent and diluted in 880 µL mobile phase. Concentration of the neurotransmitter in brain was estimated by comparing the area with the calibration curve.[92]

Y-Maze Test

Adult male Wistar rats (150-200 g) were divided into five experimental groups of seven animals each as per the given treatment: (normal control, vehicle-treated control, donepezil at 5 mg/kg, compound **23e** at 5 mg/kg and 10 mg/kg). The animals were anesthetized with ketamine (100 mg/kg, ip) and xylazine (30 mg/kg, ip) and mounted in a stereotaxic apparatus (Stoelting, USA). All the groups (except the vehicle-treated control group which received an equal volume of normal saline) were injected with 2 µL of $A\beta_{1-42}$ (4 µM/µL in normal saline) unilaterally at the following coordinates: -4.0 mm anteroposterior, -2.5 mm mediolateral, and -3.5 mm dorsoventral from Bregma. Donepezil at 5 mg/kg and compound **23e** at 5 mg/kg and 10 mg/kg in 0.1% CMC were administered perorally to the respective experimental group animals for 15 consecutive days after 5 days of surgical recovery.[59] The Y-maze test was adopted for the assessment of immediate working memory. The test was performed during the last 5 days of the treatment period in the animals which were subjected to icv injection of $A\beta_{1-42}$. Each animal from the treated groups was kept at the end of any one arm of the maze and allowed to explore all the three arms. The sequence and the number of arm entries were recorded visually for each rat over a period of 5 min. An actual "alteration" was defined as entries in all three arms in consecutive choices (i.e., ABC, BCA, or CAB but not BAB). Repeat arm entry was considered as a sign of memory impairment. The

number of arm entries indicated locomotor activity. The "alteration score" for each rat was calculated using the equation:

% spontaneous alteration performance = [No of altered entries/ No. of repeated entries-2] *100

Acute Toxicity Study

Swiss albino mice (20−25 g) were used to determine the acute toxicity of the test compound **23e**. During the experiment, animals were maintained with free access of food and water ad libitum. Compound **23e** was suspended in 0.5% CMC-Na and given orally to the experimental groups. After administration of the test compound, the animals were observed continuously for the first 4 h for any abnormal behavior and mortality. Afterward, the animals were observed intermittently for the next 24 h and occasionally for 14 consecutive days after administration of compound **23e**. After 14 days, the animals were sacrificed and examined macroscopically for possible damage to the heart, liver, and kidneys.

Computational studies

Docking studies

Docking studies were performed with Glide module of Schrodinger Suite. Glide is projected for screening of probable ligands based on binding mode and affinity for a given receptor molecule. It performs grid-based ligand docking and searches for promising interactions between ligand molecules and a macromolecule, typically a protein. The 3D structures of ligand molecules were built within Maestro[93] using the Build module, and a single low energy conformation search was carried out for all molecules under study using OPLS_2005 force field at physiological pH condition using LigPrep module of Schrödinger, keeping all the parameters at standard values. The 3D crystallographic structures of AChE (PDB Code: 2CKM, 1B41) and of BuChE (PDB Code:

71

4BDS) were obtained from RCSB Protein Data Bank[94] and prepared for docking with protein preparation wizard of Schrödinger. The grid was generated on the active site of the respective receptor structure and was validated by re-docking the preexisting co-crystallized ligand structures. Docking calculations for the minimized 3D ligand structures were performed in extra precision (XP) mode within the active sites of the receptor structures. This docking protocol was validated by comparing the interactions of the docked conformer of donepezil in the active site of AChE with the reported literature.[95]

Molecular dynamics simulations

Maestro–Desmond (based on OPLS-2005 force field) was used to perform the molecular dynamics simulation study of the molecule **23e**.[96-98] To begin with, the system was solvated with the TIP3P water model in orthorhombic box of 10 Å^3, and neutralized by Na^+ ions for AChE and by Cl^- ions for BuChE. The long-range electrostatic interactions were studied by Smooth particle-mesh Ewald (PME) approximation and the non-bonded interactions were analyzed by using a MSHAKE algorithm with a cutoff of 9 Å. The default 'six step relaxation protocol' was followed to relax the system, which was involved with both restrained as well as unrestrained minimizations (2 steps) chased by the equilibration processes (4 steps). The productive MD was carried out for 20 ns with NPT ensemble at 300 K and 1 atm pressure using Nose-Hoover thermostat and Martyna–Tuckerman–Klein barostat. The coordinates and energies were noted at every 10 and 1.2 ps respectively. The ligand protein complex stability was analyzed by determining the root-mean-square deviation of the protein (RMSD-P), root-mean-square fluctuation of the protein (RMSF-P) and root-mean-square deviation of the ligand (RMSD-L), molecular surface area (MolSA), solvent-accessible surface area (SASA), radius-of-gyration (rGyr) and polar surface area (PSA).

In-silico prediction of physicochemical and pharmacokinetics parameters

In-silico prediction of physicochemical and pharmacokinetic properties were carried out with QikProp program v 3.5 (Schrodinger LLC, New York, USA).[71] The structures of the ligand molecules were built within the Maestro using the Build module and a single low energy conformation search was carried out for all molecules under study using OPLS_2005 force field at physiological pH condition using LigPrep module of Schrödinger. These structures were used for Qik-Prop to determine various physicochemical and pharmacokinetic descriptors. There were 51 properties predicted by the software. The major descriptors that were considered in this study were Lipinski's rule of 5 (Rule of 5), NRB: number of rotatable bonds, PSA: polar surface area, SASA: total solvent accessible surface area, CNS: Predicted central nervous system activity, QPPMDCK: Predicted apparent MDCK cell permeability, QPPCaco: Caco-2 cell permeability in nm/s, QPlogBB: brain/blood partition coefficient, QPlogKhsa: binding to human serum albumin, QPlogS: Predicted aqueous solubility and Percent Human-Oral Absorption: human oral absorption.

Supporting Information

HPLC methods, spectral data of synthesized compounds, docking poses of compound **23e** within AChE and BuChE, and in vitro blood-brain barrier permeation assay data are provided in Supporting information.

Author Information

Corresponding author. Mange Ram Yadav[*]

UGC-BSR Faculty Fellow

Tel.: +91 265 2434187; fax: +91 265 2418927.

E-mail address: mryadav11@yahoo.co.in

Author Contributions

MRY designed the whole study. DVP, NRP and AVK performed synthesis and collected data. DDK, SBP, PNU, KBP, DBS contributed reagents, materials and assisted in synthesis and data collection. AMK designed and performed computational studies. KVP drafted the biological evaluation studies. SPP, AS, ARM performed biological studies and collected data. PRM and NKP helped in synthesis and data interpretation. DVP and NRP wrote the manuscript. MRY conceived, designed and approved the final version of the manuscript.

Acknowledgements

Conflicts of interest

There are no conflicts of interest to disclose.

Abbreviations used

ACh, Acetylcholine; AChE, Acetylcholinesterase; AD, Alzheimer's disease; ADME, Absorption, distribution, metabolism, and excretion; ATCI, Acetylthiocholine iodide; BBB, Blood-brain barrier; BTCI, Butyrylthiocholine iodide; BuChE, Butyrylcholinesterase; CAS, catalytic active

74

site; CAT, Catalase; ChEs, cholinesterases; DMEM, Dulbecco's modified eagle medium; DPPH, 1,1-Diphenyl-2-picrylhydrazyl; DSC, Differential scanning calorimetry; DTNB, 5,5′-Dithiobis(2-nitrobenzoic acid); ELT, Escape latency time; FBS, Fetal bovine serum; % HOA, Human oral absorption percent; IAEC, Institutional animal ethics committee; mCPBA, meta-Chloroperbenzoic acid; MDA, Malondialdehyde; MolSA, Molecular surface area; MTDLs, Multitarget-directed ligands; MTT, 3-(4,5-Dimethylthiazol-2-yl)-2,5-diphenyltetrazolium bromide; MWM, Morris water maze; NCE, New chemical entity; NRB, Number of rotatable bonds; PAMPA, parallel artificial membrane permeation assay; PAS, Peripheral anionic site;PBL, Porcine brain lipid; PBS, Phosphate buffer saline; PSA, Polar surface area; rGyr, Radius-of-gyration; RMSD-L, Root-mean-square deviation of the ligand; RMSD-P, Root-mean-square deviation of the protein; RMSF-P, Root-mean-square fluctuation of the protein; ROS, Reactive oxygen species; SASA, Solvent-accessible surface area; SI, selectivity index; TBARS, Thiobarbituric acid reactive substances; THF, Tetrahydrofuran; TLC, Thin layer chromatography; TPSA, Topological polar surface area; UV, ultraviolet; XP, Extra precision

References:

(1) Scheltens, P.; Blennow, K.; Breteler, M. M. B.; de Strooper, B.; Frisoni, G. B.; Salloway, S.; Van der Flier, W. M. Alzheimer's disease. *The Lancet* **2016,** *388*, 505-517.

(2) Patterson, C. World Alzheimer Report 2018. *The State of the Art of Dementia Research: New Frontiers* **2018**, pp. 32-36.

(3) Talesa, V. N. Acetylcholinesterase in Alzheimer's disease. *Mech. Ageing Dev.* **2001,** *122*, 1961-1969.

(4) Selkoe, D. J. Folding proteins in fatal ways. *Nature* **2003,** *426*, 900.

(5) Hardy, J. A.; Higgins, G. A. Alzheimer's disease: the amyloid cascade hypothesis. *Science* **1992,** *256*, 184.

(6) Maccioni, R. B.; Farías, G.; Morales, I.; Navarrete, L. The revitalized tau hypothesis on Alzheimer's disease. *Arch. Med. Res.* **2010,** *41*, 226-231.

(7) Chu, D.; Liu, F. Pathological changes of tau related to Alzheimer's Disease. *ACS Chem. Neurosci.* **2018,** *10*, 931-944.

(8) Greenough, M. A.; Camakaris, J.; Bush, A. I. Metal dyshomeostasis and oxidative stress in Alzheimer's disease. *Neurochem. Int.* **2013,** *62*, 540-555.

(9) Bonda, D. J.; Wang, X.; Perry, G.; Nunomura, A.; Tabaton, M.; Zhu, X.; Smith, M. A. Oxidative stress in Alzheimer disease: a possibility for prevention. *Neuropharmacology* **2010,** *59*, 290-294.

(10) Maruszak, A.; Żekanowski, C. Mitochondrial dysfunction and Alzheimer's disease. *Prog. Neuropsychopharmacol. Biol. Psychiatry.* **2011,** *35*, 320-330.

(11) Heneka, M. T.; Carson, M. J.; El Khoury, J.; Landreth, G. E.; Brosseron, F.; Feinstein, D. L.; Jacobs, A. H.; Wyss-Coray, T.; Vitorica, J.; Ransohoff, R. M. Neuroinflammation in Alzheimer's disease. *Lancet Neurol.* **2015,** *14*, 388-405.

(12) Fu, W. Y.; Wang, X.; Ip, N. Y., Targeting neuroinflammation as a therapeutic strategy for alzheimer's disease: mechanisms, drug candidates, and new opportunities. *ACS Chem. Neurosci.* **2019**. *10*, 872-879.

(13) Del Pino, J.; Marco-Contelles, J.; Lopez-Munoz, F.; Romero, A.; Ramos, E. Neuroinflammation signaling modulated by Ass234, a multitarget small molecule for Alzheimer's disease therapy. *ACS Chem. Neurosci.* **2018,** *9*, 2880-2885.

(14) Agis-Torres, A.; Sollhuber, M.; Fernandez, M.; Sanchez-Montero, J. Multi-target-directed ligands and other therapeutic strategies in the search of a real solution for Alzheimer's disease. *Curr. Neuropharmacol.* **2014,** *12*, 2-36.

(15) Bajda, M.; Guzior, N.; Ignasik, M.; Malawska, B. Multi-target-directed ligands in Alzheimer's disease treatment. *Curr. Med. Chem.* **2011,** *18*, 4949-4975.

(16) Oset-Gasque, M. J.; Marco-Contelles, J. Alzheimer's disease, the "one-molecule, one-target" paradigm, and the multitarget directed ligand approach. *ACS Chem. Neurosci.* **2018,** *9*, 401-403.

(17) Wang, T.; Liu, X. H.; Guan, J.; Ge, S.; Wu, M. B.; Lin, J. P.; Yang, L. R. Advancement of multi-target drug discoveries and promising applications in the field of Alzheimer's disease. *Eur. J. Med. Chem.* **2019,***169*, 200-223.

(18) Csermely, P.; Agoston, V.; Pongor, S. The efficiency of multi-target drugs: the network approach might help drug design. *Trends Pharmacol. Sci.* **2005,** *26*, 178-182.

(19) Morphy, J. R. The challenges of multi-target lead optimization. In *Designing Multi-Target Drugs*; Morphy, J. R., Harris, C. J., Eds.; Royal Society of Chemistry, **2012**; pp 141-154.

(20) Cavalli, A.; Bolognesi, M. L.; Minarini, A.; Rosini, M.; Tumiatti, V.; Recanatini, M.; Melchiorre, C. Multi-target-directed ligands to combat neurodegenerative diseases. *J. Med. Chem.* **2008,** *51*, 347-372.

(21) Greig, N. H.; Lahiri, D. K.; Sambamurti, K. Butyrylcholinesterase: an important new target in Alzheimer's disease therapy. *Int. Psychogeriatr.* **2002,** *14*, 77-91.

(22) Jing, L.; Wu, G.; Kang, D.; Zhou, Z.; Song, Y.; Liu, X.; Zhan, P. Contemporary medicinal-chemistry strategies for the discovery of selective butyrylcholinesterase inhibitors. *Drug Discov. Today.* **2019,** *24*, 629-635.

(23) Sussman, J. L.; Harel, M.; Frolow, F.; Oefner, C.; Goldman, A.; Toker, L.; Silman, I. Atomic structure of acetylcholinesterase from Torpedo californica: a prototypic acetylcholine-binding protein. *Science* **1991,** *253*, 872-879.

(24) De Ferrari, G. V.; Canales, M. A.; Shin, I.; Weiner, L. M.; Silman, I.; Inestrosa, N. C. A structural motif of acetylcholinesterase that promotes amyloid β-peptide fibril formation. *Biochemistry* **2001,** *40*, 10447-10457.

(25) Dinamarca, M. C.; Sagal, J. P.; Quintanilla, R. A.; Godoy, J. A.; Arrázola, M. S.; Inestrosa, N. C. Amyloid-β-Acetylcholinesterase complexes potentiate neurodegenerative changes induced by the Aβ peptide. Implications for the pathogenesis of Alzheimer's disease. *Mol. Neurodegener.* **2010,** *5*, 4.

(26) Wang, Y.; Wang, H.; Chen, H. AChE inhibition-based multi-target-directed ligands, a novel pharmacological approach for the symptomatic and disease-modifying therapy of Alzheimer's disease. *Curr. Neuropharmacol.* **2016,** *14*, 364-375.

78

(27) Hartmann, J.; Kiewert, C.; Duysen, E. G.; Lockridge, O.; Greig, N. H.; Klein, J. Excessive hippocampal acetylcholine levels in acetylcholinesterase-deficient mice are moderated by butyrylcholinesterase activity. *J. Neurochem.* **2007,** *100*, 1421-1429.

(28) Arendt, T.; Bigl, V.; Walther, F.; Sonntag, M. Decreased ratio of CSF acetylcholinesterase to butyrylcholinesterase activity in Alzheimer's disease. *The Lancet* **1984,** *323*, 173.

(29) Kosak, U.; Brus, B.; Knez, D.; Zakelj, S.; Trontelj, J.; Pislar, A.; Sink, R.; Jukic, M.; Zivin, M.; Podkowa, A. The magic of crystal structure-based inhibitor optimization: development of a butyrylcholinesterase inhibitor with picomolar affinity and in vivo activity. *J. Med. Chem.* **2017,** *61*, 119-139.

(30) Geula, C.; Mesulam, M. Cholinesterases and the pathology of Alzheimer disease. *Alzheimer Dis. Assoc. Disord.* **1995**.

(31) Guillozet, A.; Mesulam, M. M.; Smiley, J.; Mash, D. Butyrylcholinesterase in the life cycle of amyloid plaques. *Ann. Neurol.* **1997,** *42*, 909-918.

(32) Mishra, P.; Kumar, A.; Panda, G. Anti-cholinesterase hybrids as multi-target-directed ligands against Alzheimer's disease (1998-2018). *Bioorg. Med. Chem.* **2019**, *27*, 895-930.

(33) Jakob-Roetne, R.; Jacobsen, H. Alzheimer's disease: from pathology to therapeutic approaches. *Angew. Chem. Int. Ed.* **2009,** *48*, 3030-3059.

(34) Uttara, B.; Singh, A. V.; Zamboni, P.; Mahajan, R. Oxidative stress and neurodegenerative diseases: a review of upstream and downstream antioxidant therapeutic options. *Curr. Neuropharmacol.* **2009,** *7*, 65-74.

(35) Zhao, Y.; Zhao, B. Oxidative stress and the pathogenesis of Alzheimer's disease. *Oxid. Med. Cell. Longev.* **2013,** *2013,* 316523.

79

(36) Mecocci, P.; Polidori, M. C. Antioxidant clinical trials in mild cognitive impairment and Alzheimer's disease. *Biochim. Biophys. Acta* **2012,** *1822*, 631-638.

(37) Sharma, V.; Kumar, P.; Pathak, D. Biological importance of the indole nucleus in recent years: a comprehensive review. *J. Heterocycl. Chem.* **2010,** *47*, 491-502.

(38) Kaushik, N.; Kaushik, N.; Attri, P.; Kumar, N.; Kim, C.; Verma, A.; Choi, E. Biomedical importance of indoles. *Molecules* **2013,** *18*, 6620-6662.

(39) Zhou, J. N.; Liu, R. Y.; Kamphorst, W.; Hofman, M. A.; Swaab, D. F. Early neuropathological Alzheimer's changes in aged individuals are accompanied by decreased cerebrospinal fluid melatonin levels. *J. Pineal Res.* **2003,** *35*, 125-130.

(40) Wu, Y. H.; Feenstra, M. G.; Zhou, J. N.; Liu, R. Y.; Toranõ, J. S.; Van Kan, H. J.; Fischer, D. F.; Ravid, R.; Swaab, D. F. Molecular changes underlying reduced pineal melatonin levels in Alzheimer disease: alterations in preclinical and clinical stages. *J. Clin. Endocrinol. Metab.* **2003,** *88*, 5898-5906.

(41) Wu, Y. H.; Swaab, D. F. The human pineal gland and melatonin in aging and Alzheimer's disease. *J. Pineal Res.* **2005,** *38*, 145-152.

(42) Pandi-Perumal, S. R.; Srinivasan, V.; Maestroni, G.; Cardinali, D.; Poeggeler, B.; Hardeland, R. Melatonin: Nature's most versatile biological signal. *FEBS J.* **2006,** *273*, 2813-2838.

(43) Feng, Z.; Zhang, J. T. Melatonin reduces amyloid β-induced apoptosis in pheochromocytoma (PC12) cells. *J. Pineal Res.* **2004,** *37*, 257-266.

(44) Espinar, A.; García-Oliva, A.; Isorna, E. M.; Quesada, A.; Prada, F. A.; Guerrero, J. M. Neuroprotection by melatonin from glutamate-induced excitotoxicity during development of the cerebellum in the chick embryo. *J. Pineal Res.* **2000,** *28*, 81-88.

80

(45) Aydogan, S.; Yerer, M. B.; Goktas, A. Melatonin and nitric oxide. *J. Endocrinol. Invest.* **2006,** *29*, 281-287.

(46) Rodríguez-Franco, M. I.; Fernández-Bachiller, M. I.; Pérez, C.; Hernández-Ledesma, B.; Bartolomé, B. Novel tacrine-melatonin hybrids as dual-acting drugs for Alzheimer disease, with improved acetylcholinesterase inhibitory and antioxidant properties. *J. Med. Chem.* **2006,** *49*, 459-462.

(47) Pachon-Angona, I.; Refouvelet, B.; Andrýs, R.; Martin, H.; Luzet, V.; Iriepa, I.; Moraleda, I.; Diez-Iriepa, D.; Oset-Gasque, M. J.; Marco-Contelles, J. Donepezil-chromone-melatonin hybrids as promising agents for Alzheimer's disease therapy. *J. Enzyme Inhib. Med. Chem.* **2019,** *34*, 479-489.

(48) Lopez-Iglesias, B.; Pérez, C. N.; Morales-Garcia, J. A.; Alonso-Gil, S.; Pérez-Castillo, A.; Romero, A.; López, M. G.; Villarroya, M.; Conde, S.; Rodríguez-Franco, M. I. New melatonin-*N*, *N*-dibenzyl (*N*-methyl) amine hybrids: Potent neurogenic agents with antioxidant, cholinergic, and neuroprotective properties as innovative drugs for Alzheimer's disease. *J. Med. Chem.* **2014,** *57*, 3773-3785.

(49) Yanovsky, I.; Finkin-Groner, E.; Zaikin, A.; Lerman, L.; Shalom, H.; Zeeli, S.; Weill, T.; Ginsburg, I.; Nudelman, A.; Weinstock, M. Carbamate derivatives of indolines as cholinesterase inhibitors and antioxidants for the treatment of Alzheimer's disease. *J. Med. Chem.* **2012,** *55*, 10700-10715.

(50) Kumar, R.; Sirohi, T.; Singh, H.; Yadav, R.; Roy, R.; Chaudhary, A.; Pandeya, S. 1,2,4-triazine analogs as novel class of therapeutic agents. *Mini Rev. Med. Chem.* **2014,** *14*, 168-207.

(51) Irannejad, H.; Amini, M.; Khodagholi, F.; Ansari, N.; Tusi, S. K.; Sharifzadeh, M.; Shafiee, A. Synthesis and in vitro evaluation of novel 1,2,4-triazine derivatives as neuroprotective agents. *Bioorg. Med. Chem.* **2010,** *18*, 4224-4230.

(52) Veloso, A. J.; Chow, A. M.; Dhar, D.; Tang, D. W.; Ganesh, H. V.; Mikhaylichenko, S.; Brown, I. R.; Kerman, K. Biological activity of sym-triazines with acetylcholine-like substitutions as multitarget modulators of Alzheimer's disease. *ACS Chem. Neurosci.* **2013,** *4*, 924-929.

(53) Veloso, A. J.; Dhar, D.; Chow, A. M.; Zhang, B.; Tang, D. W.; Ganesh, H. V.; Mikhaylichenko, S.; Brown, I. R.; Kerman, K. sym-Triazines for directed multitarget modulation of cholinesterases and amyloid-β in Alzheimer's disease. *ACS Chem. Neurosci.* **2012,** *4*, 339-349.

(54) Tripathi, P. N.; Srivastava, P.; Sharma, P.; Tripathi, M. K.; Seth, A.; Tripathi, A.; Rai, S. N.; Singh, S. P.; Shrivastava, S. K. Biphenyl-3-oxo-1,2,4-triazine linked piperazine derivatives as potential cholinesterase inhibitors with anti-oxidant property to improve the learning and memory. *Bioorg. Chem.* **2019,** *85*, 82-96.

(55) Russell, M. G.; Carling, R. W.; Street, L. J.; Hallett, D. J.; Goodacre, S.; Mezzogori, E.; Reader, M.; Cook, S. M.; Bromidge, F. A.; Newman, R. Discovery of imidazo[1,2-*b*][1,2,4]triazines as GABAA α2/3 subtype selective agonists for the treatment of anxiety. *J. Med. Chem.* **2006,** *49*, 1235-1238.

(56) Leach, M. J.; Marden, C. M.; Miller, A. A. Pharmacological studies on lamotrigine, a novel potential antiepileptic drug. *Epilepsia* **1986,** *27*, 490-497.

(57) Misra, U.; Hitkari, A.; Saxena, A.; Gurtu, S.; Shanker, K. Biologically active indolylmethyl-1,3,4-oxadiazoles, 1,3,4-thiadiazoles, 4*H*-1,3,4-triazoles and 1,2,4-triazines. *Eur. J. Med. Chem.* **1996,** *31*, 629-634.

82

(58) Ansari, N.; Khodagholi, F.; Ramin, M.; Amini, M.; Irannejad, H.; Dargahi, L.; Amirabad, A. D. Inhibition of LPS-induced apoptosis in differentiated-PC12 cells by new triazine derivatives through NF-κB-mediated suppression of COX-2. *Neurochem. Int.* **2010,** *57*, 958-968.

(59) Sinha, A.; Tamboli, R. S.; Seth, B.; Kanhed, A. M.; Tiwari, S. K.; Agarwal, S.; Nair, S.; Giridhar, R.; Chaturvedi, R. K.; Yadav, M. R. Neuroprotective role of novel triazine derivatives by activating Wnt/β catenin signaling pathway in rodent models of Alzheimer's disease. *Mol. Neurobiol.* **2015,** *52*, 638-652.

(60) Tamboli, R. S.; Giridhar, R.; Gandhi, H. P.; Kanhed, A. M.; Mande, H. M.; Yadav, M. R. Design, green synthesis and pharmacological evaluation of novel 5,6-diaryl-1,2,4-triazines bearing 3-morpholinoethylamine moiety as potential antithrombotic agents. *J. Enzyme Inhib. Med. Chem.* **2016,** *31*, 704-713.

(61) Shidore, M.; Machhi, J.; Shingala, K.; Murumkar, P.; Sharma, M. K.; Agrawal, N.; Tripathi, A.; Parikh, Z.; Pillai, P.; Yadav, M. R. Benzylpiperidine-linked diarylthiazoles as potential anti-Alzheimer's agents: synthesis and biological evaluation. *J. Med. Chem.* **2016,** *59*, 5823-5846.

(62) Kanhed, A. M.; Sinha, A.; Machhi, J.; Tripathi, A.; Parikh, Z. S.; Pillai, P. P.; Giridhar, R.; Yadav, M. R. Discovery of isoalloxazine derivatives as a new class of potential anti-Alzheimer agents and their synthesis. *Bioorg. Chem.* **2015,** *61*, 7-12.

(63) Saxena, A.; Redman, A. M.; Jiang, X.; Lockridge, O.; Doctor, B. Differences in active site gorge dimensions of cholinesterases revealed by binding of inhibitors to human butyrylcholinesterase. *Biochemistry* **1997,** *36*, 14642-14651.

(64) Kedare, S. B.; Singh, R. Genesis and development of DPPH method of antioxidant assay. *J. Food Sci. Technol.* **2011,** *48*, 412-422.

(65) Mathew, M.; Subramanian, S. In vitro screening for anti-cholinesterase and antioxidant activity of methanolic extracts of ayurvedic medicinal plants used for cognitive disorders. *PloS one* **2014,** *9*, e86804.

(66) Porcal, W.; Hernández, P.; González, M.; Ferreira, A.; Olea-Azar, C.; Cerecetto, H.; Castro, A. Heteroarylnitrones as drugs for neurodegenerative diseases: synthesis, neuroprotective properties, and free radical scavenger properties. *J. Med. Chem.* **2008,** *51*, 6150-6159.

(67) Dahlgren, K. N.; Manelli, A. M.; Stine, W. B.; Baker, L. K.; Krafft, G. A.; LaDu, M. J. Oligomeric and fibrillar species of amyloid-β peptides differentially affect neuronal viability. *J. Biol. Chem.* **2002**, *277*, 32046-32053.

(68) Di, L.; Kerns, E. H.; Fan, K.; McConnell, O. J.; Carter, G. T. High throughput artificial membrane permeability assay for blood–brain barrier. *Eur. J. Med.Chem.* **2003,** *38*, 223-232.

(69) Di, L.; Kerns, E. H.; Bezar, I. F.; Petusky, S. L.; Huang, Y. Comparison of blood–brain barrier permeability assays: in situ brain perfusion, MDR1-MDCKII and PAMPA-BBB. *J. Pharm Sci.* **2009,** *98*, 1980-1991.

(70) Wang, J.; Urban, L. The impact of early ADME profiling on drug discovery and development strategy. *Drug Discov. World* **2004,** *5*, 73-86.

(71) QikProp, version 3.5, Schrödinger, LLC, New York, NY, 2012.

(72) Lipinski, C. A.; Lombardo, F.; Dominy, B. W.; Feeney, P. J. Experimental and computational approaches to estimate solubility and permeability in drug discovery and development settings. *Adv. Drug Deliv. Rev.* **1997,** *23*, 3-25.

(73) Veber, D. F.; Johnson, S. R.; Cheng, H. Y.; Smith, B. R.; Ward, K. W.; Kopple, K. D. Molecular properties that influence the oral bioavailability of drug candidates. *J. Med. Chem.* **2002,** *45*, 2615-2623.

84

(74) Kelder, J.; Grootenhuis, P. D.; Bayada, D. M.; Delbressine, L. P.; Ploemen, J. P. Polar molecular surface as a dominating determinant for oral absorption and brain penetration of drugs. *Pharm. Res.* **1999,** *16*, 1514-1519.

(75) Pajouhesh, H.; Lenz, G. R. Medicinal chemical properties of successful central nervous system drugs. *NeuroRx* **2005,** *2*, 541-553.

(76) Waterhouse, R. N. Determination of lipophilicity and its use as a predictor of blood-brain barrier penetration of molecular imaging agents. *Mol. Imaging Biol.* **2003,** *5*, 376-389.

(77) Wang, Q.; Rager, J. D.; Weinstein, K.; Kardos, P. S.; Dobson, G. L.; Li, J.; Hidalgo, I. J. Evaluation of the MDR-MDCK cell line as a permeability screen for the blood-brain barrier. *Int. J. Pharm.* **2005,** *288*, 349-359.

(78) Chen, J.; Long, Y.; Han, M.; Wang, T.; Chen, Q.; Wang, R. Water-soluble derivative of propolis mitigates scopolamine-induced learning and memory impairment in mice. *Pharmacol. Biochem. Behav.* **2008,** *90*, 441-446.

(79) Lee, M. R.; Yun, B. S.; Park, S. Y.; Ly, S. Y.; Kim, S. N.; Han, B. H.; Sung, C. K. Anti-amnesic effect of Chong–Myung–Tang on scopolamine-induced memory impairments in mice. *J. Ethnopharmacol.* **2010,** *132*, 70-74.

(80) Goverdhan, P.; Sravanthi, A.; Mamatha, T. Neuroprotective effects of meloxicam and selegiline in scopolamine-induced cognitive impairment and oxidative stress. *Int. J. Alzheimers Dis.* **2012,** *2012,* 1-8.

(81) Morris, R. Developments of a water-maze procedure for studying spatial learning in the rat. *J. Neurosci. Methods* **1984,** *11*, 47-60.

(82) Chumakov, I.; Nabirotchkin, S.; Cholet, N.; Milet, A.; Boucard, A.; Toulorge, D.; Pereira, Y.; Graudens, E.; Traoré, S.; Foucquier, J. Combining two repurposed drugs as a promising approach for Alzheimer's disease therapy. *Sci. Rep.* **2015,** *5*, 7608.

(83) Rosenbrock, H.; Giovannini, R.; Schmid, B.; Kramer, G.; Arban, R.; Dorner-Ciossek, C.; Wunderlich, G. Improving cognitive function in rodents via increasing glycine levels in brain by the novel glycine transporter-1 inhibitor BI 425809. *Alzheimer's Dement. J. Alzheimer's Assoc.* **2016,** *12*, 1018.

(84) Rosenbrock, H.; Desch, M.; Kleiner, O.; Dorner-Ciossek, C.; Schmid, B.; Keller, S.; Schlecker, C.; Moschetti, V.; Goetz, S.; Liesenfeld, K. H. Evaluation of pharmacokinetics and pharmacodynamics of BI 425809, a novel GlyT1 inhibitor: translational studies. *Clin. Transl. Sci.* **2018,** *11*, 616-623.

(85) Camacho, A.; Massieu, L. Role of glutamate transporters in the clearance and release of glutamate during ischemia and its relation to neuronal death. *Arch. Med. Res.* **2006,** *37*, 11-18.

(86) Sattler, R.; Rothstein, J. Regulation and dysregulation of glutamate transporters. In *Neurotransmitter Transporters. Handbook of Experimental Pharmacology,* Sitte H. H., Freissmuth M., Eds.; Springer, Berlin, Heidelberg, **2006**, vol 175, pp 277-303.

(87) Mattson, M. P., Calcium and neurodegeneration. *Aging cell* **2007,** *6*, 337-350.

(88) Yan, J. J.; Cho, J. Y.; Kim, H. S.; Kim, K. L.; Jung, J. S.; Huh, S. O.; Suh, H. W.; Kim, Y. H.; Song, D. K. Protection against β-amyloid peptide toxicity in vivo with long-term administration of ferulic acid. *Br. J. Pharmacol.* **2001,** *133*, 89-96.

(89) OECD, *Test No. 423: Acute Oral toxicity - Acute Toxic Class Method*. **2002**.

(90) El Sayed, H.; Hamid, H. M. A.; Hagar, M. Microwave irradiation for accelerating each step for the synthesis of 1,2,4-triazino [5,6-*b*]indole-3-thiols and their derivatives from isatin and 5-chloroisatin. *Synlett* **2004,** *2004*, 723-725.

(91) Hou, D. R.; Cheng, H. Y.; Wang, E. C. Efficient syntheses of oncinotine and neooncinotine. *J. Org. Chem.* **2004,** *69*, 6094-6099.

(92) Monge-Acuna, A. A.; Fornaguera-Trías, J., A high performance liquid chromatography method with electrochemical detection of gamma-aminobutyric acid, glutamate and glutamine in rat brain homogenates. *J. Neurosci. Methods* **2009,** *183* (2), 176-181.

(93) Maestro, version 9.0; Schrodinger, LLC, New York, NY, U.S., 2009.

(94) Protein Data Bank. www.rcsb.org/pdb/home/home.do (accessed Jan. 09, 2019).

(95) Cheung, J.; Rudolph, M. J.; Burshteyn, F.; Cassidy, M. S.; Gary, E. N.; Love, J.; Franklin, M. C.; Height, J. J. Structures of human acetylcholinesterase in complex with pharmacologically important ligands. *J. Med. Chem.* **2012,** *55*, 10282-10286.

(96) Patel, N. R.; Patel, D. V.; Kanhed, A. M.; Patel, S. P.; Patel, K. V.; Afosah, D.; Desai, U. R.; Karpoormath, R.; Yadav, M. R. 2-Aminobenzamide-based factor Xa inhibitors with novel mono-and bi-aryls as S4 binding elements. *ChemistrySelect* **2019,** *4*, 802-809.

(97) Bowers, K. J.; Chow, D. E.; Xu, H.; Dror, R. O.; Eastwood, M. P.; Gregersen, B. A.; Klepeis, J. L.; Kolossvary, I.; Moraes, M. A.; Sacerdoti, F. D. In *Scalable algorithms for molecular dynamics simulations on commodity clusters*, SC 2006 conference, proceedings of the ACM/IEEE, IEEE: **2006**, 43-43.

(98) Tuckerman, M.; Berne, B. J.; Martyna, G. J. Reversible multiple time scale molecular dynamics. *J. Chem.Phys.* **1992,** *97*, 1990-2001.

87

Table of Contents graphic

Vicinal diaryltriazines
ChE inhibition
Neuroprotection

Molecular hybridization

MeO

Melatonin
Anti-oxidant
Neuroprotection

Cholinesterase Inhibition

AChE $IC_{50} = 0.56 \pm 0.02$ μM
BuChE $IC_{50} = 1.17 \pm 0.09$ μM

Neuroprotective activity
against H_2O_2/Aβ-induced toxicity

Anti-oxidant activity

RP of DPPH
54.9 ± 1.8 at 10 μM conc.
64.3 ± 2.8 at at 20 μM conc.

Neurochemical analysis

MWM Test

Behavioral study

Y-Maze Test

QikProp

MW 338.45

LogP$_{o/w}$ 3.196

PSA 69.799

NRB 8

HBA 5.5

HBD 2

Lipinski's rule of five √

Veber's rule √

PAMPA CNS+

Acute toxicity study

$LD_{50} > 2000$ mg/kg